Spring 2013

# The effects of rapid stretch injury on rat neocortical cultures

George Constandinos Magou
*New Jersey Institute of Technology*

# Copyright Warning & Restrictions

The copyright law of the United States (Title 17, United States Code) governs the making of photocopies or other reproductions of copyrighted material.

Under certain conditions specified in the law, libraries and archives are authorized to furnish a photocopy or other reproduction. One of these specified conditions is that the photocopy or reproduction is not to be "used for any purpose other than private study, scholarship, or research." If a, user makes a request for, or later uses, a photocopy or reproduction for purposes in excess of "fair use" that user may be liable for copyright infringement,

This institution reserves the right to refuse to accept a copying order if, in its judgment, fulfillment of the order would involve violation of copyright law.

Please Note: The author retains the copyright while the New Jersey Institute of Technology reserves the right to distribute this thesis or dissertation

Printing note: If you do not wish to print this page, then select "Pages from: first page # to: last page #" on the print dialog screen

## ABSTRACT

### THE EFFECTS OF RAPID STRETCH INJURY ON RAT NEOCORTICAL CULTURES

**by**
**George Constandinos Magou**

Several key biological mechanisms of traumatic injury to axons have been elucidated using *in vitro* stretch injury models. These models, however, are based on the experimentation of single cultures keeping productivity slow. Indeed, low yield has hindered important and well founded investigations requiring high throughput methods such as proteomic analyses. To meet this need, a multi-well high throughput injury device is engineered to accelerate and accommodate the next generation of traumatic brain injury research. This modular system stretch-injures neuronal cultures in either a 24-well culture plate format or six individual wells simultaneously. Custom software control allows the user to accurately program the pressure pulse parameters to achieve the desired substrate deformation and injury parameters.

Classically, *in vitro* research in TBI has shown increases in $[Ca^{2+}]_i$ levels following injury. The $Ca^{2+}$ sensitive fluorescent dye, Fluo-4AM, is used to observe the effects of strain rate on the changes in $[Ca^{2+}]_i$ levels following injury. Neuronal cultures are injured at three strain levels: 20%, 40% and 60% strain. At each of these strain levels, two strain rates are applied; $30s^{-1}$ (slow) and $70s^{-1}$ (rapid). At each strain level, the data show that neurons injured at $70s^{-1}$ experience larger maximum $F/F_0$ and longer sustained $Ca^{2+}$ fluorescence than neurons injured at $30s^{-1}$. It is also shown that at high strain rates TTx no longer blocks increases in $[Ca^{2+}]_i$ levels after injury.

Traumatic injury to the brain is known to cause dysfunction in surviving neurons. The effects of simulated traumatic injury of rat neocortical neurons cultures are investigated. These neurons are subjected to a stretch injury of 60% strain over 20 ms using a custom *in vitro* injury device. Spontaneous and stimulated electrical properties are measured 20-60 minutes after stretch using current and voltage clamp techniques. The same measurements are performed in non-stretched neurons. All neurons display TTX-inhibitable action potentials when basal membrane potential was set at -60 mV, and many display bursting behavior in response to depolarizing current injection. No differences in resting membrane potential (-40 ± 1 mV [n=20]) or input resistance (1.0 ± 0.1 GΩ [n=20]) are observed in injured and non-injured neurons. Interestingly, stretch injury reduces the frequency of spontaneous action potentials (33 ± 6 $min^{-1}$ [n=13] and 11 ± 3 $min^{-1}$ [n=16] in non-injured and injured neurons, respectively) and decreases spontaneous bursting activity by almost 90%. $ADP_{50}$ and action potential amplitude are unchanged. However, $ADP_{90}$ is significantly prolonged in injured neurons and characterized by a less pronounced action potential after-hyperpolarization. These data are consistent with an alteration in kinetics of $K^+$ currents in injured neurons. Since spontaneous action potentials are blocked by 20 μM bicuculline and 3 mM kyneurinic acid, the frequency of subthreshold depolarizations is measured to estimate overall neuronal network activity. The frequency of spontaneous subthreshold depolarizations is not significantly different in injured and non-injured neurons. These data show that spontaneous electrical signaling is acutely altered and suggest that action potential initiation is reduced by *in vitro* stretch in neuronal cell cultures.

# THE EFFECTS OF RAPID STRETCH INJURY ON RAT NEOCORTICAL CULTURES

**by**
**George Constandinos Magou**

**A Dissertation**
**Submitted to the Faculty of**
**New Jersey Institute of Technology**
**in Partial Fulfillment of the Requirements for the Degree of**
**Doctor of Philosophy in Materials Science and Engineering**

**Interdisciplinary Program in Materials Science and Engineering**

**May 2013**

.

**APPROVAL PAGE**

**THE EFFECTS OF RAPID STRETCH INJURY ON RAT NEOCORTICAL CULTURES**

**George Constandinos Magou**

---

Dr. Bryan J. Pfister, Dissertation Advisor — Date
Associate Professor of Biomedical Engineering, NJIT

---

Dr. Joshua R. Berlin, Co-Advisor — Date
Professor of Pharmacology and Physiology, UMDNJ

---

Dr. Michael Jaffe, Committee Member — Date
Research Professor of Biomedical Enginering, NJIT

---

Dr. Raquel Perez-Castillejos, Committee Member — Date
Assistant Professor of Biomedical Engineering, NJIT

---

Dr. Camelia Prodan, Committee Member — Date
Associate Professor of Physics, NJIT

---

Dr. Andrew Hill, Committee Member — Date
Assistant Professor of Biological Sciences, Rutgers University

## BIOGRAPHICAL SKETCH

**Author:** George Constandinos Magou

**Degree:** Doctor of Philosophy

**Date:** May 2013

**Undergraduate and Graduate Education:**

- Doctor of Philosophy in Materials Science and Engineering,
  New Jersey Institute of Technology, Newark, NJ, 2013

- Bachelor of Science in Biomedical Engineering,
  New Jersey Institute of Technology, Newark, NJ, 2006

**Major:** Materials Science and Engineering

**Presentations and Publications:**

George C. Magou, Bryan J. Pfister, and Joshua R. Berlin, "Effect of acute stretch injury on action potential and network activity of rat neocortical neurons in culture," The 57$^{th}$ annual meeting of the Biophysical Society, Philadelphia, PA, February 2013.

George C. Magou, Yi Guo, Mridusmita Choudhury, Linda Chen, Nicolae Hususan, Stephanie Masotti, and Bryan J. Pfister, "Engineering a high throughput axon injury system," Journal of Neurotrauma, 28, pp. 2203-2218, November 2011.

George C. Magou and Bryan J. Pfister, "Engineering a high throughput axon injury system," 2010 National Neurotrauma Symposium. Las Vegas, NV, June 2010.

I would like to dedicate this work to my parents, George and Susana, for never letting me give up on my dreams. Their constant encouragement, love, and support has been the backbone of my success.

## ACKNOWLEDGMENT

This work could not have been accomplished without the continued support and dedication of Dr. Bryan Pfister. His guidance, creativity and motivation have been vital to my success. I would like to thank him for allowing me the opportunity to work in his lab. Very special thanks are given to Dr. Joshua Berlin. This work would not have been possible without his expertise, insight, and support. Thank you to both Dr. Bryan Pfister and Dr. Joshua Berlin for their mentorship, guidance, and for the opportunity to train and work alongside them. I would also like to acknowledge Dr. Michael Jaffe, Dr. Andrew Hill, Dr. Raquel Perez-Castillejos, and Dr. Camelia Prodan for serving on my committee and for their continued support. Special thanks to John Hoinowski for his creativity, time, advice, and immense talent. Without him, my designs could not have come to fruition. I would to thank my colleagues, Joseph Loverde, Mevan Siriwardane, Mat Long, and Yi Guo for their long-time encouragement, insight and support. It has been a pleasure working alongside each of them. I would like to thank my beautiful girlfriend, Stephanie, for her encouragement and unwavering support over the years. Lastly, I would like to thank my parents, George and Susana, my brother, Nick, and my sister, Stephanie who have always been a great source of encouragement and support.

## TABLE OF CONTENTS

**TABLE OF CONTENTS**
**(Continued)**

**Chapter** **Page**

**TABLE OF CONTENTS**
**(Continued)**

**Chapter** **Page**

**TABLE OF CONTENTS**
**(Continued)**

## LIST OF TABLES

## LIST OF FIGURES

## LIST OF FIGURES
## (Continued)

# CHAPTER 1

# INTRODUCTION

## 1.1 Traumatic Brain Injury and Diffuse Axonal Injury

Nearly 2 million cases of traumatic brain injury (TBI) occur in the United States every year, (Smith & Meaney, 2000) TBI cases makes up a third of all injury related deaths in the United States. The leading causes of TBI are falls, motor vehicle related injuries, blows to the head, and assault .

Due to complexity of the disease, TBI has been categorized into two major types of trauma; "focal" and "diffuse", (Adams *et al.*, 1983; Gennarelli, 1993; Smith & Meaney, 2000). Focal trauma is described as an injury caused by a blow to the head and is generally associated with the presence of contusions and/or hematomas in the brain, (Adams *et al.*, 1983; Graham *et al.*, 1983; Gennarelli, 1993). Diffuse injury is a result of rapid rotational head movements. Large acceleration/deceleration of the head coupled with the large mass of the brain creates inertial forces in the brain. Brain tissue, being known to have viscoelastic properties, (Thibault *et al.*, 1992; Meaney *et al.*, 1995; Smith *et al.*, 1999), deforms against the skull when subjected to these inertial forces. Due to the differences in material integrity of the brain (viscoelastic) and the skull (rigid), shear forces develop on a macroscopic level between brain tissue and the skull. These shear forces translate microscopically to uniaxial stretch and compression of axon fibers. This type of injury commonly referred to as diffuse axonal injury (DAI), (Figure 1.1). One of the most challenging aspects of treating DAI is diagnosing the disease. In severe DAI cases, patients often times experience tears in brain tissue due to extreme uniaxial loading of white matter (Smith & Meaney, 2000). This type of pathology is macroscopic and is

identifiable via modern brain imaging techniques. However, many mild to moderate cases may not yield such obvious evidence of DAI. At its core DAI is microscopic and commonly present without evidence of macroscopic tissue damage. Often times it can only be identified post-mortem in humans and animals using histological methods (Adams *et al.*, 1989; Graham *et al.*, 1993; Smith & Meaney, 2000).

This type of mechanical loading to the brain is believed to be

To study the progression of traumatic axonal injury, the relationship between mechanical deformation and the evolution of structural and functional alterations of the neuron needs to be investigated. *In vitro* models offer the advantage of studying injury dynamics *in real time,* making it easier to explore biomechanical and biological factors involved in the progression of axonal pathology. Importantly, the mechanisms identified from *in vitro* modeling represent an important first step that can be used for further study and verification in animal models.

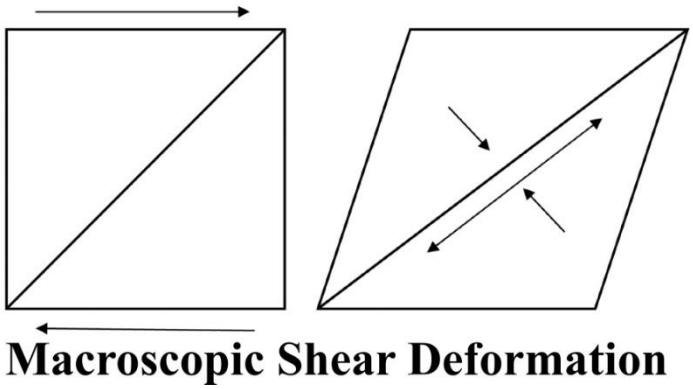


**Figure 1.1** A representative block of brain tissue under shear deformation translating into a uniaxial stretch of axon fibers along the diagonal. Likewise, compression occurs perpendicular to the diagonal.

## 1.2 *In Vitro* Models of DAI

*In vitro* models of DAI have been useful in identifying different aspects of neuronal injury associated with TBI. Since, in its essence, DAI is simply described as a stretch induced injury, these models hinge on this concept. Many labs dedicated to TBI research have created their own "stretch injury" devices to provide the mechanical forces needed to induce DAI in cultured cells. Each model provides a unique and creative method of stretching cells. Some models injure cells with equibiaxial stretch, whereas other models apply uniaxial stretch. In this section three noteworthy stretch injury systems are described.

Ellis *et al.* (1995) describe a device that employs a pneumatic pressure pulse to create equibiaxial stretch to cultured cells. Cells were grown on commercially available Flex Plates who's bottoms consisted of a 2mm thick flexible silastic bottom. Injuries are performed through the use of a Cell Injury Controller (Figure 1.2). This device regulates the magnitude and duration of the applied pressure pulse via a valve and timer. The controller has two inlets. One inlet is connected to a tank of compressed air, while the second inlet is connected to an airtight plug that is fitted to the top of a well on the Flex Plate. The user defines the magnitude and duration of the pressure pulse.

An alternative method of inducing stretch injury is described in a study done by Geddes and Cargill (2001). In this model of stretch injury neurons are stretched via cell straining apparatus (CSA). Cells are grown on silicone membrane attached to an aluminum washer. The aluminum washer is attached to a cantilevered translating arm and positioned below an indenter. Equibiaxial stretch was induced by displacing the arm vertically allowing the membrane to stretch over the indenter, (Figure 1.3). A key

difference in this system is that it allows for epifluorescent imaging before, during, and after mechanical injury; an option not available to the Ellis model.

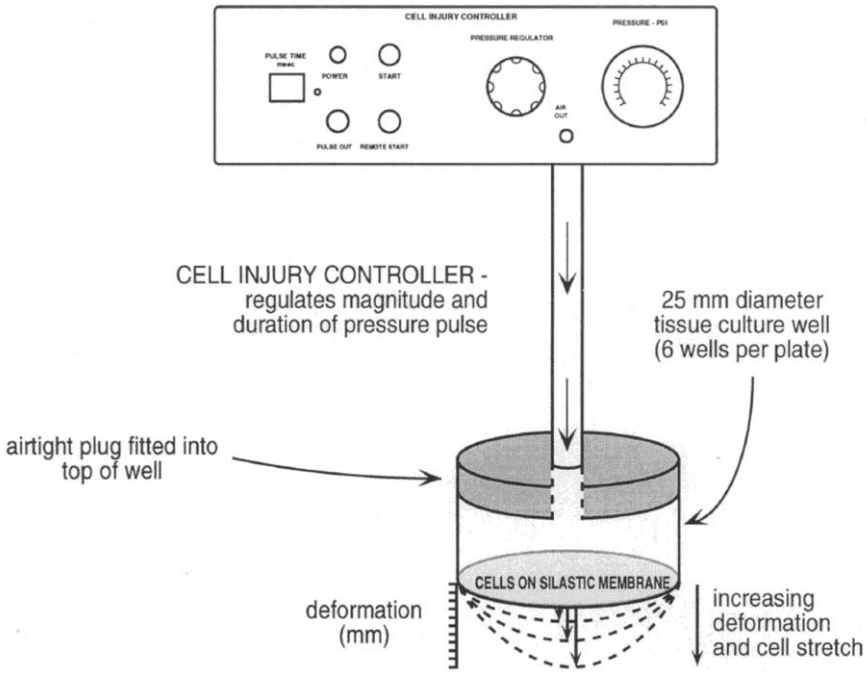


**Figure 1.2** Experimental set-up. Cells grown to confluency on silastic-bottomed tissue culture wells are subjected to a controlled amount of stretch by an air pressure pulse of controlled magnitude and duration. Variations in the pressure pulse produce varying silastic membrane deformation and cell stretch (not drawn to scale), (Ellis *et al.*, 1995).

The model described in Smith *et al.* (1999) is different from the previous models described in two major ways; 1) this model was designed to create uniaxial stretch as opposed to equibiaxial stretch, 2) this model uses a unique plating technique to isolate only axons for injury. Similar to the Ellis model, the Smith model utilizes a pneumatic driven stretch. Cells are plated on silicone substrates in custom designed wells. During plating a clear silicone barrier is placed on the membrane to create an area free of cell bodies. The cells were allowed to attach and the barrier was removed at 24hrs. As the cultures develop this creates and axon rich area of the culture. Culture wells are placed in

a sealed pressure chamber and the axon rich area of the culture was aligned with a rectangular slit plate. This plate restricts the deformation of the membrane creating

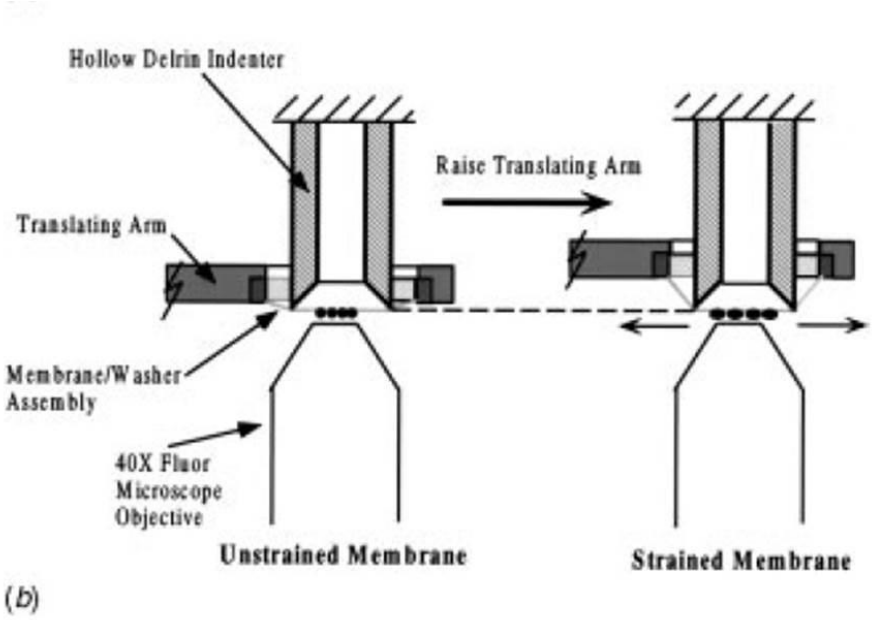


**Figure 1.3** Schematic of the CSA deformation mechanism, the epifluorescence microscope, and the membrane/washer assembly. Cells grown on a silicone membrane are imaged with the inverted epifluorescence microscope. Upon displacement of the translating arm, the membrane is stretched over the fixed, flat circular surface of the Delrin form, resulting in a transfer of strain onto the attached cells. The cells remain in the same focal plane throughout the membrane stretch, as shown by the dotted line. The microscope objective is positioned just below the membrane and images the cells throughout the deformation period, (Geddes, 2001).

uniaxial stretch. Cultures are exposed to a controlled air pulse via a control system similar to the Ellis model. This model included a "viewing window" in the pressure chamber to allow for live imaging.

Each of these models provides a means of studying DAI *in vitro* in real time. However, these models only allow for injury of individual cultures. The need for high throughput methods appears pertinent in TBI research. High throughput methods applied to TBI research would afford researchers the capability to screen for biomarkers, study

mechanisms of therapeutics, and generate large tissues samples for running genomic and protein assays. It is for these reasons that an *in vitro* model of TBI with the capabilities of producing a large number of samples is needed. Concurrently, given the nature of TBI this model

## 1.3 Neuronal Stretch Injury Studies

In this section the work that has been previously done using models of axon stretch injury and discuss their relevance to my research are discussed.

### 1.3.1 Delayed Elastic Response

A study done by Smith *et al.* (1999) showed that shortly after injury, axons have been found to display signs of delayed elastic response in the form of undulations (waves), (Figure 1.4). Undulated axons often times recover over time (~ 45 minutes) and the degree with which axons are undulated is proportional to the degree of injury (Smith *et al.*, 1999).

However, as the axons recover, they develop axonal swellings, (Figure 1.5). Immunohistochemical staining of neurofilament, a fundamental component of axonal cytoskeletal structure, showed that axonal swellings were comprised of large accumulations of neurofilament. It was hypothesized that these axonal swellings signified a deficit in axonal transport. This *in vitro* study presents a morphological changes in axons in response to DAI that are also commonly observed *in vivo* in patients that have experienced traumatic brain injury, (Adams *et al.*, 1989; Povlishock, 1992). Ultimately, this study shows that *in vitro* modeling can be used to observe similar phenomena seen *in vivo*. Data such as those presented in this study are helpful in

identifying future areas of research in DAI that are necessary for beginning to understand the mechanisms that underlie this pathology.

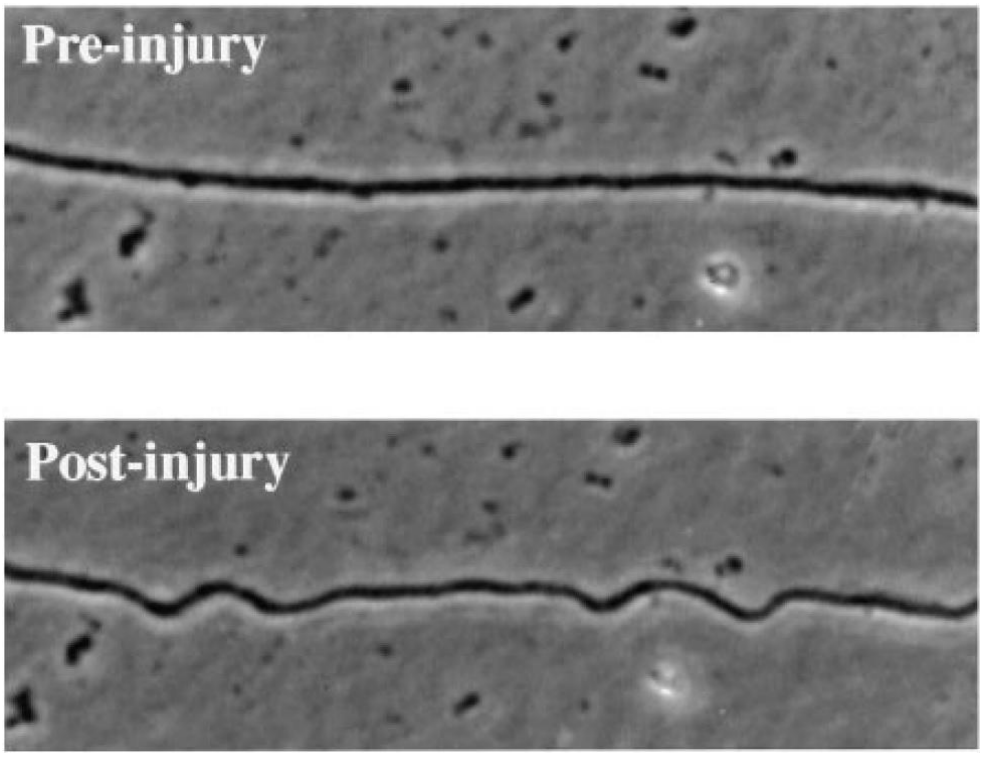


**Figure 1.4** Development of undulations in axons immediately after injury as a result of diffuse axonal injury (DAI) (Smith *et al*., 1999).

### 1.3.2 Studies of Intracellular Free $Ca^{2+}$ Levels Following Stretch Injury

It is well established that intracellular free $Ca^{2+}$ levels are elevated post mechanical injury (Geddes & Cargill, 2001; Wolf *et al.*, 2001; Iwata *et al.*, 2004; Lusardi *et al.*, 2004b; von Reyn *et al.*, 2009). Elevated levels of $[Ca^{2+}]i$ have been suggested to be responsible for secondary injury to axons, such as Wallerian degeneration and activation of deleterious proteases (Smith *et al*., 1999; Iwata *et al*., 2004; von Reyn *et al*.,2009). In the study described in Wolf et al 2001, a variety pharmacological agents were used to explore potential mechanisms for $Ca^{2+}$ entry as a result of stretch injury.

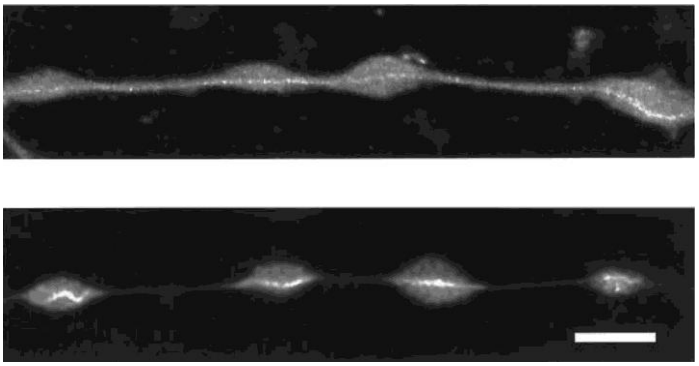

**Figure 1.5** Accumulation of neurofilament in axons by 2 hr after dynamic stretch injury. Confocal (*top*) and deconvolution (*bottom*) microscopy demonstrates multiple swellings along injured axons immunostained to reveal neurofilament protein. Both confocal and deconvolution microscopy reveals what appears to be a central core of neurofilament in the swellings represented by more intense immunostaining. In some of the swellings, this central core appears disturbed from its original orientation with a tortuous course, even though the axons as a whole had returned to their straight preinjury orientation, (Smith *et al.*, 1999).

Experiments were done on N-Tera2 cl/D1 cell line because of their ability to differentiate into neuron-like cells. The following pharmacological agents were used to treat cultures: TTx (voltage gated sodium channel blocker), ω-conotoxin MVIIC (P/Q and N-type voltage gated $Ca^{2+}$ channel blocker), and Bepridil ($Na^{+}$-$Ca^{2+}$ exchanger blocker). In addition to these agents, cells were injured in $Ca^{2+}$ free solution by replacing $CaCl_2$ with $MgCl_2$ as well as a $Na^{+}$ free solution by replacing NaCl with N-methyl-D-glucamine (NMG). Cultures were stained with the fluorescent $Ca^{2+}$ indicator, Fluo-4AM and injured using the model described in Smith *et al.* (1999). Fluorescent imaging was performed before and after injury.

The results showed that cells treated with TTx, 0mM $Ca^{2+}$,and 0mM $Na^{+}$ prior to injury exhibited no significant change in fluorescent $Ca^{2+}$ intensity, whereas untreated cells showed significant increases in $[Ca^{2+}]_i$ intensity after injury. This implied that elevations in $[Ca^{2+}]_i$ post injury were not only governed by $Na^{+}$ entry through voltage gated sodium channels, but also that the main source of $Ca^{2+}$ entry was from the

extracellular space. In the presence of ω-conotoxin and Bepridil, $Ca^{2+}$ entry into stretch injured cells was substantially decreased, suggesting that P/Q and N-type voltage gated $Ca^{2+}$ channels and the $Na^{+}$-$Ca^{2+}$ exchanger are also avenues for intracellular $Ca^{2+}$ entry.

A study described in Iwata *et al.* (2004) examined the secondary effects of elevated $[Ca^{2+}]_i$ levels following injury. It was believed that prolonged elevation of $[Ca^{2+}]_i$ levels due to stretch injury activates proteases. These proteases ultimately cleave the III-IV intracellular loop of the sodium channel (Iwata *et al*., 2004; von Reyn *et al*., 2009). This loop may represent the inactivation gate of the sodium channel, and as such plays a major role in halting $Na^{+}$ flux into the neuron during action potentials. These changes in the sodium channel have been seen as soon as 20 minutes following injury. It has been shown that treatment with TTx prior to injury blocks elevated levels of $[Ca^{2+}]_i$ associated with injury in the N-Tera2 cl/D1 cell line. Since it is believed that elevated $Ca^{2+}$ is responsible for cleavage of the sodium channel's inactivation gate, TTx was used to investigate the possibility of preventing proteolysis of the III-IV loop of the sodium channel.

Neuronal cultures were stained with the fluorescent $Ca^{2+}$ indicator, Fluo-4 and injured using the model described in Smith *et al.* (1999). Fluorescent imaging was performed before and after injury. Neurons were treated with TTx prior to injury.

The results showed that blocking with TTx prior to injury dramatically reduced fluorescent measurements of $[Ca^{2+}]_i$ following stretch injury. Western blot analysis also showed that pretreatment with TTx preserved the integrity of voltage gated sodium channels. In contrast, Western blot analysis of cultures not treated with TTx prior to

injury exhibited shifts to lower weights in the bands that represent voltage gated sodium channels, which may indicate proteolysis of III-IV loop of the sodium channel.

It is indicated by this study that rises in $[Ca^{2+}]_i$ due to stretch injury are mediated by TTx sensitive sodium channels. It was also found that blocking influx of $Ca^{2+}$ into the neuron via blocking sodium channels with TTx, prevents proteolysis of these channels. This work done in this study not only provides an approach to understanding the nature of the progression of DAI, but also the beginnings of understanding the mechanism of this progression.

### 1.3.3 Electrophysiology of Stretch Injured Neurons

*N*-methyl-D-aspartate receptor (NMDA) and the α-amino-3-hydroxy-5-methyl-4-isoxazolepropionic acid receptor (AMPA) are responsible for the primary excitatory currents transmitted at the synapse. These currents promote excitatory post-synaptic potentials (EPSPs) to the post-synaptic membrane; a process that is necessary for signal transduction. Prior research has been aimed at investigating the effects of stretch injury on the function of these receptors and their kinetics.

A mechanical injury system (Ellis *et al.*, 1995), similar to the system described in Chapter 2, has been used to show that there are significant changes in NMDA receptors after injury (Zhang *et al.*, 1996). In this study, NMDA receptors of injured neurons showed a large increase in conductance at hyperpolarized potentials following mechanical injury. This study ultimately concluded that the effect was due to a loss in sensitivity of NMDA receptors to $Mg^{2+}$ block. The study also showed that the ability of $Mg^{2+}$ to block NMDA currents at higher concentrations was severely diminished as well (Zhang *et al.*, 1996).

Another study showed that mechanical injury alters AMPA receptor function (Kao *et al.*, 2004). In this study, injured neurons had significantly larger AMPA induced currents than non-injured neurons. These cells also exhibited larger average steady state current densities and longer decay time constants.

Contrary to AMPA and NMDA receptors, the γ-aminobutyric-acid (GABA) receptor regulates the primary inhibitory current at the synapse. Similarly, research has shown that stretch injury induces changes in $GABA_A$ currents (Kao *et al.*, 2004). Neurons that were exposed to stretch injury have shown dramatic increase in $GABA_A$ potentiation and current density.

### 1.4 Viscoelasticity and the Brain

The brain has often been described as having viscoelastic properties (Margulies *et al.*, 1990; Arbogast *et al.*, 1997; Arbogast & Margulies, 1998; 1999; Smith & Meaney, 2000; Coats & Margulies, 2006). Before one can consider the effects of mechanical perturbations to the brain, one must consider the mechanical properties of viscoelastic materials. When undergoing deformation, viscoelastic materials exhibit properties of both viscous and elastic materials (Palsson & Bhatia, 2004; Callister, 2007). Viscous materials respond to applied stresses in a time-dependant manner, while elastic materials deform instantaneously. In contrast, elastic materials completely recover from applied stresses, while viscous materials do not. Upon loading, viscoelastic materials exhibit instantaneous elastic strain followed by time-dependant strain response, which is largely recoverable over long periods of time.

The behavior of viscoelastic materials is largely dependent on time and temperature. Stress relaxation is a type of measurement that is used to quantify this type

of behavior. This is done by subjecting a specimen to a predetermined amount of strain and measuring the amount of stress needed to maintain that strain level. At constant temperatures, stress is found to decrease as a function of time. This result is due to relation in the molecular structure of viscolelastic polymers and is often referred to as the relaxation modulus of a material (Callister, 2007). The relaxation modulus of a material can be defined as:

$$E_r(t) = \frac{\sigma(t)}{\varepsilon_0} \tag{1.1}$$

where $\sigma(t)$ is the measured time-dependent stress and $\varepsilon_0$ is the predetermined applied strain. The relaxation modulus also represents the temperature dependent properties of viscoelastic materials. With changes in temperature, the $E_r$ of viscoelastic materials can vary from glassy, rubbery, or viscous. Increases in temperature cause a reduction in $E_r$ and allowing viscoelastic materials to become more ductile and behave as rubbery or viscous materials. In contrast, as temperature is reduced, $E_r$ is increased, causing viscoelastic materials to become brittle and glassy (Callister, 2007).

These changes in elastic modulus are also dependent on the rate of deformation, also known as strain rate. Simply put, strain rate is the rate of change in strain of a material with respect to time. Viscoelastic materials subjected to slow deformations behave as if they have a low elastic modulus, allowing them to withstand large strains. In contrast, high strain rates cause viscoelastic materials to behave as if they have a high elastic modulus, making them brittle and glassy. In addition, by increasing the rate of deformation, larger forces are translated to the material. Because these forces are

generated at such a high rate, the material cannot accommodate to the imposed strain, thus making these forces damaging to the material.

Consideration of these material properties is crucial for understanding the complex nature of DAI. Review of the literature shows that the mechanical forces and physiological responses underlying DAI are complex and there is still much research that needs to be performed. One aspect of DAI that has yet to be fully investigate is strain rate. However, if one considers the viscoelastic properties of the brain, it becomes evident that strain rate may play just as an important role as strain in the pathology of DAI.

*In-situ* models have been used to study the biomechanics of DAI. One such model (Meaney *et al*., 1995) utilized a cleaned and emptied porcine skull filled with silicone gel, a viscoelastic material that acted as a surrogate for brain tissue (Meaney *et al*., 1995). An orthogonal grid was positioned within the skull between two layers of gel. The skull was then secured in an aluminum can fitted with a cover plate and o-ring (Figure 1.6). The aluminum can was fitted to an apparatus designed to apply rotational acceleration/deceleration to the brain tissue surrogate.

High-speed video (1000 frames/s) was taken to capture the distortion of the orthogonal grid during rotational acceleration/deceleration (Figure 1.7). This data was used to analyze the biomechanical response of the brain tissue surrogate during rotational acceleration/deceleration. The data in this paper was referenced in a recent doctoral dissertation on the topic of axonal injury (Pfister, 2001). In this dissertation, the author calculates strain rate based on the data presented in (Meaney *et al*., 1995) and reports

strain rates upwards of $52s^{-1}$. Most studies propose injuries with strain rates ranging from $20\text{-}35s^{-1}$ (Smith *et al*., 1999; Wolf *et al*., 2001; Iwata *et al*., 2004). In light of this data,

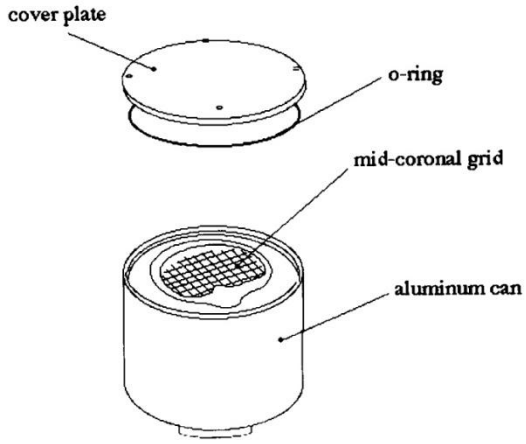


**Figure 1.6** Illustration of the physical model used in this study. A clean, dried porcine skull was embedded within an aluminum can and filled with a silicone gel that acted as a surrogate for brain tissue. An orthogonal grid placed between two gel layers was used to estimate the mechanical response of the brain surrogate to a coronal plane, rotational acceleration (Meaney *et al*., 1995).

the proposed strain rates of modern *in vitro* studies seem low when compared with strain implied in the discussed *in-situ* study.

If the brain is to be considered as a viscoelastic material, then its responses to mechanical forces must be also considered as viscoelastic. With these point considered, it is the central hypothesis of this dissertation to understand the implications of strain rate on injured neurons. This will be done using *in vitro* modeling and in consideration of the strain rates proposed implied in (Meaney *et al*., 1995). In order to investigate the effects of strain rates, a stretch injury system that can independently, accurately, and reliably control strain and strain rate must be designed. This system must also be designed with the capability to explore strain rates greater than $52s^{-1}$.

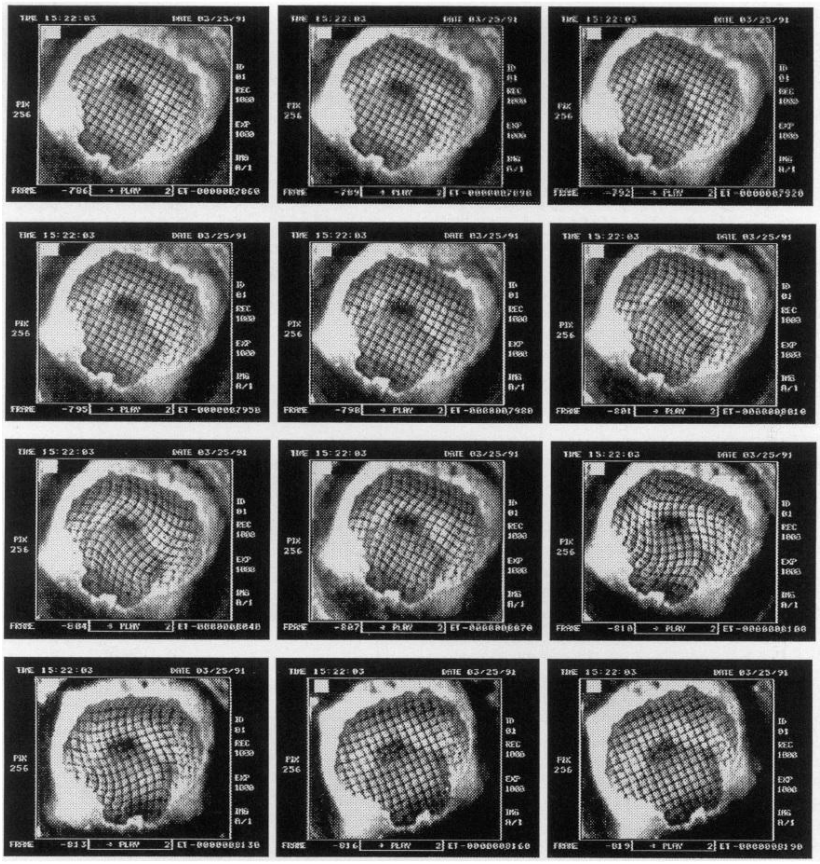

**Figure 1.7** High-speed video (1000 frames/s) captured the distortion of the grid within the physical model in response to a biphasic rotational acceleration/deceleration. Analysis of a consecutive series of grid frames allowed for the calculation of strain throughout the grid plane of the physical model (Meaney *et al*., 1995).

# CHAPTER 2

# ENGINEERING A HIGH THROUGHPUT STRETCH INJURY SYSTEM

## 2.1 Background and Significance

DAI is microscopic, commonly present without evidence of macroscopic tissue damage, and can only be identified post-mortem in humans and animals using histological methods, (Adams *et al.*, 1989; Graham *et al.*, 1993; Smith & Meaney, 2000). Likewise, injury-induced functional alterations due to subcellular changes must also be explored ex vivo (Santhakumar *et al.*, 2001; Cohen *et al.*, 2007). To study the progression of traumatic axonal injury, the relationship between mechanical deformation and the evolution of structural and functional alterations of the neuron needs to be investigated, a difficult task using any type of animal model. On the other hand, *in vitro* models offer the advantage of studying injury dynamics in real time, making it easier to explore biomechanical and biological factors involved in the progression of axonal pathology. Importantly, the mechanisms identified from *in vitro* modeling represent an important first step that can be used for further study and verification in animal models.

Biomedical engineers have been instrumental in building laboratory models to gain understanding of the characteristics of a TBI. In particular, several *in vitro* injury models have been developed that apply mechanical perturbations to cultured neurons,(Galbraith *et al.*, 1993; Ellis *et al.*, 1995; Cargill & Thibault, 1996; LaPlaca & Thibault, 1997; Morrison *et al.*, 1998b; Smith *et al.*, 1999; Pfister, 2001; Lusardi *et al.*, 2004a; LaPlaca *et al.*, 2005). These models have been in use for many years and replicate many of the morphological and ultrastructural changes observed *in vivo*, such as

alterations in neurofilament structure and membrane permeability (Meaney *et al.*, 1998; Morrison *et al.*, 1998b; Smith *et al.*, 1999; Smith & Meaney, 2000; Geddes & Cargill, 2001; Geddes *et al.*, 2003a; Geddes *et al.*, 2003b; Lusardi *et al.*, 2003; Lusardi *et al.*, 2004a; Lusardi *et al.*, 2004b; LaPlaca *et al.*, 2005). *In vitro* modeling has had significant impact in the field by identifying many important post-injury biological processes in neurons including an immediate rise the $[Ca^{2+}]_i$ levels, protease activation, electrophysiogical alterations, and changes in ion homeostasis (Galbraith *et al.*, 1993; Tavalin *et al.*, 1995; Gallant & Galbraith, 1997; Tavalin *et al.*, 1997; LaPlaca & Thibault, 1998; Rzigalinski *et al.*, 1998; Geddes *et al.*, 2003a; Lusardi *et al.*, 2003; Iwata *et al.*, 2004; Kao *et al.*, 2004; Lusardi *et al.*, 2004b; Pfister *et al.*, 2004; LaPlaca *et al.*, 2005; Prado *et al.*, 2005; Morrison *et al.*, 2006; Cohen *et al.*, 2007; Spaethling *et al.*, 2008; Miller *et al.*, 2009; von Reyn *et al.*, 2009; Yuen *et al.*, 2009).

*In vitro* modeling of mechanical injury to neuronal cultures is based on the experimentation of single custom designed cultures, one-by-one. Often, productivity is slow and extensive experience is required to gain consistent results. Consequently, pharmaceutical and neuroscience research environments can view TBI research as an expensive and low-yield effort that can only be accomplished through animal models. The discovery of biological mechanisms and treatments for many diseases has been accelerated with the use of high throughput tissue culture techniques. They are cost effective and provide an efficient method for investigating cellular and molecular alterations in real time or screening for biomarkers and potential therapies. Accordingly, a next big step for *in vitro* TBI models is to provide the similar efficiency and throughput the multi-well plate brought to tissue culture experimentation.

Here, a modular, multi-well high throughput *in vitro* axon injury system was engineered with the aim of accelerating the study of TBI mechanisms. The premise of the design was based on the technique of a well established *in vitro* stretch injury device (Smith *et al.*, 1999; Wolf *et al.*, 2001; Iwata *et al.*, 2004; Lusardi *et al.*, 2004a; Chen *et al.*, 2009). In particular, this technique was selected based on its ability to injure isolated tracks of axons to study the direct effect of mechanical stretch on the evolution of axonal pathology (Smith *et al.*, 1999). The injury format of this single specimen device was expanded to create a 24 well plate for protein analysis and biochemical assays and a 6 dish system for experiments requiring individual and time course measurements. The engineering goals for this study were to design and build a system with the capability to rapidly screen for biomarkers and potential interventions, study mechanisms of therapeutics, and generate large tissue samples often necessary for proteomic and genomic analyses. In addition, this system was designed to be automatic and not require a high level of expertise to operate.

## 2.2 Materials and Methods

### 2.2.1 Description of *In Vitro* Neuronal Stretch Injury Model

The neuronal stretch injury model consists of culturing neurons on a thin elastic silicone membrane, which is then rapidly deformed by applying a pressure-pulse to the substrate, distending the membrane like a balloon. Since neuronal cultures adhere tightly to the silicone substrate, they deform with the membrane, (Figure 2.1, A) (Morrison *et al.*, 1998b; Smith & Meaney, 2000; Cohen *et al.*, 2007). The biomechanics of head injury has shown that injurious head rotations cause macroscopic shear deformation of brain tissue

(Margulies *et al.*, 1990; Meaney *et al.*, 1995). This translates microscopically to rapid uniaxial stretching or compression of axon fibers (Smith & Meaney, 2000; Pfister *et al.*, 2003). By placing a rigid mask under the membrane, the silicone can be restricted to deform only within a long rectangular opening to create a uniaxial stretch (Smith *et al.*, 1999; Lusardi *et al.*, 2004a), (Figure 2.1, C).

The stretch of neuronal cultures has been reported in terms of strain, which is defined as the ratio of the total deformation of a given body to its original form or configuration (i.e. membrane strain of 30% denotes that membrane has been deformed 30% relative to its original conformation). The rate of injury is measured in terms of strain rate, which is the rate at which a specified strain is delivered to neuronal cultures, (i.e. 30% strain delivered over a period of 10msec is reported as a strain rate of $30s^{-1}$). The damaging deformations to brain tissue during a TBI event are rapid (Margulies *et al.*, 1985; Margulies *et al.*, 1990; Meaney & Thibault, 1990; Margulies & Thibault, 1992; Meaney *et al.*, 1993; Meaney *et al.*, 1995). *In vitro*, axons are injured on the order of > 50-60% strain at strain rates measuring up to $25\text{-}30s^{-1}$. The pressure pulse generally used to model this level of TBI is typically 7psi delivered in 20msec (Smith *et al.*, 1999; Wolf *et al.*, 2001; Lusardi *et al.*, 2003).

### 2.2.2 System Overview

The injury system created in this study consisted of four components: A) a control system run via a LabVIEW (National Instruments, Austin, Texas) interface, B) an input pressure regulation system, C) a valve control system, and D) a modular injury chamber equipped with pressure sensor, (Figure 2.2). Control System: The pressure pulse parameters were controlled via the LabVIEW computer interface. Here, the user set the input reserve tank

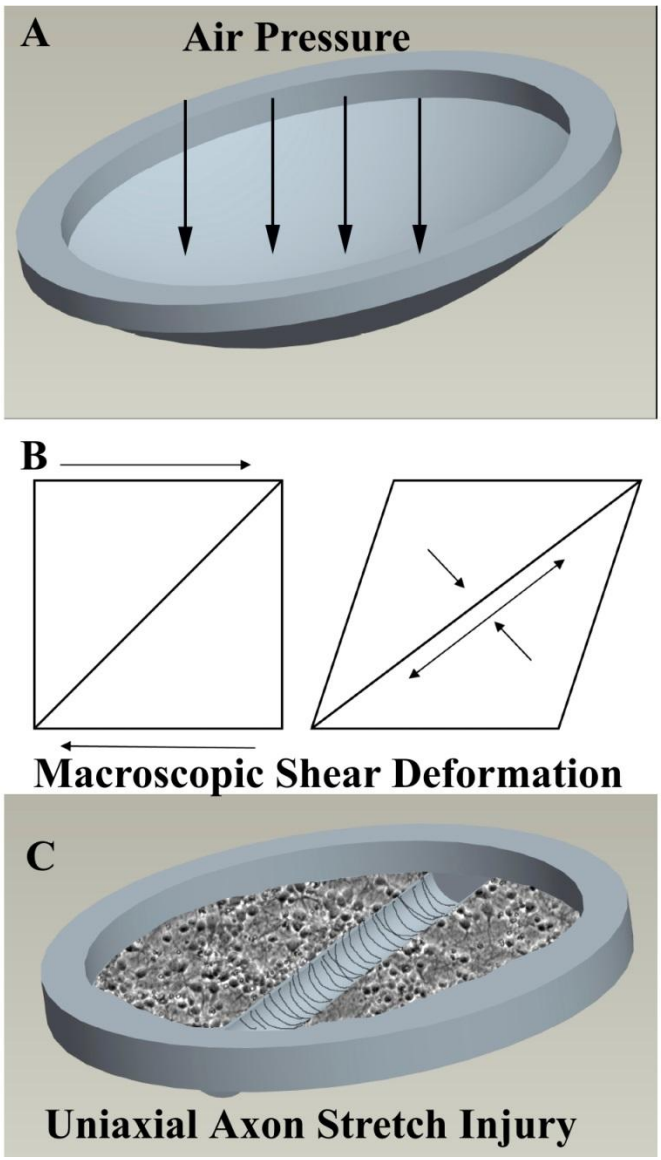


**Figure 2.1** Principles of stretch injury. (A) An equibiaxial stretch. Air pressure is used to deform an elastic silicone membrane. (B) A representative block of brain tissue under shear deformation translating into a uniaxial stretch of axon fibers along the diagonal. Likewise, compression occurs perpendicular to the diagonal. (C) Uniaxially stretched axons spanning a cell-free zone between two populations of cortical neurons.

pressure and timing of the valve based on the type of injury desired. Input Pressure Regulation: An electronic pressure controller (VSO-EP, Parker Hannifin, Life Sciences, Hollis, NH) regulated the user set input pressure (ranging from 0-100psi) from a main compressed air tank into a secondary reserve tank. The VSO monitored the pressure in the secondary reserve tank until it reached the user set input pressure. As a safety precaution, a mechanical blow-off valve of 150psi prevented damage to the VSO. Valve Control: Once the desired pressure was reached, the control system signaled the valve driver circuit (OEM, Parker Hannifin). The valve driver circuit controlled the opening and closing of the valve based on the user set valve timing signal from the LabView interface. The valve was a three-way, normally closed, fast acting solenoid valve, connecting the secondary reserve tank to the injury chamber to deliver a controlled pressure pulse to the neuronal cultures. Key elements of the fast acting solenoid valve were the large orifice size (0.116") and fast response time (2-3ms), which allow for precise control of the pressure pulse. Modular Injury Chamber: The injury chamber pressure was monitored and recorded using an EPX-V01-25P Pressure Sensor (Measurement Specialties, Les Clayes-sous-Bois, France, 2.076mV/psi sensitivity). The pressure sensor was coupled with a transducer amplifier (IAM, Measurement Specialties, gain of 201.8) to amplify the signal voltage to 0-10V. The pressure pulse waveform readout was recorded in the LabVIEW interface and saved to a Microsoft Excel spreadsheet.

The system was designed to be modular, giving the user two options when performing injury experiments. There were two major points that make this system modular: 1) the design of two distinct tissue culture vessels and 2) the design of two

injury chambers that were complimentary to each tissue culture vessel, (Figure 2.3). For high-throughput experiments, the 24-well module would be used, featuring a custom made 24-well tissue culture plate. However, if the study required a smaller number of samples, 6-well module featuring individual wells for tissue culture would be chosen.

### 2.2.3 6-well Stretch Injury Module

The 6-well module incorporated individual wells so that the user could injure as many as 6 samples at once, (Figure 2.3, A). The independent wells could be convenient for single sample studies such as electrophysiology and time-lapse $Ca^{2+}$ imaging. Based on an existing method, uniaxial stretch of neuronal cultures was accomplished by using a mask that restricted the deformation of the silastic membrane within a rectangular slit (Smith *et al.*, 1999). Here, deformation masks for the 6-well module were designed using ProEngineer software (PTC, Needham, MA) and fabricated out of ABS (acrylonitrile butadiene styrene) plastic using a 3-dimensional rapid prototyping system (SST 1200es, Dimension, Inc., Eden Prairie, MN). For injuring isolated axons, the mask aligned precisely with a cell free zone spanned by axons (described below). The masks for the 6-well module incorporated either a 1.5mm or 2.00mm slit. Solid masks were also created to act as a sham to injured cultures. Prior to stretch injury, deformation masks were attached to the underside of culture wells and placed in the injury chamber.

### 2.2.4 Preparation and Assembly

To prepare the injury wells for cell culture, the PEEK rings were washed thoroughly using Sparkleen (Fisher Scientific Co.) laboratory detergent and sonicated if rigorous cleaning was necessary. The PEEK rings were then thoroughly rinsed

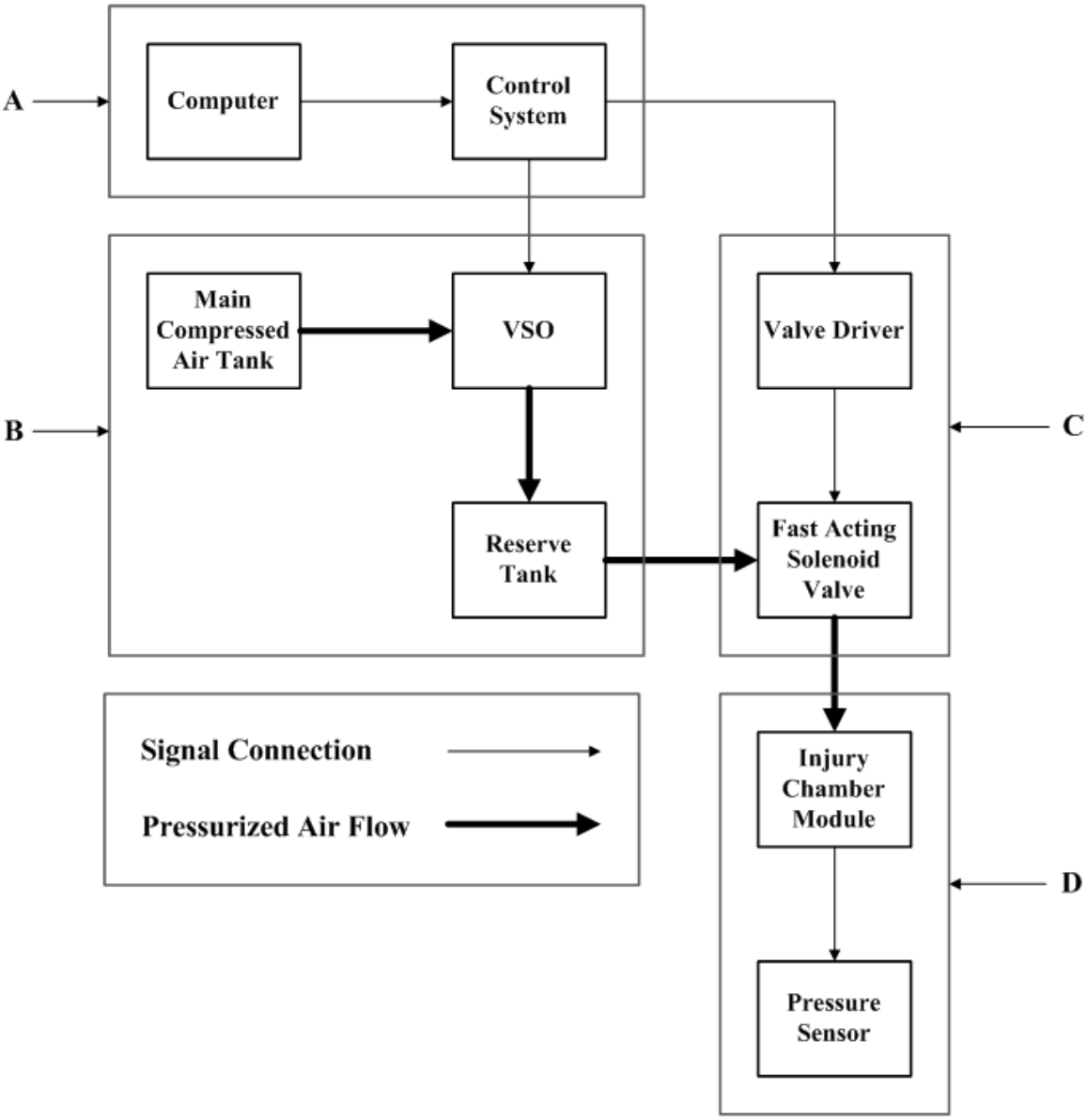


**Figure 2.2** Schematic of the injury system displaying both air and electrical connections. (A) Control system runs via LabVIEW interface. Outputs control the pressure pulse valve and input pressure; inputs monitor input pressure and injury chamber pressure. (B) Input pressure regulation system. The computer signals the VSO pressure regulator to set the pressure in the reserve tank while the measured pressure is sent back to the computer for monitoring. The air flows from a compressed air tank, through the VSO regulator to the reserve tank. (C) Valve control system to deliver the injury pressure pulse. The computer signals the valve driver to open and close the valve, allowing air to flow from the reserve tank to the injury chamber. (D) Modular injury chamber. The chamber pressure is monitored with a pressure sensor, which is recorded by the computer.

using reverse osmosis (RO) water. The silicone membrane (0.005" Gloss/Gloss silicone sheeting Specialty Manufacturing, Saginaw, MI) was cut into 1.5 x 1.5cm squares, briefly rinsed with RO water, and dried on lint free Kimwipes.

The well design allowed for rapid assembly by press-fitting two concentric PEEK rings together. The smaller of the PEEK rings contains a groove for the insertion of an O-ring. This O-ring served three purposes: 1) it applied pre-stretch to the silicone membrane, 2) it held the well together, and 3) it acted as a gasket to prevent media leakage. A square of silicone membrane was placed flat over the larger ring, wrinkles in the membrane were straightened and the smaller ring was gently pressed into the larger. The circular geometry ensured that the membrane was pre-stretched equibiaxially and uniformly throughout the well (Lee *et al.*, 1996; Sotoudeh *et al.*, 1998). Close examination of the substrate pre-stretch from assembly of the wells (method below) produced average radial strains of 7.03%±0.95% with little shear 0.5%±0.19%. Completed wells were filled with RO water and steam autoclaved for 1 hour.

### 2.2.5 24-well Stretch Injury Module

The 24-well module consisted of a one piece tissue culture plate made from PEEK that was designed to match the dimensions of commercially available 24-well tissue culture plates. The plate was designed without a bottom to allow for attaching a silicone membrane as the substrate. For uniaxial stretch injury, a one-piece mask that self-aligns under the 24 well injury plate was created. The deformation mask was made from a 1mm thick sheet of stainless steel and was designed to align a 1.5mm slit across the center of each well, (Figure 2.3, A). To provide sham controls on the plate, laboratory tape was used to cover the slits of select wells.

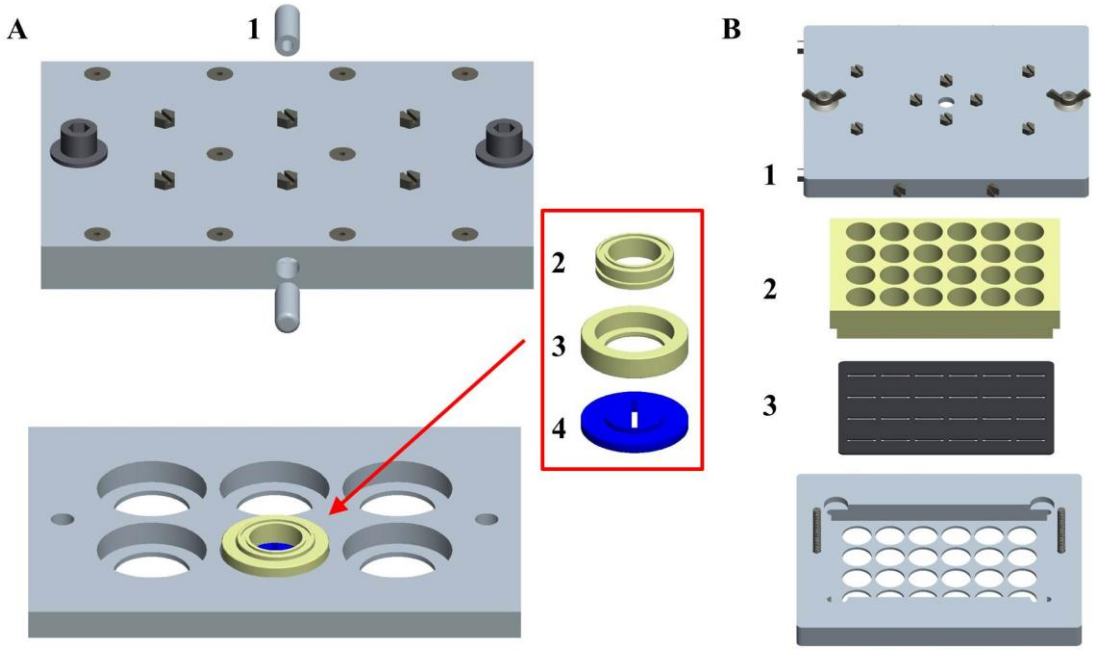


| | Module A (6-well) | Module B (24-well) |
|---|---|---|
| **1** | Pressure inlet | Pressure inlet |
| **2** | 6-well vessel (top ring) | 24-well plate |
| **3** | 6-well vessel (bottom ring) | Deformation mask |
| **4** | Deformation mask | - |

**Figure 2.3** Injury system modules. CAD drawings of the 6-well pressure chamber with individually removable wells and deformation masks (A), and the 24-well pressure chamber with 24-well tissue culture plate and deformation mask (B).

### 2.2.6 Preparation and Assembly

Each 24-well PEEK plate was lightly abraded with 100-grit sandpaper on the underside to enhance adhesion of the silicone membrane. The PEEK plate was then washed thoroughly using Sparkleen (Fisher Scientific Co.) laboratory detergent and then thoroughly rinsed using RO water. A silicone membrane (0.005 inch Gloss/Gloss silicone sheeting Specialty Manufacturing, Saginaw, MI) was cut to 15.25x15.25cm, briefly rinsed with RO water and allowed to dry.

A device was created to uniformly pre-stretch and hold the membrane prior to gluing to the PEEK plate. The membrane was sandwiched in between a two-piece Plexiglas frame, removing any wrinkles. The framed square of membrane was then stretched over a block of high-density polyethylene (HDPE) and held in place with small clamps. Close examination of the substrate pre-stretch indicated a pre-stretch of 4.92%±1.78% in the X direction, 6.22%±1.82% in the Y direction with little shear 0.68%±0.28%. The membrane pre-stretch was uniform across the membrane with exception of the corners of the stretched sheet, which were kept sufficiently away from the 24-well plate during gluing. RTV Sealant (Dow Corning #732) was applied to the bottom of the 24-well PEEK plate with a small roller to achieve uniform coating. The PEEK plate was then placed over the pre-stretched silicone membrane and cured overnight. To maximize membrane adhesion, a heavy weight was applied to the top of the plate during gluing.

### 2.2.7 Neuronal Culture

After autoclaving, all PEEK tissue culture plates and wells were allowed to dry and cool to room temperature in a sterile tissue culture hood. Silicone substrates were then coated with poly-L-lysine solution (0.05mg/mL, PLL, Peptides International, Louisville, KY). Coated wells were allowed to incubate at 37°C overnight to allow for maximal PLL adsorption. Afterwards, PLL solution was aspirated and wells were rinsed three times with RO water.

Cortices were isolated from E17 Sprague-Dawley rats and stored in ice cold HBSS containing $Ca^{2+}$ and $Mg^{2+}$. Before dissociation, cortices were rinsed in $Ca^{2+}$ and $Mg^{2+}$ free HBSS. Following rinsing, neuronal tissue was digested for 25 minutes at 37°C in 0.25% trypsin containing EDTA (0.2 g/L) and DNase I (1.5 mg/mL). Trypsin was removed and deactivated by rinsing neuronal tissue with a solution of 10% fetal bovine serum prepared in $Ca^{2+}$ and $Mg^{2+}$ free HBSS. Following trypsin deactivation, neuronal tissue was triturated and centrifuged at 3000 RPM for 3 minutes. Supernatant was removed and the pellet was resuspended in NeuroBasal media containing 2% B-27, 1% penicillin-streptomycin, and 0.4mM L-glutamine. The cell containing solution was filtered with a Nylon mesh basket to remove large pieces of tissue. Filtering was performed using a 100µm pore sized filter followed by a 50µm pore sized filter. A 100µL sample of filtered cell suspension was diluted in 900µL of Trypan blue and counted. Cells were plated at an average density of 175,000 cells/cm2 onto elastic membranes treated with 0.14 mg/mL poly-L-lysine.

Neuronal cultures were maintained at 37°C (5% CO2) in NeuroBasal media containing 2% B-27, 1% penicillin-streptomycin and 0.4mM L-glutamine. Cultures were fed at 24 hours and every two days thereafter.

### 2.2.8 Isolated Axons for Stretch Injury

An existing method was used to create a cell free zone to isolate axons for stretch injury (Smith *et al.*, 1999). Here, a plating insert was designed to create a 1.5-2 mm region free of cell bodies that precisely aligns with the underlying deformation mask. Plating inserts were molded out of polydimethylsiloxane elastomer (PDMS NuSil Technology LLC, Carpinteria, CA). Molds were designed on ProEngineer (PTC, Needham, MA) and created out of Acrylonitrile butadiene styrene (ABS) plastic using a 3-dimensional rapid prototyping system (SST 1200es, Dimension, Inc., Eden Prairie, MN). The cell-plating fixture covers the silicone substrate and prevents plated neurons from adhering to the cell free region. Once the cells had properly adhered to the substrate (~ 24hr after plating), plating inserts were removed. Cultures were grown for 10 days to allow sufficient time for axons to traverse the cell free zone.

### 2.2.9 Neuronal Viability Assay

At DIV10 the viability of injured and non-injured cultures was assessed. At 24 hours post injury, cultures were treated for 20 minutes at 37°C with membrane permeable acridine orange (5µg/mL, stains all DNA) and membrane impermeable propidium iodide (5µg/mL, stains DNA of dead cells only) in phosphate buffered saline (PBS) solution. After staining, cultures were rinsed with PBS and imaged using a Nikon TS2000E. Viability was calculated by counting the total number of cells stained with acridine

orange ($N_t$) and the total number of non-viable cells stained with propidium iodide ($N_n$). Using the equation:

$$\%\, Viability = \frac{N_t - N_n}{N_t} \times 100\% \tag{2.1}$$

### 2.2.10 Device Characterization

**2.2.10.1 Defining the Pre-stretch of the Silicone Membrane.** A vector analysis of the strain and shear stress was done for both modules to test for excessive or uneven pre-stretch in the membrane during assembly using a previously described method (Pfister *et al.*, 2003). A grid was drawn on the silicone membrane and three points were chosen. Pictures of these three points were taken before (no pre-stretch) and after (pre-stretched) assembly for each module. From the three points two vectors, $dX^{(1)}$ and $dX^{(2)}$, were defined. These vectors represent the membrane before assembly, without any pre-stretch. Then two vectors were defined to describe the membrane with pre-stretch: $dx^{(1)}$ and $dx^{(2)}$. From this the deformation gradient tensor, F, could be defined such that:

$$dx^{(1)} = FdX^{(1)}, dx^{(2)} = FdX^{(2)} \tag{2.2}$$

From this **F** is defined as:

$$F = \left(dx^{(1)} \middle| dx^{(2)}\right)\left(dX^{(1)} \middle| dX^{(2)}\right)^{-1} \quad (2.3)$$

From this the Cauchy-Green deformation tensor:

$$C = F^T F \quad (2.4)$$

Finally, using the deformation the Lagrangian finite strain tensor was derived:

$$E = \frac{(C - I)}{2} \quad (2.5)$$

The diagonal terms of tensor E provides strain information in the x, y directions as well as information on shear stresses in the off diagonal terms.

**2.2.10.2 Deformation of the Substrate.** Polystyrene fluorescent beads (Invitrogen) were used to measure the deformation of the silicone membrane, using a previously established protocol (Pfister *et al.*, 2003). Briefly, beads were diluted to $10^3$ beads/mL from stock solution in RO water and allowed to adhere to the silicone for 2-3 hours. Wells were rinsed to remove non-adherent beads and allowed to dry. A picture of the adherent beads was taken in the undeformed state (0psi). The chamber pressure was

increased incrementally (1-15psi) and pictures were taken of the membrane in its deformed state. Pressures were recorded using an EPX-V01-25P Pressure Sensor (Measurement Specialties, Les Clayes-sous-Bois, France).

All measurements were done using deformation masks to create a uniaxial deformation. The strain tensor E (above) verified that membrane stretch under the influence of a deformation mask is indeed uniaxial. Since the stretch in each well is considered to be uniaxial as a result of the deformation mask, strain was calculated using the equation:

$$\% \, Strain = \frac{l_f - l_0}{l_0} \times 100\% \tag{2.6}$$

Pairs of fluorescent beads were selected for measurement based on two factors: 1) pairs must be aligned within 5° of the stretch direction [where Cosine (5°) ≈ 1] as to not affect linear measurement and 2) ability to visualize the bead pair throughout the entire sequence of images. Using image analysis in Matlab (MathWorks, Inc., Natick, MA), a pair of beads in a well was chosen. The distance between the selected pair of beads was measured in the undeformed state in terms of relative number of pixels ($l_0$). This measurement was repeated for the same pair of beads for pictures of the membrane in its deformed state ($l_f$).

## 2.3 Results

### 2.3.1 Uniform Pressure

Injury to axons was delivered by a pneumatic pressure pulse; therefore control of the injury was as accurate as the control of the pressure pulse. In this high throughput system, the pressure chamber has larger dimensions and volume than the commonly used single well designs in the literature. Therefore, delivery of the pressure pulse was examined throughout the chamber to ensure uniform injury to all wells.

For the 24-well module, an input pressure of 40psi was programmed into the control system with valve timing of 20ms. The pressure pulse was delivered to the pressure chamber and recorded by the pressure transducer at nine distinct locations located along the top plate of the pressure chamber, (Figure 2.3, B). Analysis of the pressure pulse waveforms gave mean (±standard deviation) rise times of 14.89±0.33ms, peak pressures of 3.45±0.08psi, and decays of 59.89±1.17ms.

For the 6-well module, an input pressure of 30psi was programmed into the control system with valve timing of 20ms. The pressure pulse was delivered to the pressure chamber and recorded by the pressure transducer above each of the six wells, (Figure 2.3, A). Pressure pulse rise times were 14.17±0.41ms, peak pressures were 13.16±0.26psi, and decays were 21±0.00ms. The low standard deviation in the data for both modules indicated that pressure pulses are distributed evenly throughout each well in the pressure chambers.

### 2.3.2 Pressure Pulse Delivery

The amount of time the valve was open (valve timing) controls the flow of pressurized air from the reserve tank to the pressure chamber. Accordingly, the peak pressure reached in

the pressure chamber was directly affected by valve timing. The 6-well module was programmed with an input pressure of 30psi. Pressure pulses were delivered at valve timings of 10, 15, and 20ms, (Figure 2.4, A). The 24-well module was programmed with an input pressure of 80psi. Pressure pulses were delivered at valve timings of 5, 10, 15, and 20ms (Figure 2.4, C). The valve timing was found to have no the affect on the slope of the rising phase, but linearly affects the peak pressure achieved in the injury chamber.

On the other hand, input pressure controlled the slope of the pressure pulse. Using the 6-well module, the valve timing was programmed for 10ms. Input pressures ranging from 20-70psi were tested to look at the relationship between reserve pressure and peak pressure (Figure 2.4, B). The same protocol was followed for the 24-well module, but with a valve timing of 10ms, (Figure 2.4, D). The input pressure was found to be directly related to the slope of the rising phase as well as the peak pressure.

To assist the user with choosing the correct input pressure and valve open time, the pressure dynamics of each module was mapped for different combinations of valve timings and input pressures, (Figure 2.5). Input pressure was set to 20 psi and pressure pulse data was recorded for four valve timings: 5, 10, 15, and 20 ms. This was repeated for input pressures of 30, 40, 50, 60, 70 and 80 psi.

### 2.3.3 Silicone Membrane Deformation

The pressure-deformation relationship of the membrane was measured by deforming the membrane uniaxially using the deformation mask, (Figure 2.1, C). A region in the center

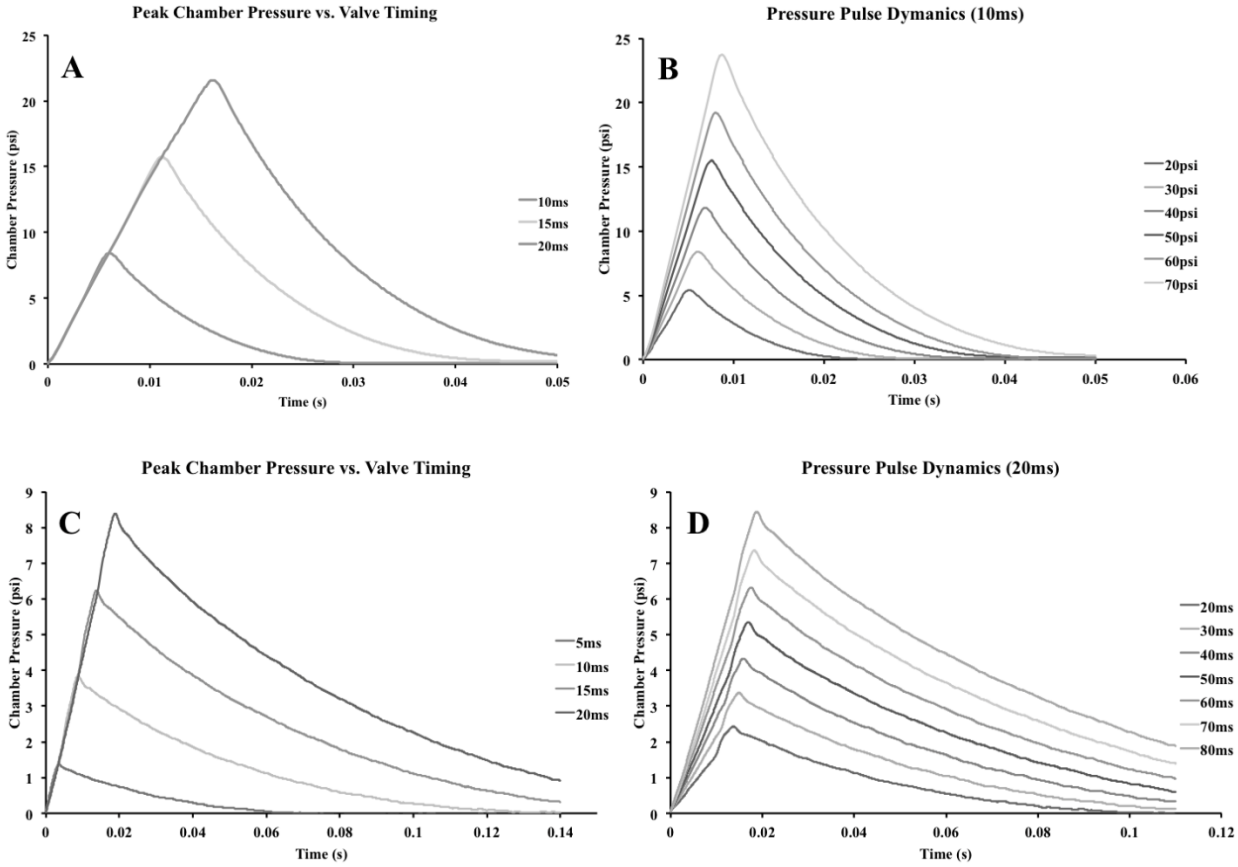


**Figure 2.4** Pressure pulse dynamics. (A) 6-well module pressure pulse traces at a constant input pressure of 30 psi. (B) 6-well module pressure pulse traces at a constant valve open time of 10 msec. (C) 24-well module pressure pulse traces at a constant input pressure of 80 psi. (D) 24-well module pressure pulse traces at a constant valve open time of 20 msec.

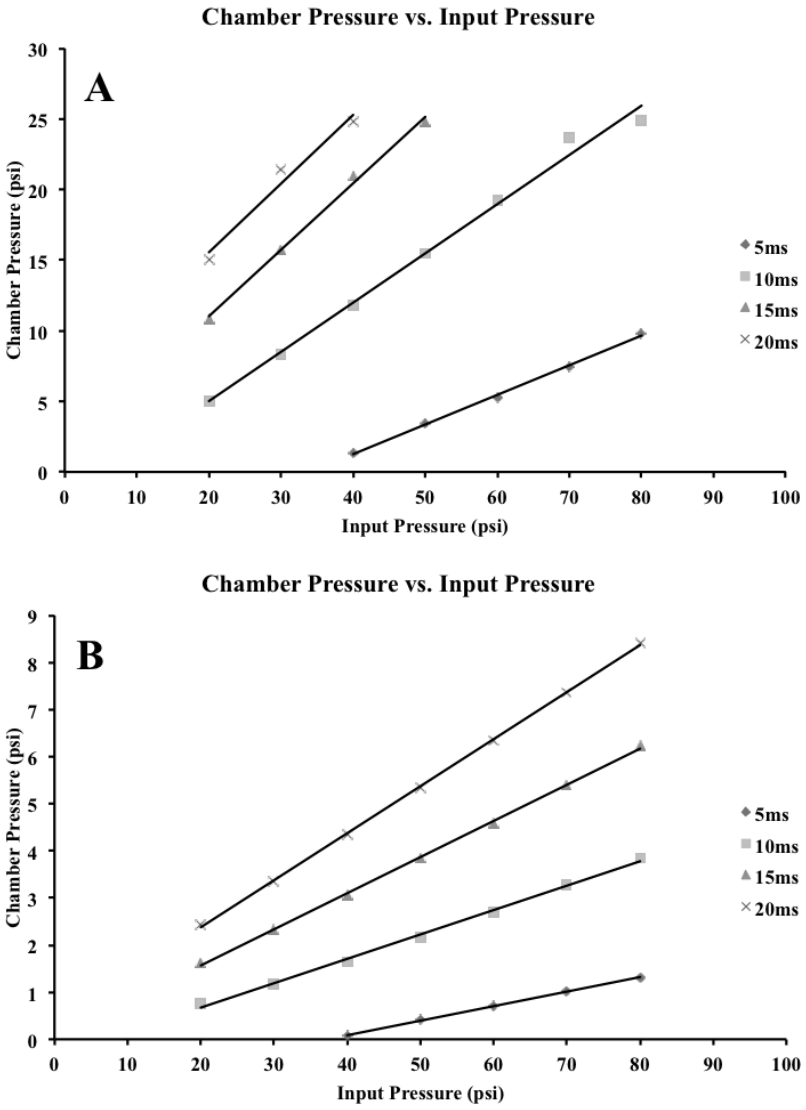


**Figure 2.5** Modular performance characterization maps. Each line represents the relationship between input pressure and peak chamber pressure at valve timings of 5, 10, 15, and 20 msec. (A) The 6-well module; (B) the 24-well module. User may use this map along with substrate deformation data to determine what parameters must be set to achieve desired injury levels.

of the membrane was randomly chosen for imaging. Beads were imaged in each well under static pressures of 0, 3, 6, 10 and 15 psi. Uniaxial substrate strain was calculated in all wells for the 6-well module (n=18) and 24-well module (n=72) and averaged over three trials, Table 2.1. The results displayed a linear behavior in both modules within the deformation ranges needed to replicate axon stretch injury, (Figure 2.6).

The 6-well and 24-well modules performed similarly using the 1.5mm mask, reaching 46.73% and 50.02% respectively. To study the effect of mask slit width on substrate deformation, 1.5mm and 2mm widths were tested in the 6-well module. As anticipated, a larger slit width required lower pressures to achieve the same level of deformation, where at 15psi, the 1.5mm mask produces 46.73% strain the 2.0mm produced a strain of 65.05%, (Table 2.1).

**Table 2.1** Mean pressure-deformation results for both modules using a 0.005" membrane and two deformation masks.

| Pressure | 6-well (1.5 mm mask) | 6-well (2 mm mask) | 24-well (1.5 mm mask) |
|---|---|---|---|
| **0** | 0 | 0 | 0 |
| **3** | 4.14 ± 1.77 | 7.29 ± 1.90 | 7.13 ± 2.79 |
| **6** | 12.51 ± 1.70 | 20.73 ± 2.83 | 17.66 ± 2.56 |
| **10** | 27.61 ± 3.42 | 45.56 ± 6.98 | 34.31 ± 4.53 |
| **15** | 46.73 ±4.97 | 65.05 ± 6.89 | 50.02 ± 12.47 |

The effects of membrane thickness on substrate strain was investigated. A sample sheet of 0.002” silicone membrane was obtained from Specialty Manufacturing (no

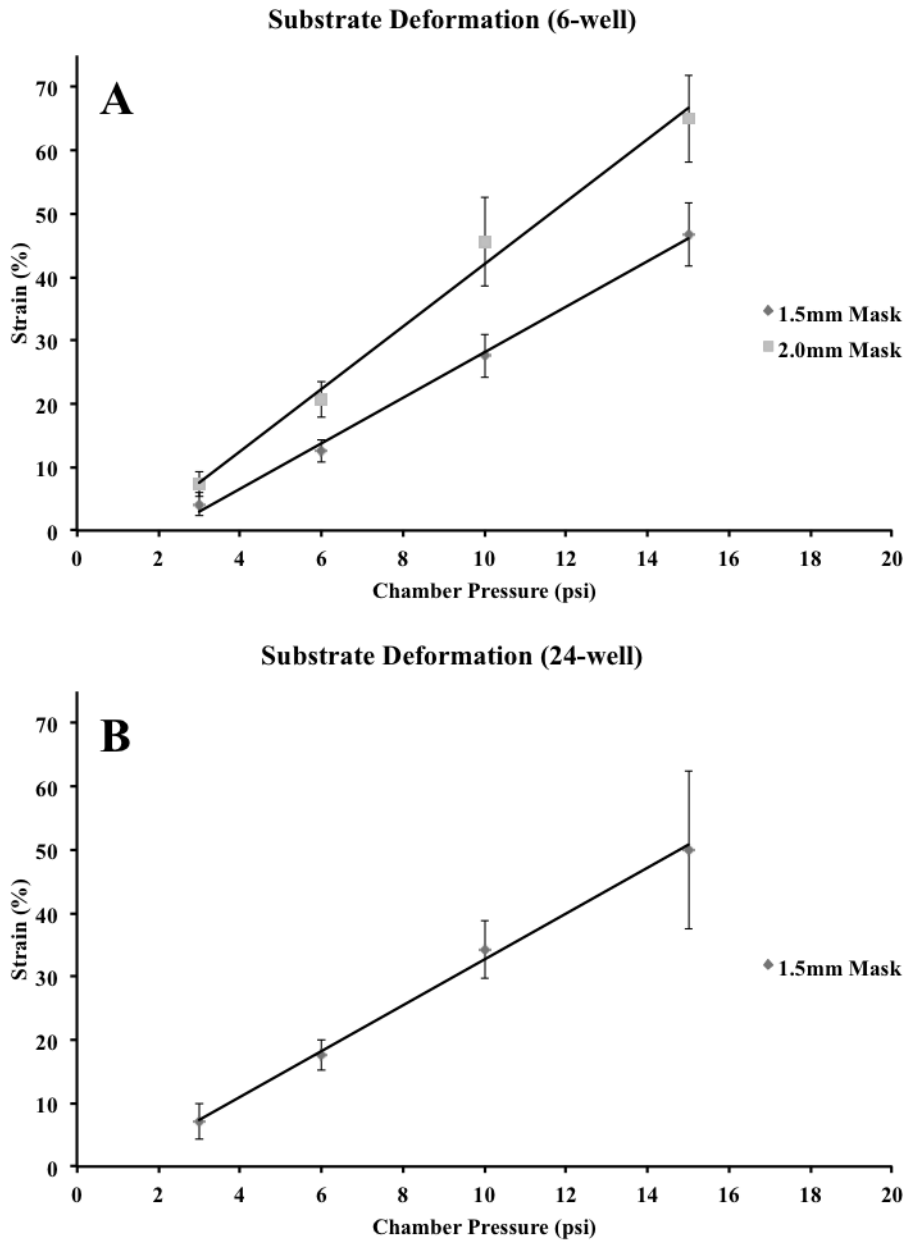


**Figure 2.6** Substrate deformation characterization maps. Plots represent the relationship between substrate deformation and chamber pressure. Measurements were made using the deformation mask to induce uniaxial deformation in the membrane. The 6-well (A) and 24-well (B) modules perform similarly through the use of a deformation mask with a 1.5mm gap. However, by increasing the gap width to 2mm, higher substrate strains were achieved.

longer available) which is 60% thinner than the 0.005" membrane used in this study. Due to the limited amount of substrate available, analysis was done using the 6-well module. Significantly lower pressures were required to achieve substrate strains; specifically using the 0.002" membrane 7 psi yielded 47.16% strain compared to 15 psi for the 0.005" membrane, Table 2.2. Importantly, it was found that the standard deviation in the strain measurements also decreased significantly where the 0.002" membrane yielded 47.16%±1.92% compared to the 0.005" membrane of 45.59%±6.98%.

**Table 2.2** Pressure deformation results using a 0.002" membrane with the 6-well module

| Pressure | % Strain (2mm mask) |
|---|---|
| **0** | 0 |
| **2** | 10.39 ± 1.86 |
| **4** | 25.78 ± 1.95 |
| **6** | 40.57 ± 2.02 |
| **7** | 47.16 ± 1.92 |

To further investigate the large variability (standard deviations in Table 2.1) in substrate strain at higher pressures, an intra-well study of the substrate deformation properties was conducted. Using the 6-well module and 0.005" membrane, strain of the membrane was measured at five different locations in each well. All experiments were done using the 2.00 mm deformation mask and all strain measurements were taken at a static pressure of 15 psi. When single measurements were compared from well to well, an average strain of 46.75%±6.89% was found. When five measurements are averaged within the same well, a strain of 46.52%±6.77% was measured. Interestingly, the

variability of strain at different locations within the same well is similar to the variability of strain measured from one well to another.

### 2.3.4 Neuronal Compatibility with Materials

Custom culture environments can affect culture viability due to material compatibility. To assess compatibility with the PEEK material, the viability of cortical cells cultured in the 24-well plates with silicone membrane substrates was tested. Morphology of cultures grown on silicone membranes resembled controls grown on tissue culture plastic. Cultures displayed no signs of irregular growth or toxicity such as aggregation of cell bodies. The viability of neuronal cultures in the 24-well module at 10DIV over three tissue isolations (n=59 wells) was quantified. Images were taken in two locations in each well and total number of cells ($N_t$) and non-viable cells ($N_n$) were counted. The average viability for each of the three populations was 97.84% ±0.83, 97.85% ±0.67 and 97.20% ±0.58 (±StDev). In all subsequent experiments cultures were consistently healthy by visual inspection.

### 2.3.5 Maximizing the Region of Isolated Axons

Increasing the width of the uniaxial deformation gap and region of isolated axons would provide a mechanical advantage and allow a larger substrate deformation at a lower pressure. In addition, injuring a larger span of axons would increase the yield of tissue that could be collected from each 24-well culture plate for analysis; an obvious goal of the high throughput system. Here, the maximum distance axons could traverse across an increasing gap widths was considered. During plating, cell free zones were created in cell culture dishes using strips of silicone ranging from 1.5 mm to 3 mm. Images were

taken of axon outgrowth every 2-3 days, (Figure 2.7). Healthy cultures were able to traverse the 1.5mm gap in 7DIV and the 2mm gap in 9DIV. However, cultures were found unable to consistently traverse the 2.5mm and 3mm gaps.

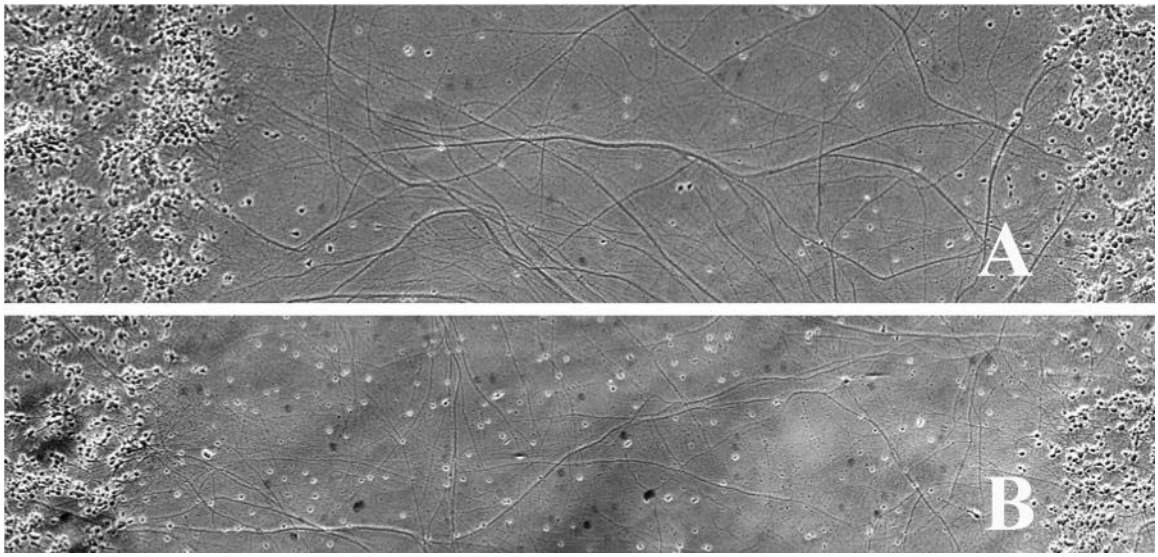


**Figure 2.7** Axons spanning the cell free zone. Axons were able to traverse a 1.5mm gap in 7 DIV (A) and a 2mmgap in 9 DIV (B).

### 2.3.6 Injury to Neuronal Cultures

To assess the uniformity and consistency of injury to neuronal cultures, experiments were performed to replicate common morphology of traumatic axon injury and neuronal viability. The pressure deformation map (Figure 2.6) and the characterization map (Figure 2.5), was used to determine injury the injury parameters needed to achieve 50% strain in each module. An input pressure of 80psi and a valve timing of 20 ms was used for the 24-well module, whereas, an input pressure of 50 psi and valve timing of 10 ms was used for the 6-well module. At 10 DIV axons were injured in both modules and observed under phase microscopy. All injuries displayed evidence of axonal undulations immediately after injury, (Figure 2.8, A). 12 hours after injury, swellings in injured axons were apparent, (Figure 2.8, B). A viability study was conducted using the 24-well

module (n=30) 24 hours after injury to assess neuronal viability after injury. At 24 hours average neuronal viability was 84.82%±5.77%.

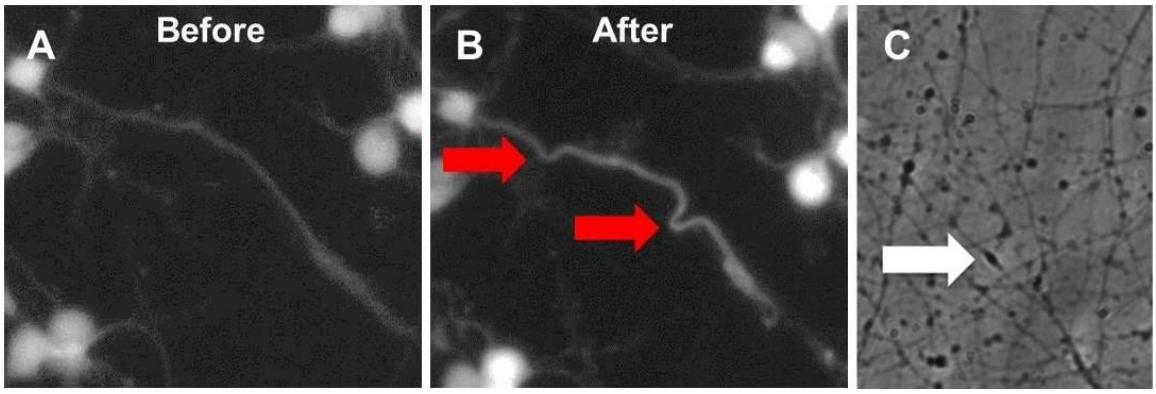


**Figure 2.8** Common morphological markers of axon stretch injury. Images of an axon before (A) and after (B) injury. Undulations developed immediately following the injury as indicated by red arrows. Axonal beading developed within 12 h post-injury (C) as indicated by white arrow.

## 2.4 Discussion

Many advanced tissue culture models are emerging and driving the discovery of novel biological processes involved in traumatic brain injury (Lighthall *et al.*, 1989; Lucas, 1992; Meaney *et al.*, 1998; Morrison *et al.*, 1998b; Cohen *et al.*, 2007; Chen *et al.*, 2009). In particular, *in vitro* mechanical deformation injury models have contributed to the discovery of key biological mechanisms of traumatic injury to neuronal cultures (Ellis *et al.*, 1995; LaPlaca & Thibault, 1998; Morrison *et al.*, 1998a; Morrison *et al.*, 1998b; Smith *et al.*, 1999; Geddes *et al.*, 2003b; Lea *et al.*, 2003; Pfister *et al.*, 2003; Iwata *et al.*, 2004; Kao *et al.*, 2004; LaPlaca *et al.*, 2005; Prado *et al.*, 2005).

*In vitro* stretch injury of neuronal cultures uses a rapid pressure-pulse to stretch an elastic silicone membrane on which neural cells are cultured. The resulting deformation can be either biaxial (e.g., an inflating balloon), or uniaxial (e.g., stretching a rubber band). Uniaxial stretching of the axon may be the more mechanically relevant

deformation in traumatic axonal injury, discussed below (Smith & Meaney, 2000; Pfister *et al.*, 2003; Iwata *et al.*, 2004). Importantly, uniaxial stretch models replicate many of the morphological and ultrastructural changes observed *in vivo*, including alterations in neurofilament structure, axolemma permeability, and axonal swelling formation (Smith *et al.*, 1999; Smith & Meaney, 2000; Pfister *et al.*, 2003; Pfister *et al.*, 2004). Here, the injury format of the device developed by Smith and Meaney was adopted (Smith *et al.*, 1999); allowing this device to be operated for either biaxial or uniaxial stretch injury of cultures.

While mechanical injury models are elucidating many important injury mechanisms, the experimentation of single cultures, one-by-one, limits productivity. Unfortunately, these custom designed models also typically require extensive experience to gain consistent results. The complexity combined with low experimental yield has limited the use of these powerful *in vitro* models to just a few research laboratories. Indeed, low experimental yield has prevented important and well founded investigations where high throughput methods are required, such as protein and genomic analyses or treatment screening. For instance, it can take several months to generate sufficient experimental yield for routine analyses such as Western blot (Iwata *et al.*, 2004; von Reyn *et al.*, 2009).

In absence of a high throughput TBI model, many great *in vitro* experimental ideas have been waived due to a high economy of the question. The purpose of this engineering effort was to create a multi-well high throughput neural injury device based off the format of a well-established stretch injury model (Smith *et al.*, 1999). To provide the similar efficiency and throughput the multi-well plate brought to tissue culture

experimentation, a 24-well and 6-well stretch injury system was created. This system has the capability to rapidly screen for biomarkers and potential interventions, study mechanisms of therapeutics, and generate large tissue samples necessary for proteomic and genomic analyses. For easy implementation in any laboratory, this system is automatic and does not require a high level of expertise to operate.

### 2.4.1 Modules and Flexibility in Design

The ability to simultaneously injure 24 independent populations of neuronal cultures made this device convenient for high-throughput scenarios or collecting protein for western blot analysis.

This system was created in a modular format allowing the user more freedom in experimental design. If high throughput tissue generation is important to the experimental design, the investigator has the option of using the 24-well module. Alternatively, if the experiment calls for time course of measurements, the user can use the 6-well module. From this prospective, the 6-well module offers a bit more flexibility in experimental design. Unlike the 24-well module, the individual wells may be injured separately or in any combination up to six wells at once. This is useful for time point studies where all samples must be injured together, returned to the incubator and analyzed individually. Furthermore, future needs could drive the development of different modules such as 12 or 96 well modules.

The design of the 6-well module with discrete wells offered a number of advantages over the 24-well module. The most obvious design feature of the 6-well module that surpasses those of the 24-well module was the ability to quickly assemble culture vessels without the need for silicone glue; a step that requires 2 days. The 6-well

module utilizes a two-part snap fit design for the culture vessel. The silicone substrate is pre-stretched equibiaxially and secured between the two concentric rings that make up the culture vessel and an O-ring that is fitted around the inner ring of the well. This design is currently being adapted to the 24-well module. Another critical design advantage of the 6-well module is a large reduction in volume of the pressure chamber. This key feature allows the 6-well module to achieve higher chamber pressures at lower reserve pressure settings than the 24-well module.

**2.4.1.1 Uniaxial Axon Stretch Injury.** Biomechanical studies on closed head injury have shown that rotational motion (opposed to linear motion) of the head induces a large deformation of the brain. The soft brain tissues react slower to the rotation of the head causing large intracranial shear deformation within the brain with respect to the comparatively rigid skull (Holbourn, 1945; Margulies & Thibault, 1992; Meaney *et al.*, 1995; Smith & Meaney, 2000; Pfister *et al.*, 2003). Macroscopic shear deformation of brain tissue translates microscopically to rapid longitudinal or uniaxial stretching along the diagonal of a representative cube, (Figure 2.1, B). Axon fibers aligned along the diagonal will be stretched while perpendicular fibers will be compressed. It is believed that axons are mostly damaged by the stretching forces, whereas compression forces would simply release damaging forces and cause the axon to undulate.

Stretch injury models were initially designed to apply a rapid pressure-pulse and cause biaxial deformation of the membrane, (Figure 2.1, A). Since uniaxial (longitudinal) stretching of the axon is the more mechanically relevant deformation in axonal injury, two models have been implemented to deliver a uniaxial stretch injury (Smith *et al.*, 1999; Pfister *et al.*, 2003; Lusardi *et al.*, 2004a). To injure isolated axons in

a uniaxial fashion, Smith and Meaney developed a protocol to create a cell free gap across which cultured axons grow (Smith *et al.*, 1999). Cells are restricted from adhering to a 1.5-2mm line across the well by covering the region with a silicone divider. Neurons are seeded on both sides of the divider and allowed to adhere to the substrate. Upon removal of the divider, developing axons grow across the gap in about 10DIV. This isolated axonal region is stretched by placing a complementary mask underneath the silicone substrate, only allowing deformation of this region, (Figure 2.1, C).

Plating procedures and alignment of the deformation mask with the cell free zone has been a manual and often inaccurate procedure. This procedure was simplified by creating a self-aligning deformation mask and plating fixtures. PDMS dividers were designed to be self-centering and easy to insert into each well. The deformation mask was designed to be complementary to the 24-well plate so as to align with the cell free zones during assembly of the pressure chamber. For the 6-well device, individual masks are needed for each well; however, they are simply aligned during assembly by aligning markings on the masks, wells, and pressure chamber.

**2.4.1.2 Controlling the Pressure Pulse.** Commonly used stretch injury devices use a pressure pulse to drive the deformation of the silicone substrate and the attached neurons. Since injury is related to the degree of substrate strain, accuracy is only as good as the control and reliability of the pressure pulse dynamics. The input pressure serves as a driving force for the pressure pulse and affects the rise time of the pressure waveform, (Figure 2.4, B&D). Accordingly, the rising phase of the pressure pulse can be altered by small inaccuracies in manually set pressures or a drop in the input pressure during operation (common issues with pressures set by air cylinder regulators). Here, a

secondary reserve pressure tank is used to supply a large reservoir of compressed air so that the input pressure remains constant during operation. The reserve tank's pressure is set by the user via LabVIEW software interface and automatically controlled with an electronic pressure controller to prevent user inaccuracies in the setting.

Controlling valve timing was critical in order to accurately set a precise peak of the pressure pulse. How long the valve is open is directly related to substrate strain, (Figure 2.4, A&C). Accordingly, the pressure pulse is directly affected by the response of the solenoid valve. The specified 2-3ms response time of the fast acting solenoid valve is the time required to energize the solenoid and open the valve. Specifically, if the valve is sent a signal to open for 20 ms the valve is closed for the first 2-3 ms. Accordingly, this response time adds a delay to the opening of the valve, which becomes more apparent at shorter opening times. Furthermore, it was observed that the speed at which the valve opens is also a function of the pressure bias across it. Work is currently being done to compensate for these delays in the control software. Analysis of the pressure pulse uniformity throughout the pressure chambers yielded small standard deviations and convincingly demonstrated that the system could repeatedly produce accurate pressure pulse dynamics uniformly throughout both pressure chamber modules.

The performance map for 24-well module shows a range of peak pressures upwards of 8.5 psi, on the contrary, the data for 6-well module shows a much wider range of peak pressures upwards of 25psi, (Figure 2.5). This disparity in performance is directly related to the large difference in volume between the two modules. The internal volume of the 6-well module is substantially smaller than that of the 24-well module and accounts for the difference in their respective pressure pulse dynamics. Because of the

24-well module's large volume it inherently requires a higher input pressure and longer valve open time to perform similarly to the 6-well module. While both systems can produce the same rising phase of the pressure pulse, the control system settings are different for each module.

### 2.4.2 Analysis of Substrate Deformation

At high pressures, the substrate deformation measurements for the 0.005" membrane had rather large deviations about the mean. Since the delivery of the pressure pulse of the device was extremely accurate, it was believed that the pressure waveform was not the major contributor to the inconsistencies in substrate deformation. There are two other possibilities that could cause the variability in substrate strain 1) variation in the properties of the silicone membrane and 2) uneven stresses produced by the membrane pre-stretch process when assembling the wells. Close examination of the substrate pre-stretch process for both the 24-well and 6 well modules produced nicely uniform strain across the membrane and negligible shear strain. This rules out pre-stretch as a major contributor of the deformation inconsistency.

The other cause could be changes in membrane thickness that would clearly affect local deformation. According to the manufacturer, the membrane thickness can vary from 0.002" to 0.007" (Specialty Manufacturing, personal communication). If this were true, then strain measures within the same well should vary similarly to measures from one well to the next. Using the 6-well module, strain measurements were taken at five different locations in five different wells. The variation in these 25 intra-well measurements was the same as the deformation measurements where a single strain measurement was made in each well, (Figure 2.9), first two bars. If it was concluded that

the variation in strain is membrane dependent, the accuracy of the device is only as good as the membrane used. However, one could consider the measurements in each well to be part of a population and averaged, thus reducing measurement the variation between wells. Indeed, a common practice in biology is to average measurements of a population of cells to get a more representative result.

To further investigate the variation in deformation due to membrane thickness, a 0.002" membrane that has less thickness variability and yields higher strains at lower pressures, Table 2.2, was analyzed. When histograms of 0.005" and 0.002" deformations are compared, membrane inconsistencies are drastically reduced with thinner membranes, (Figure 2.10). This further supports that variations in membrane thickness are affecting the consistencies of the deformation measurements recorded. Interestingly, cell viability measurements vary as much as the substrate deformation, (Figure 2.9). Viability after

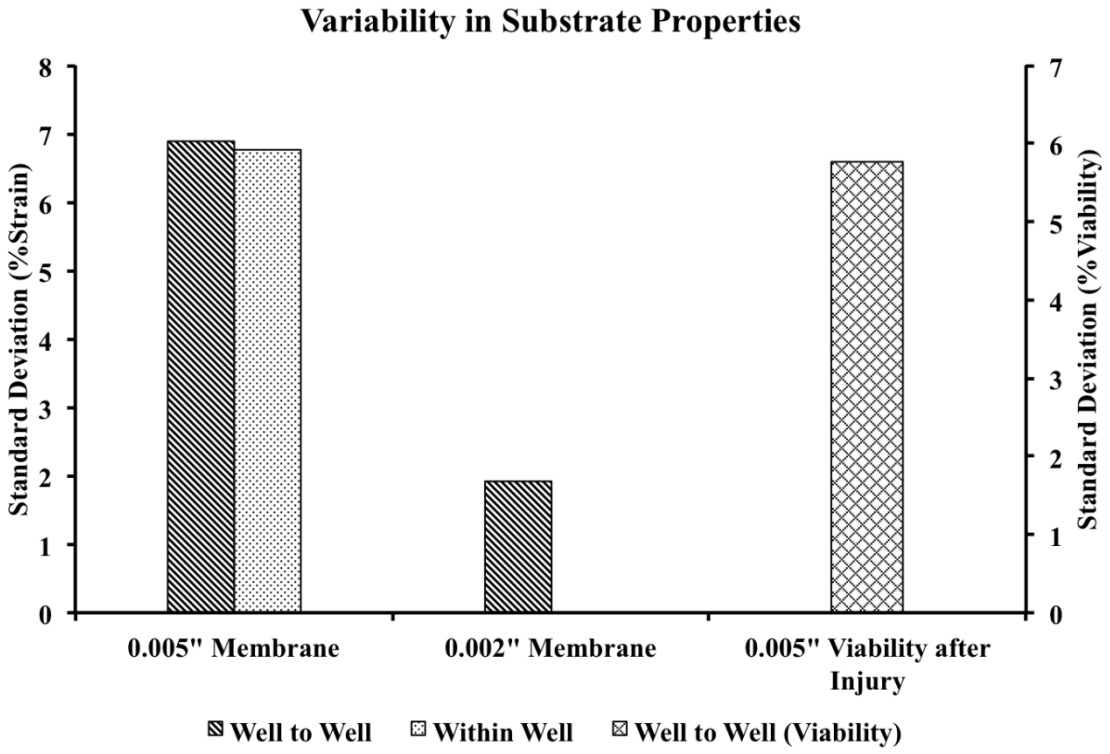


**Figure 2.9** Analysis of substrate properties and variation. First set of bars: deformation measurements were made to compare inter-well variability (well-to-well) with intra-well variability (within the same well) using the 0.005" membrane, the 2.0mm mask, and a pressure of 10 psi. Inter-well measurements took a single measurement in each of n = 18 different wells. Intra-well measurements took five measurements at different locations in each well for over five different wells for a total of n = 25. The standard deviation of the inter- and intra-well measurements of deformation showed the same variation about the mean. The middle bar shows inter-well variability using a 0.002" membrane where the standard deviation in the measurements is greatly reduced. The last bar presents the variability in the neuronal viability following injury. These comparisons suggest that inconsistencies in deformation of the membrane are a result of inconsistencies in the membrane itself and that the variability in the biological response to injury may be linked to substrate inconsistencies rather than solely biological variation.

injury was reported to be 84.82%±5.77 % (±StDev), close to the variation in substrate strain measures. This suggests that the variability in viability after injury should not be considered to be solely based on biological inconsistency.

### 2.4.3 Effects of Gap Size

One goal of the high throughput module is to generate as much injured axonal tissue as possible for each 24-well plate. Accordingly, a wider cell-free zone would allow us to injure and collect larger sections of axons. Experiments were performed by growing axons across longer cell-free zones and concluded that it was possible to reproducibly grow and isolate 2mm long axons. Axons were able to traverse the 1.5mm gap within 7 DIV, whereas the 2.0mm gap took up to 9 DIV. Importantly, the 2mm deformation mask has two major advantages. First, higher strains can be achieved at lower chamber pressures broadening the span of possible pressure-deformation combinations. Second, the dynamics of the pressure pulse are easier to control at lower pressures.

## 2.5 Conclusions

Designing and experimenting with the 6-well module has helped in identifying critical design elements that improve the operation in comparison to the 24-well module. Smaller volume in the 6-well pressure chamber has proved to show tighter control in the pressure pulse dynamics and the ability to achieve faster rise times, therefore allowing for higher peak pressures to be reached at lower reserve pressures. Work is currently being done to re-engineering the 24-well pressure chamber to reduce the interior volume. The two-part assembly method of the 6-well module allows the user to move away from the

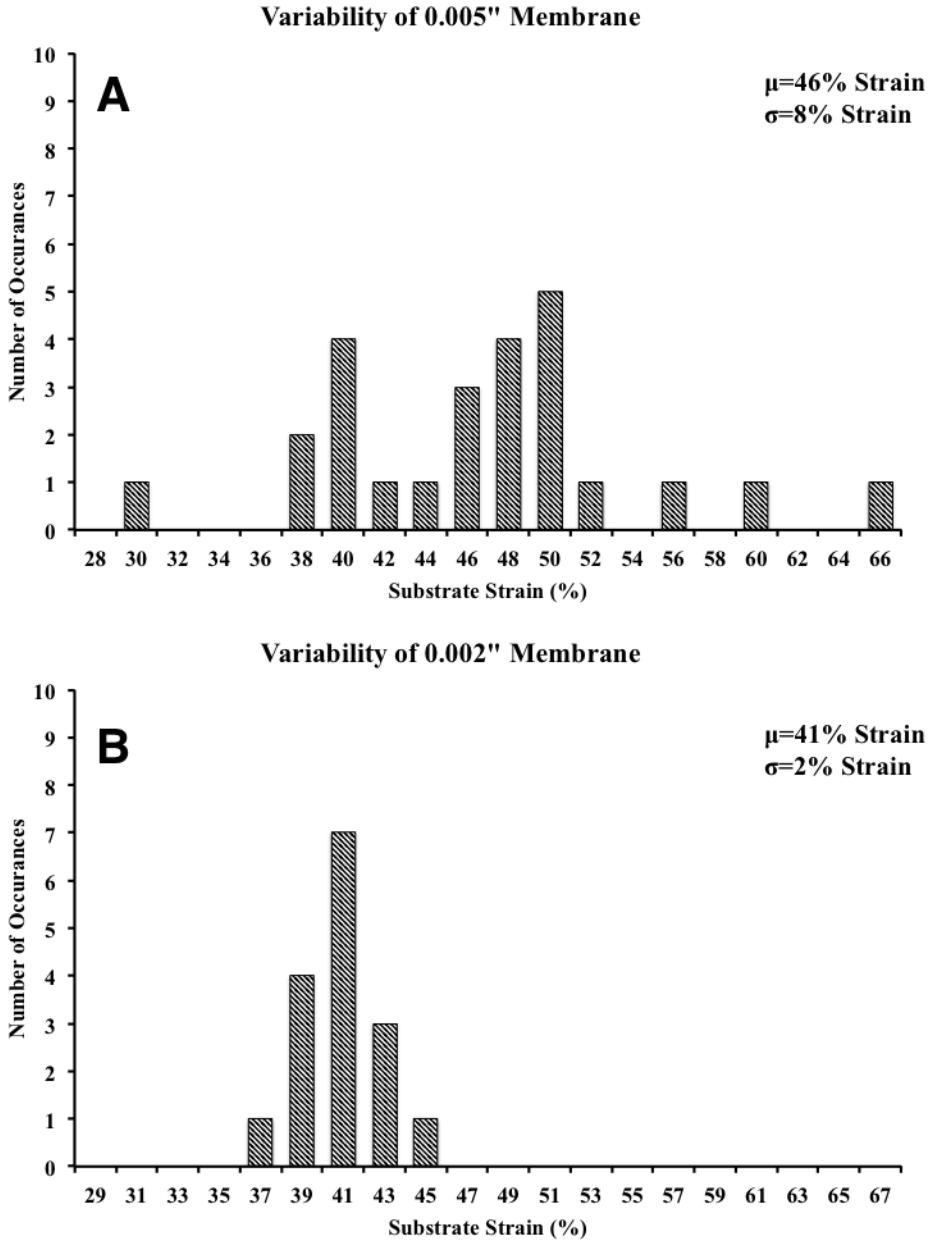


**Figure 2.10** Membrane thickness. Histogram plots were made to show the variability of the deformation measurements taken for a 0.005" thick membrane (A) and 0.002" thick membrane (B). Measurements were done identically for both membranes using the 6-well device with the 2.0mm mask. The pressure used for each thickness was adjusted to achieve similar means of 46% and 41% strain for the 0.005" and 0.002" membrane, respectively. Insets display the mean ($\mu$) and standard deviation ($\sigma$) for each membrane. The 0.002" membrane has a much smaller distribution about the mean than the 0.005" membrane, suggesting that variability in membrane thickness is the underlying cause for inconsistencies in deformation data.

difficult 24-well gluing method of substrate adhesion. Mirroring the conveniences in assembling the 6-well module, new designs for the 24-well injury plate are being evaluated. While these planned improvements will create a better-controlled model, the system has expanded upon currently used stretch injury devices. The advantage is the ability to now undertake high throughput studies that are needed for the countless number of scientific questions across the field of neurotrauma research.

# CHAPTER 3

# EXPLORING THE EFFECTS OF STRAIN RATE ON STRETCH INJURED RAT NEOCORTICAL NEURONS IN CULTURE

## 3.1 Background and Significance

Mechanical injury is known to cause dysfunction in surviving neurons. In most cases many surviving neurons die within 24 hours of mechanical injury (Choi, 1995; Lusardi *et al.*, 2004a; Magou *et al.*, 2011). It is well established that $[Ca^{2+}]_i$ levels are elevated post mechanical injury (Geddes & Cargill, 2001; Wolf *et al.*, 2001; Iwata *et al.*, 2004; Lusardi *et al.*, 2004b; von Reyn *et al.*, 2009). Consequently, many studies have been done to investigate the role that $Ca^{2+}$ plays as a second messenger to neuronal injury, dysfunction, and viability (Iwata *et al.*, 2004; von Reyn *et al.*, 2009; Yuen *et al.*, 2009). It has been shown that elevated levels of $[Ca^{2+}]_i$ play a role in the activation of proteases involved in cleavage of voltage gated sodium channels (Iwata *et al.*, 2004; von Reyn *et al.*, 2009). Interestingly, the voltage gated sodium channel blocker, tetrodotoxin (TTx), has proven useful in mitigating $[Ca^{2+}]_i$ entry of stretch injured neurons (Wolf *et al.*, 2001). Histological studies of neurons treated with TTx prior to injury showed results that suggest mitigation of voltage gated sodium channel proteolysis (Iwata *et al.*, 2004; Yuen *et al.*, 2009). Unfortunately, the mechanisms behind neuronal dysfunction and viability after mechanical injury are still unclear.

Typically, studies using *in vitro* models categorize injuries by maximum applied strain. However, other factors may play a role in the progression of neuronal injury. One

specific study used the fluorescent $Ca^{2+}$ indicator, Fluo4, to explore the hypothesis that neurons subjected to very mild injures were predisposed to secondary insults (Yuen *et al.*, 2009). Single mild injuries (3% strain) did not elicit an $[Ca^{2+}]_i$ response. However, if subjected to a secondary mild injury within 24 hours, injured neurons exhibited rises in $[Ca^{2+}]_i$ response analogous to injuries on the order of 20% strain. These data suggest that neuronal response to mechanical insult is complex in nature and is dependent on many factors. One such parameter that is often overlooked in studies utilizing mechanical injury models of neurons is rate of injury. Rate of injury can be described as the rate at which maximum mechanical deformation is achieved (i.e., 60% strain produced over a time period of 20ms is reported as a strain rate of $30s^{-1}$). The few studies that have looked at strain rate have either studied them in "neuron-like" cultures (Geddes & Cargill, 2001) or at very low rates ($0.015s^{-1}$-$24s^{-1}$) (Lusardi *et al.*, 2004b).

The central hypothesis of this study is that the rate of injury may exacerbate the injury response. More specifically, cells may exhibit a greater injury response as a result of increasing the rate of injury. Furthermore, if strain rate increases the response of injured neurons, it would be interesting to consider the capabilities of TTx as a potential blocker for this mechanism.

The following studies were performed to explore the effects of rapid strain rates ($\dot{\varepsilon} > 30s^{-1}$) on mechanically injured neurons. Measurements of $[Ca^{2+}]_i$ using the indicator, Fluo4, will serve to describe the degree of injury as a result of varying strain rate. These studies were also performed in the presence of TTx to examine the efficacy of TTx as a blocker of $[Ca^{2+}]_i$. If strain rate increases the injury response of stretch injured neurons, it is hypothesized that TTx will no longer block increases in $[Ca^{2+}]_i$.

## 3.2 Materials and Methods

### 3.2.1 Stretch Injury to Neuronal Cultures

Table 3.1 lists the injury paradigm applied to cultures. The rate of injury was reported as strain rate, which is described as the rate at which the applied strain is delivered to neuronal cultures, (i.e., 30% strain delivered over a period of 10msec is reported as a strain rate of $30s^{-1}$). For this study, the effects of strain rate on $[Ca^{2+}]_i$ levels following injury were explored. All injuries were performed on DIV 10 using the 6-well module described in Chapter 2. The experiments outlined in this chapter were performed in the absence of a cell free zone.

### 3.2.2 Neuronal Culture

All neuronal culture was performed as described in Chapter 2.

### 3.2.3 $[Ca^{2+}]_i$ Imaging

The immediate $[Ca^{2+}]_i$ response of stretch injured cultures was measured using the fluorescent $Ca^{2+}$ indicator Fluo-4AM. Fluo-4AM powder was dissolved in anhydrous dimethylsulfoxide to create a 4mM stock solution. Before loading, cultures were rinsed in HBSS containing $Ca^{2+}$ and $Mg^{2+}$ to remove debris and any non-adherent cells. Cultures were loaded with 4μM Fluo-4AM supplemented with pluronic F-127 [0.01% (w/v) final] in HBSS containing $Ca^{2+}$ and $Mg^{2+}$. Loaded cultures were incubated for 30 minutes at 37°C (5% CO2). At 30 minutes, the loading solution was removed and cultures were rinsed with HBSS to remove any nonspecifically bound indicator and then incubated for an additional 30 minutes to allow for complete de-esterfication of loaded

indicator. Prior to injury neuronal cultures were rinsed in HBSS containing $Ca^{2+}$ and $Mg^{2+}$. All experiments were performed at 25°C in HBSS containing $Ca^{2+}$ and $Mg^{2+}$.

**Table 3.1** Injury scheme for testing the effect of strain rate on different injury groups

| Strain % | Rate 1 | Rate 2 |
|---|---|---|
| 20% | $30s^{-1}$ | $70s^{-1}$ |
| 40% | $30s^{-1}$ | $70s^{-1}$ |
| 60% | $30s^{-1}$ | $70s^{-1}$ |

Fluorescent microscopy was performed on a Nikon Eclipse TE-2000S inverted microscope. Images were taken using a Photometrics CoolSNAP EZ CCD camera. Fluo4 was excited at 488 nm via xenon light source and collected at 515 nm. Time-lapse images were acquired using NIS-Elements D software. Images were taken at 1s intervals for approximately 10 seconds before injury was performed. Imaging was continuous through application of injury and for approximately 120 seconds thereafter.

### 3.2.4 Tetrodotoxin Pretreatment of Injured Neurons

Previous studies have shown that intracellular entry of $Ca^{2+}$ can be blocked by the voltage gated sodium channel blocker Tetrodotoxin (TTx) (Wolf *et al*., 2001; Iwata *et al*., 2004). However, these experiments were done under a single injury simulation. To test the effect of strain rate on the increases in $[Ca^{2+}]_i$ in the presence of TTx, cultures were subjected to 50% strain at strain rates of $20s^{-1}$ $70s^{-1}$, and $100s^{-1}$.

Images were taken at 1s intervals for approximately 10 seconds before injury was performed. Imaging was continuous through application of injury and for approximately 120 seconds thereafter.

### 3.2.5 Fluorescent Analysis

All fluorescent analysis was done using ImageJ (NIH). Three cultures were injured for each injury parameter. Within each culture 10 neurons that showed a fluorescent response were analyzed for changes in fluorescence. Neurons were excluded from the selection process if they did not show a fluorescent response to the injury. All fluorescent measurements were done in the soma; for each neuron analyzed a region of interest was drawn around the soma. Mean fluorescent intensity was measured in that region of interest for each image taken in an injury sequence. Fluorescent changes were reported as normalized intensity; a ratio between measured fluorescence (**F**) and baseline fluorescence ($\mathbf{F_0}$). To reduce the effect of background noise, three areas of background that were absent from neurites and cell bodies were sampled and averaged. Background measurements were subtracted from the raw fluorescent data. Maximal intensity for tested groups was compared and statistical significance was determined using a two-way analysis of variance (ANOVA). ANOVA was chosen for this analysis because of its ability to discern differences between different groups and its ability to attribute variances to specific components. For this study those components are considered to be strain and strain rate.

## 3.3 Results

### 3.3.1 Immediate $[Ca^{2+}]_i$ Response of Stretch Injured Neurons

Neuronal cultures were injured at 20%, 40%, and 60% strain. To investigate the role that rate of injury plays in stretch injury, strain rate was modulated from $30s^{-1}$ to $70s^{-1}$ at each of the aforementioned strain levels.

Neuronal cultures injured at 20% strain expressed different behavior when exposed to different injury rates (Figure 3.1). Neurons that were injured at a slow rate exhibited slow $[Ca^{2+}]_i$ oscillations that generally returned to baseline, whereas, neurons that were injured at a rapid rate exhibited a higher incidence of $[Ca^{2+}]_i$ oscillations that did not return to baseline. However, when maximum $Ca^{2+}$, estimated as $F/F_0$, was compared, there was no significant difference between the two groups (Figure 3.2).

Cultures that were exposed to 40% strain also expressed different behavior when strain rate was modulated (Figure 3.3). When these cultures were injured at a slow rate, they also exhibited $[Ca^{2+}]_i$ oscillations; however, most cells were not able to return to baseline. When injured at a rapid rate, cells displayed steep rises in fluorescence with a much slower decay. These cultures did not exhibit oscillations and did not return to baseline within the measurement period. When maximum $F/F_0$ was compared, the differences between the two groups were found to be statistically significant ($p < 0.05$) (Figure 3.4). Significance was determined via two-way ANOVA followed by Tukey's honesty significant difference (HSD).

When injured at a strain of 60%, neither group rate produced $[Ca^{2+}]_i$ oscillations (Figure 3.5). Instead, all cultures displayed a steep rise in $Ca^{2+}$ fluorescence, much greater than that of the 20% and 40% groups, and did not return to baseline within the

measurement period. Maximum $F/F_0$ was compared (Figure 3.6). Results of two-way ANOVA showed significant difference in the maximum $F/F_0$ between the strain rate groups ($p < 0.05$).

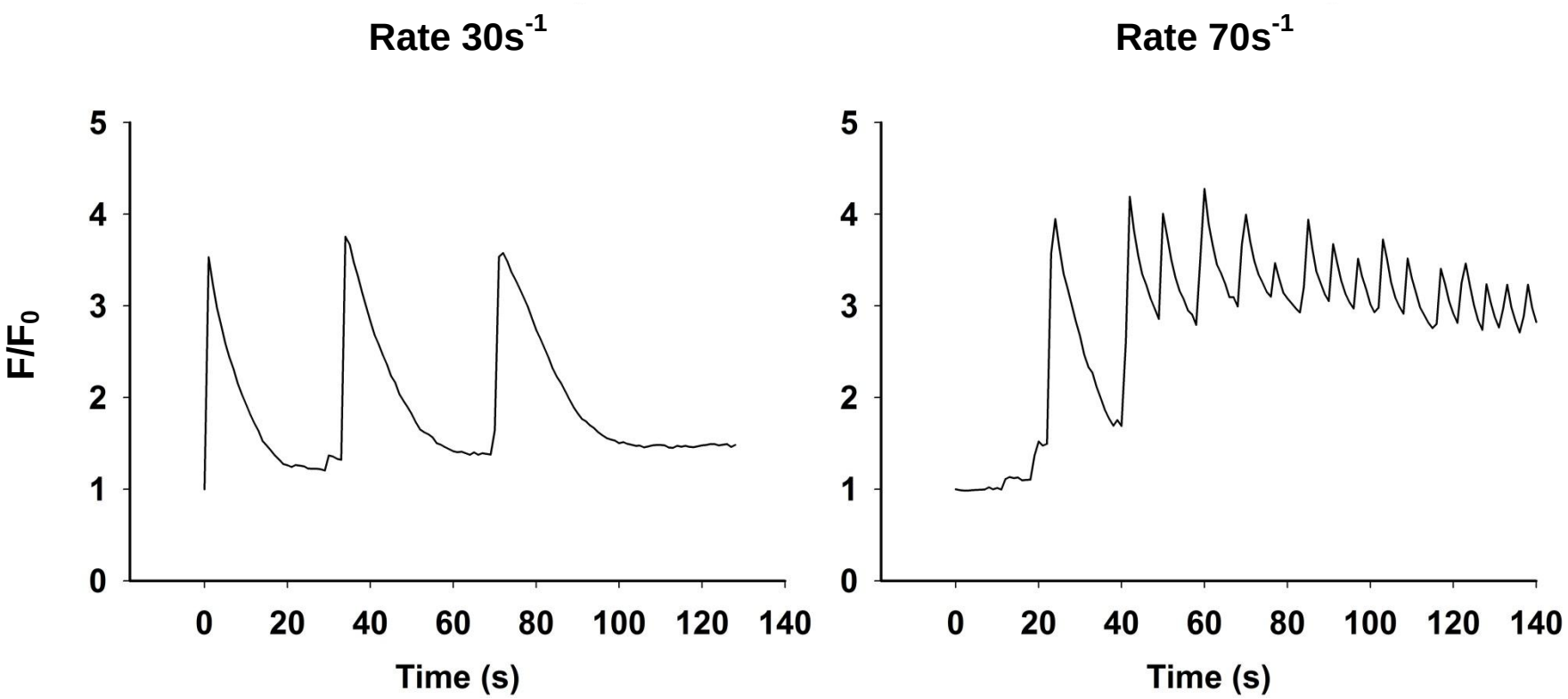


**Figure 3.1** Representative time course of $[Ca^{2+}]_i$ in neurons exposed to 20% stretch injury.

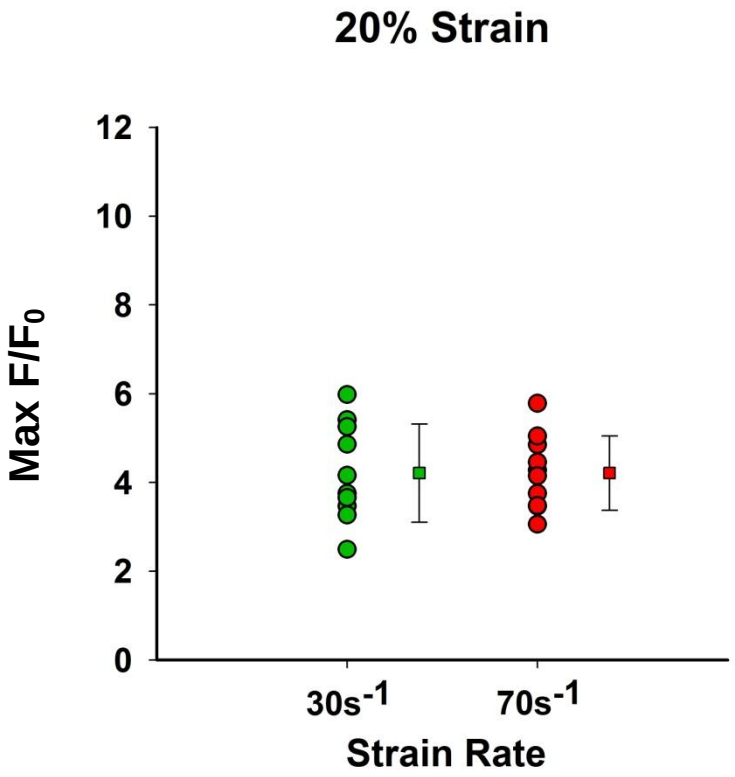


**Figure 3.2** Figure compares the Fluo4 fluorescence normalized to baseline fluorescence for slow and rapid rate injuries performed at 20% strain. Each dot represent maximum $F/F_0$ of a single cell within the specified group (n=10 cells were analyzed for each injury rate). ANOVA followed by Tukey's honesty significant difference (HSD) yielded no significant difference between the two groups.

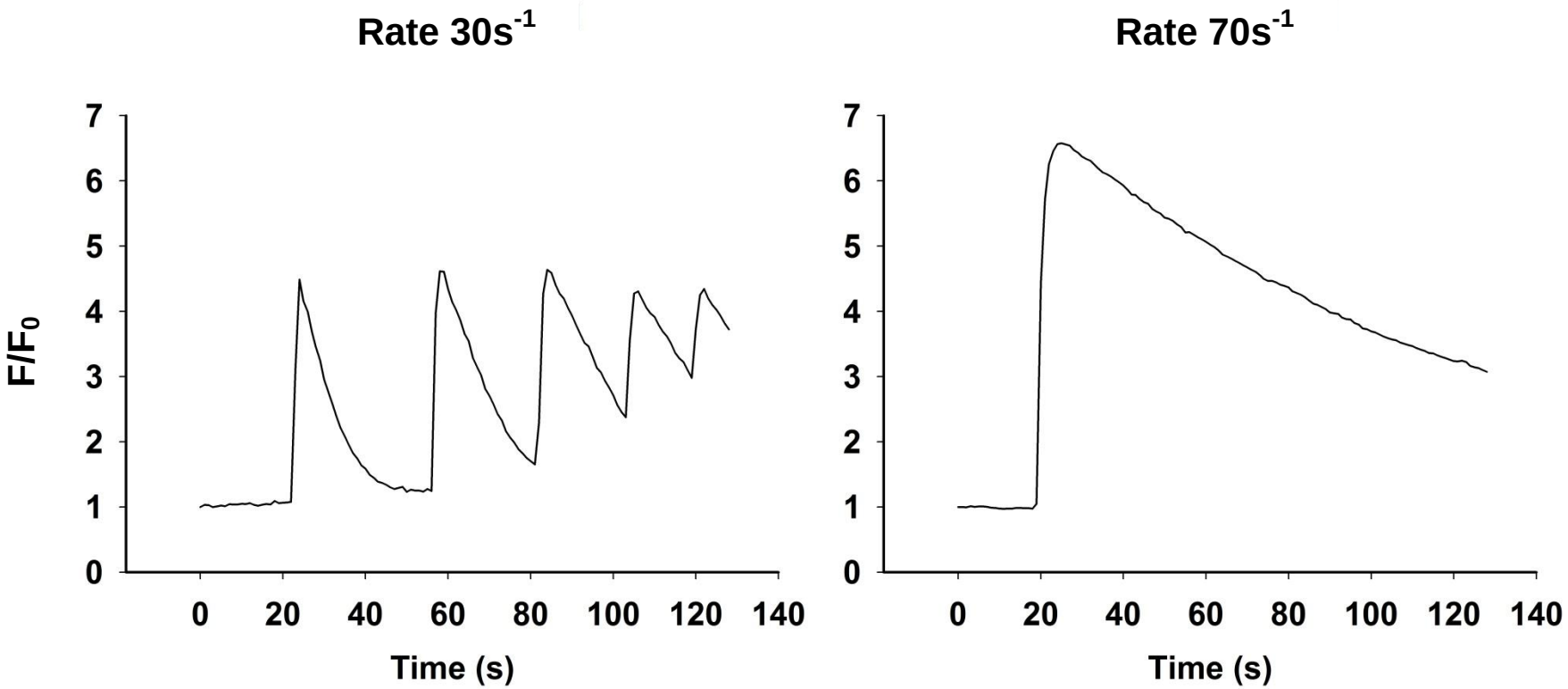


**Figure 3.3** Representative time course of $[Ca^{2+}]_i$ in neurons exposed to 40% stretch injury.

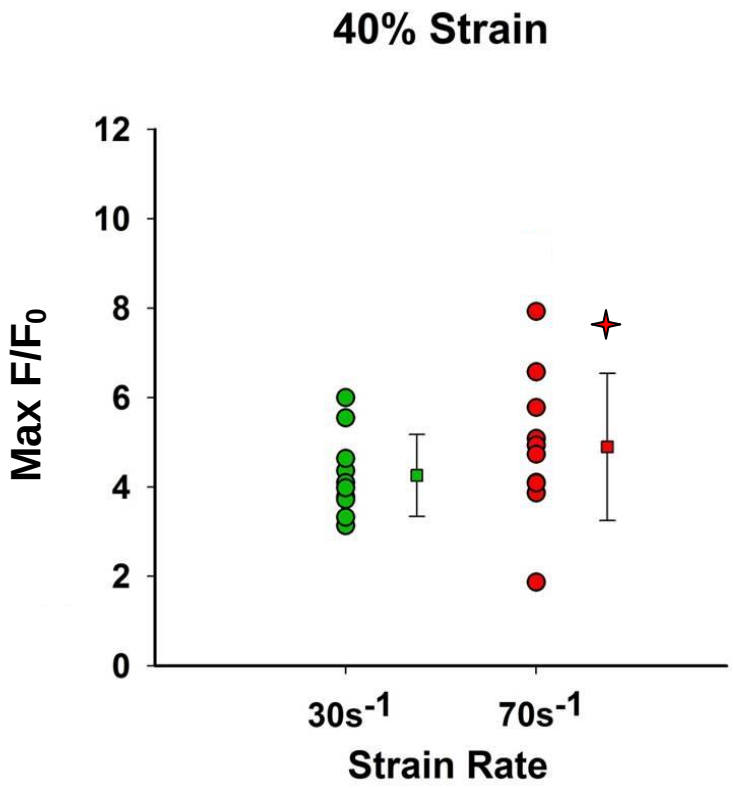


**Figure 3.4** Figure compares the Fluo4 fluorescence normalized to baseline fluorescence for slow and rapid rate injuries performed at 40% strain. Each dot represent maximum $F/F_0$ of a single cell within the specified group (n=10 cells were analyzed for each injury rate). Two- way ANOVA showed statistical difference between the two groups.

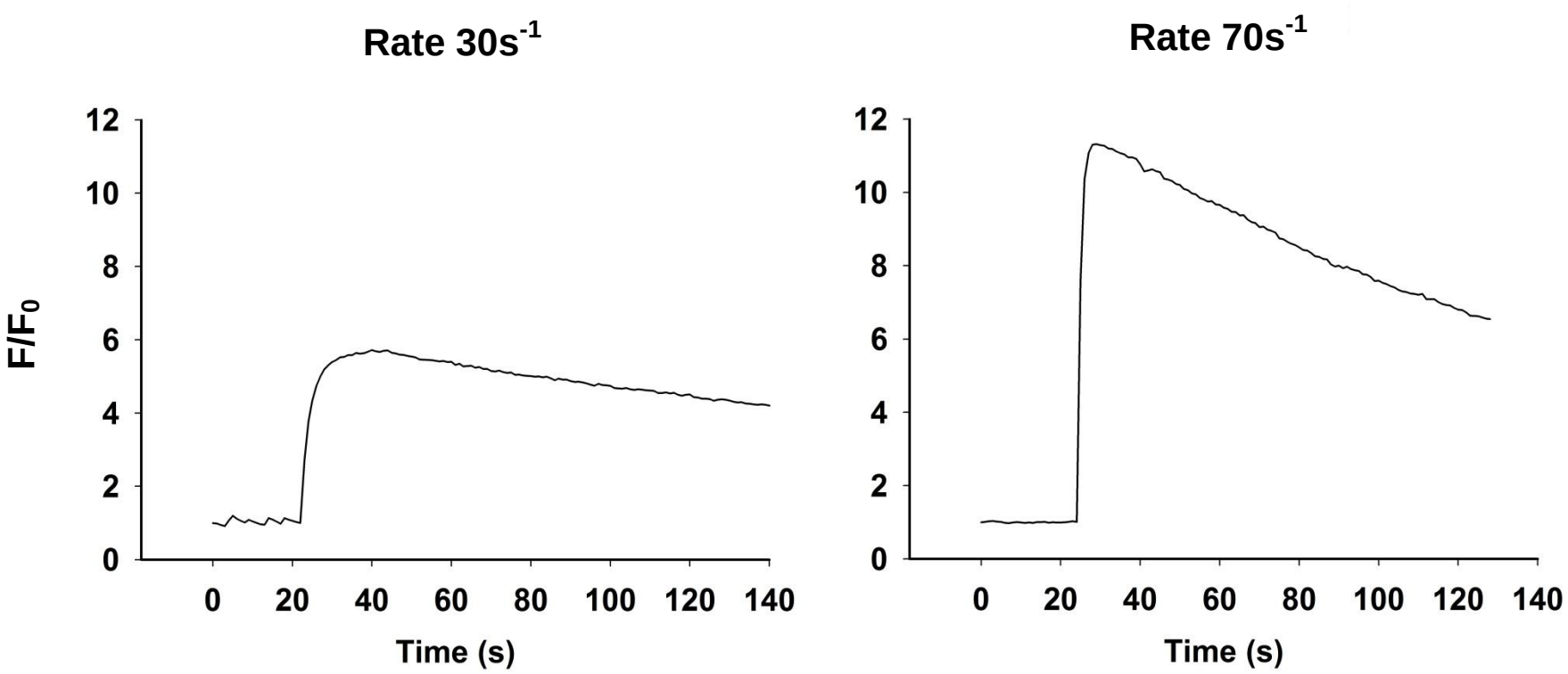


**Figure 3.5** Representative time course of $[Ca^{2+}]_i$ in neurons exposed to 60% stretch injury.

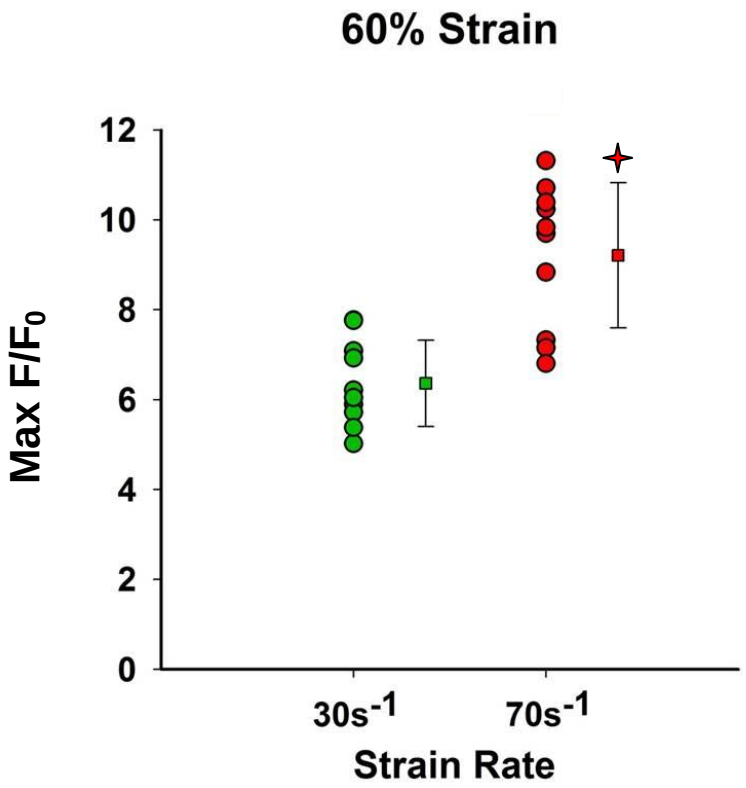


**Figure 3.6** Figure compares the Fluo4 fluorescence normalized to baseline fluorescence for slow and rapid rate injuries performed at 60% strain. Each dot represent maximum $F/F_0$ of a single cell within the specified group (n=10 cells were analyzed for each injury rate). Two- way ANOVA showed statistical difference between the two groups.

### 3.3.2 Analysis of Time Course Intensity Traces

In order to further investigate the differences due to changes in strain rate observed within each group, area under each time lapse intensity trace was calculated and compared. Area under the curve serves to represent the duration of time that cells exhibited a fold change in baseline intensity (Figure 3.7).

### 3.3.3 TTx Pretreatment of Injured Neurons

TTX has been shown to block rises in $[Ca^{2+}]_i$ levels that immediately follow stretch injury (Iwata et al 2004). However, these studies were only performed under conditions that simulated a single rate of injury ($30s^{-1}$). In this study, cultures loaded with Fluo4 indicator were treated with 1µM TTx for 10 minutes prior to injury. All experiments were performed at 50% strain to simulate a moderate traumatic event. Cultures pretreated with TTx were exposed to three strain rates $20s^{-1}$, $70s^{-1}$, and $100s^{-1}$. A positive control was injured at a rate of $20s^{-1}$ in the absence of TTx. When compared, the control group showed an increase in $F/F_0$ after injury, while the TTx treated group did not ($p < 0.05$) (Figure 3.8). Analysis of area under the time course intensity traces showed larger values in the control group when compared to the TTx treated group ($p < 0.05$).

Max $F/F_0$ for injured cultures was calculated and compared at each rate. TTx treated cultures that were injured at rates higher than $20s^{-1}$ ($70s^{-1}$ and $100s^{-1}$) showed increases in $[Ca^{2+}]_i$ that appeared to be unmitigated by TTx. Single factor ANOVA showed significance ($p < 0.05$) between the cultures injured at $20s^{-1}$vs $70s^{-1}$, cultures injured at $20s^{-1}$vs $100s^{-1}$, but not between cultures injured at $70s^{-1}$vs $100s^{-1}$. Area under the curve was calculated and compared for each rate. Single factor ANOVA showed

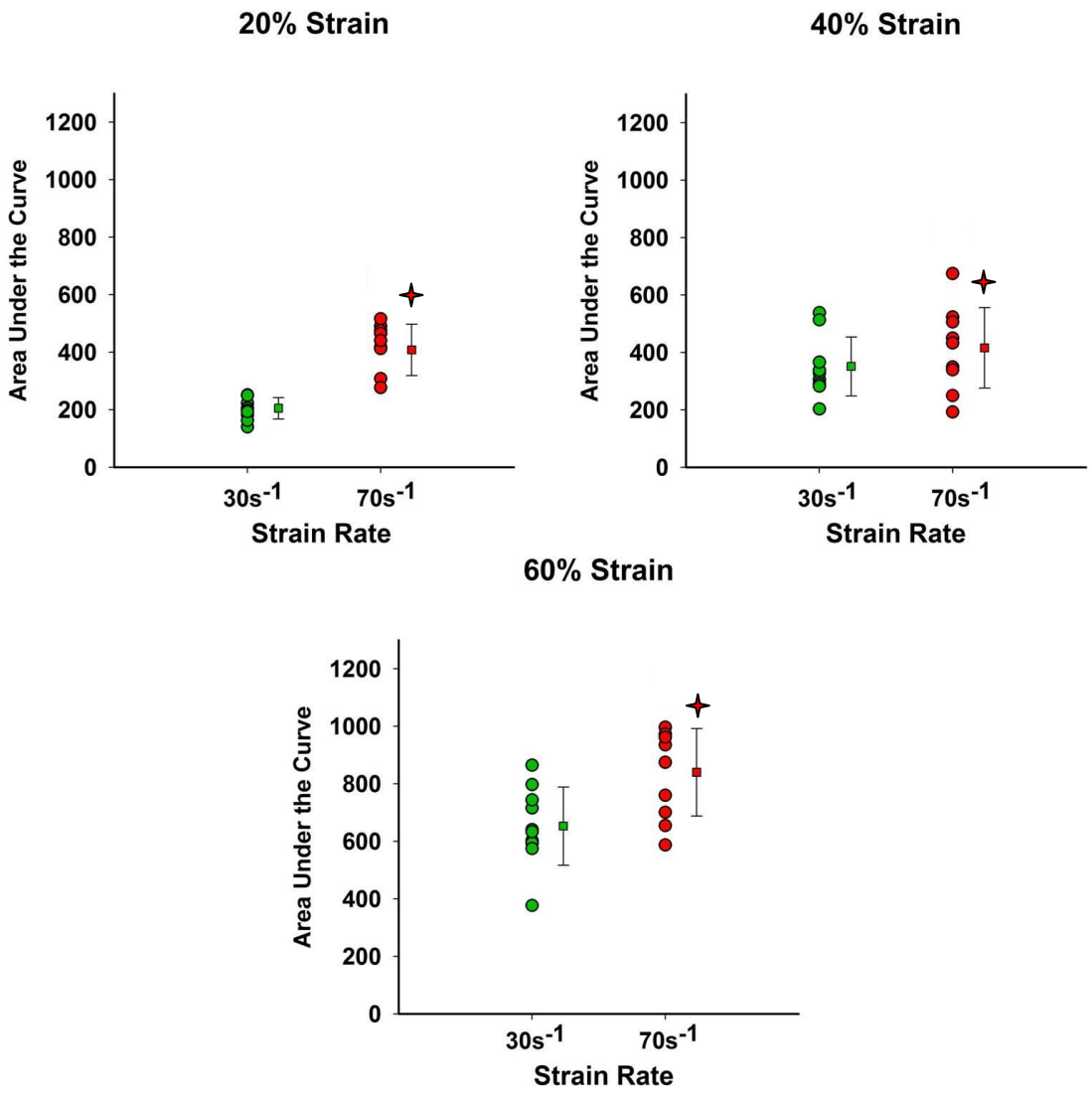


**Figure 3.7** Area under the curve analysis for slow and rapid rate injuries performed at each strain group. Each dot represent total area under the curve of a single cell within the specified group (n=10 cells were analyzed for each injury rate). Statistics were performed via ANOVA followed by Tukey's HSD. Statistical difference was found between the slow and rapid rate group for each strain experiment ($p < 0.05$).

significance ($p < 0.05$) between the cultures injured at $20s^{-1}$vs $70s^{-1}$, cultures injured at $20s^{-1}$vs $100s^{-1}$, but not between cultures injured at $70s^{-1}$vs $100s^{-1}$ (Figure 3.9).

### 3.4 Discussion

In this study data are focused on a novel aspect of neuronal stretch injury. While much research has focused on studying applied strain, this study explores the effects of rapid strain rate on neuronal injury response. Cultures were placed in three injury groups (20% strain, 40% strain, 60% strain) and injured at two rates: $30s^{-1}$ and $70s^{-1}$. Upon initial analysis of maximum $F/F_0$, the 20% injury group appeared to show no significant differences when strain rate was modulated ($p > 0.05$). However, when the time course intensity traces were compared, there were clear differences in the behavior. The $30s^{-1}$ group exhibited slow oscillating $[Ca^{2+}]_i$ that returned to baseline intensity, whereas the $70s^{-1}$ showed rapid spiking and sustained $[Ca^{2+}]_i$. This behavior may imply that cultures injured at slower rates may retain the ability to regulate elevated levels of $[Ca^{2+}]_i$ following injury. While cultures injured at higher rates experience an exacerbated effect and suffer from the inability to regulate $[Ca^{2+}]_i$ levels. To further characterize this behavior, area under the curve for each time course intensity trace was analyzed. Area under the curve represents the duration of time that cells exhibited a fold change in $[Ca^{2+}]_i$ and may represent the amount of time a cell experiences a sustained level of $[Ca^{2+}]_i$. When compared, the two groups were statistically different ($p < 0.05$). Since it has been shown that $[Ca^{2+}]_i$ fluorescence can be blocked by pretreatment with TTx, this behavior could reflect increases in TTx sensitive voltage gated sodium channel activity (Iwata et al 2004) resulting in $Ca^{2+}$ oscillations. Similar behavior can be seen in the 40%

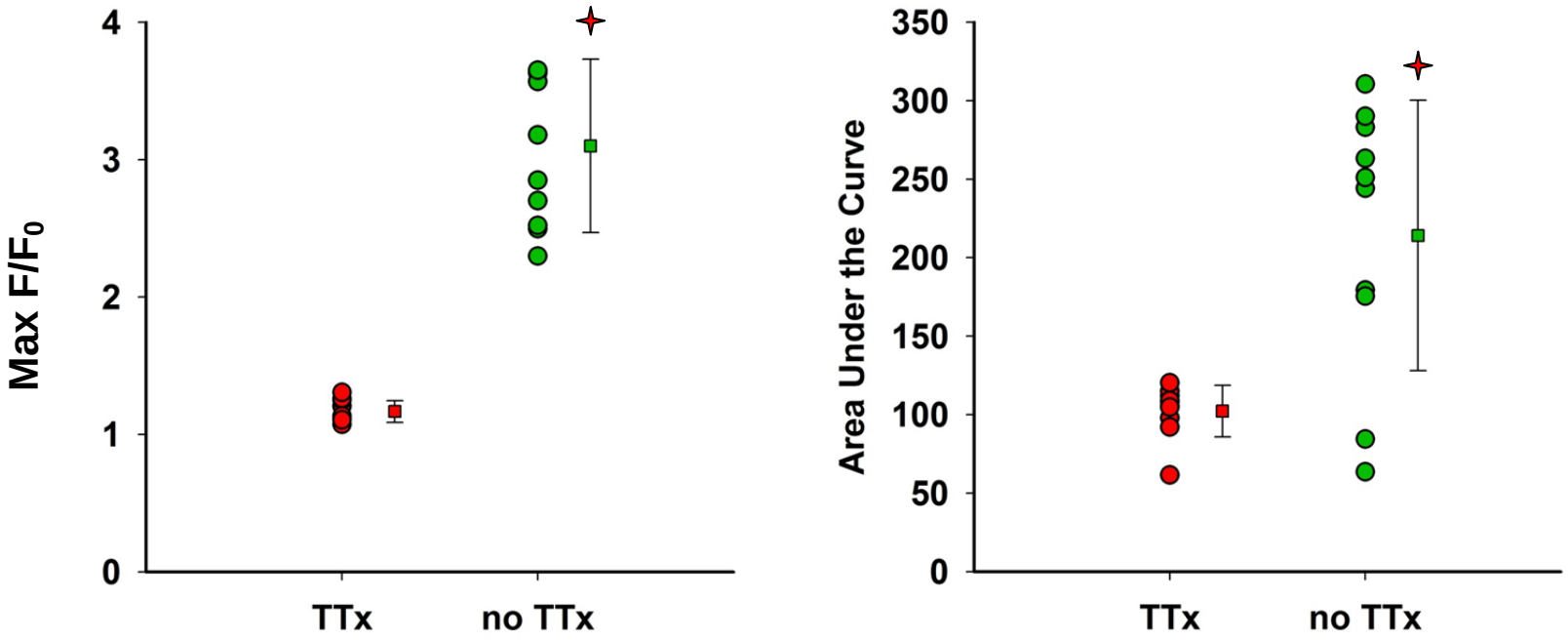


**Figure 3.8** Maximum $F/F_0$ and area under the curve analysis for cultures subjected to 50% strain at a strain rate of $20s^{-1}$ with and without TTx pretreatment. Student's t-test found the two groups to be statistically different ($p < 0.05$).

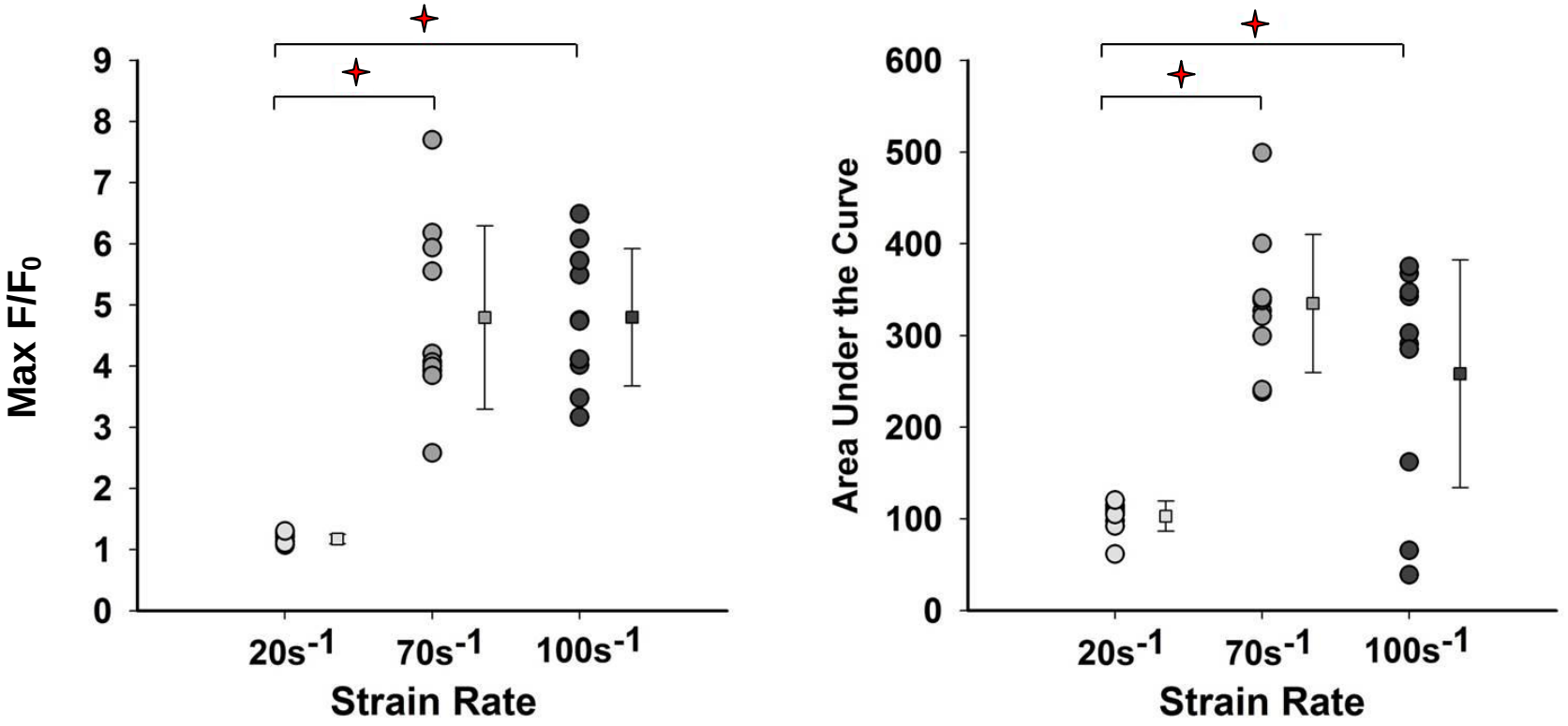


**Figure 3.9** Figure represents maximum $F/F_0$ and area under the curve analysis for cultures pretreated with 1µM TTx. Cultures were exposed to 50% strain at three different rates. Modulation of strain rate showed increases in both maximum $F/F_0$ and area under the curve for strain rates $>20s^{-1}$ despite pretreatment with 1µM TTx. These results were found to be statistically significant ($p < 0.05$).

injury group. At slower rates, cultures behaved by exhibiting slow $[Ca^{2+}]_i$ oscillations that, generally, returned to baseline. When cultures in this injury group were injured at a higher strain rates, the cells experienced steep rises in $[Ca^{2+}]_i$ and did not show signs of $[Ca^{2+}]_i$ oscillations. The maximum $F/F_0$ between the slow and rapid rate group was found to be statistically different ($p < 0.05$) as was area under the curve analysis ($p < 0.05$). Neither rate in the 60% injury group produced $[Ca^{2+}]_i$ oscillations; neither group returned to baseline fluorescence within the measurement period. Both groups showed steep increases in $F/F_0$. When compared, maximum $F/F_0$ and area under the curve for both groups were statistically different ($p < 0.05$).

The data clearly show two phenomena. Foremost, at a single strain rate, the $[Ca^{2+}]_i$ of injured neurons increased as applied strain is increased. More importantly, however, the data shows that as strain rate was increased, $Ca^{2+}$ response of injured neurons was exacerbated in each injury group. This suggests that forces exerted on cultures during mechanical injury may produce similar results under different loading conditions; i.e., cells that experience a low strain, high strain rate injury may experience similar pathology, dysfunction and viability as that of cells that experience a high strain, low strain rate injury. Consequently, when statistical analysis was done to compare the area under the curve and maximum normalized intensity for the 20% strain group injured at a strain rate of $70s^{-1}$ and the 40% group injured at a strain rate of $30s^{-1}$, there was no statistical difference between the two groups ($p > 0.05$). This was also found to be true of the maximum $F/F_0$ of cultures exposed to 40% strain at a strain rate of $70s^{-1}$ and cultures exposed to 60% strain at a strain rate of $30s^{-1}$ This suggests that cultures injured at lower strains (20-40%) may experience injury responses similar those injured at higher strains

(+60%) by simply altering the strain rate. Two-way ANOVA showed that both strain and strain rate had an effect on both the max $F/F_0$ and area under the curve. Two-way ANOVA also indicated that strain and strain rate showed a significant interaction with each other.

Iwata *et al*., (2004) proposed a mechanism for TTx blocking of $[Ca^{2+}]_i$ elevation. During injury, mechanical perturbation of the cell causes voltage gated sodium channels to open causing neurons to become depolarized. This depolarization activates voltage gated calcium channels allowing $Ca^{2+}$ to enter the cell. Due to the nature of the injury process, the cell eventually becomes overwhelmed by a massive influx of $Ca^{2+}$. This elevated level of $Ca^{2+}$ activates proteases and other enzymes. These proteases and enzymes begin a deleterious process, which ultimately ends in cellular dysfunction and/or cell death.

TTx proved capable of significantly reducing increases in $[Ca^{2+}]_i$. When compared to cultures not treated with TTx prior to injury, the two groups were found to be statistically different ($p < 0.05$). When strain rate was increased, TTx was no longer capable of blocking rises in $[Ca^{2+}]_i$. Cultures pretreated with TTx and injured at strain rates > $20s^{-1}$ showed a significant rise in $[Ca^{2+}]_i$. Maximum $F/F_0$ and area under the curve of these cultures were found to be statistically different ($p < 0.05$) when compared to pretreated cultures exposed to 50% strain at a strain rate of $20s^{-1}$. This data suggests that at high strain rates, the TTx block of voltage gated sodium channels no longer affects the fluorescent response of injured neurons. It is possible to speculate that an alternative means of elevating $[Ca^{2+}]_i$ of the cell may be activated. Wolf *et al*., (2001) demonstrated that the fluorescent response is due to an external source of $Ca^{2+}$ and is not a result of

release of intracellular stores of $Ca^{2+}$. However, because of the observed changes in fluorescent response as strain rate is increased, it is possible that a completely different type of injury, governed by different mechanisms, is being observed. Therefore, one could speculate that at high strain rates, it is possible that the exacerbated response is due to release of intracellular $Ca^{2+}$ stores.

TTx reversibly blocks voltage gated sodium channels. An alternative hypothesis is that the forces generated by high strain rate injuries are strong enough to reverse the TTx block on sodium channels.

The work described in Yuen *et al.* (2009), characterized injury conditions that yielded no $[Ca^{2+}]_i$ increases and described them as sub-threshold injuries (< 5% strain). However, repeated sub-threshold insults, within an appropriate refractory period, elicited exacerbated levels of $[Ca^{2+}]_i$ analogous to injuries on the order of 20% strain. The data presented in this study, while different in nature, holds the same underlying principle; characterizing loading conditions of traumatic brain injury models is a complex system with many variables. Characterizing severity of brain injury may not be as concrete when one considers the rate of injury. In light of the data presented, injuries that were once categorized as "mild" might actually be considered to be moderate or severe. Different mechanical loading of cells can yield similar responses with respect to the measurement technique used. These considerations become important when applying the data to larger *in vivo* and clinical models.

# CHAPTER 4

# EFFECT OF ACUTE STRETCH INJURY ON ACTION POTENTIAL AND NETWORK ACTIVITY OF RAT NEOCORTICAL NEURONS IN CULTURE

## 4.1 Background and Significance

In human patients and animal models, traumatic brain injury (TBI) can cause deficits in motor, cognitive, and behavioral function including problems with memory, attention, and task execution (Ashman *et al.*, 2006; Goforth *et al.*, 2011). These dysfunctions may reflect neuronal loss (Ellis *et al.*, 1995; Magou *et al.*, 2011), disconnection of critical network circuitry, or changes in synaptic activity (Zhang *et al.*, 1996; Goforth *et al.*, 1999; Kao *et al.*, 2004; Cohen *et al.*, 2007; Goforth *et al.*, 2011). Changes in synaptic activity may reflect an imbalance in the relationship between excitatory and inhibitory signaling in cells (Cohen *et al.*, 2007)

*N*-methyl-D-aspartate receptor (NMDA) and the α-amino-3-hydroxy-5-methyl-4-isoxazolepropionic acid (AMPA) receptor are responsible for the primary excitatory currents at the synapse. These currents promote excitatory post-synaptic potentials (EPSPs) necessary for signal transduction. Prior research has been aimed at investigating the effects of stretch injury on the function of these receptors and their kinetics.

A mechanical injury system (Ellis *et al.* (1995), similar to the system described in Chapter 2, has been used to show that there are significant changes in NMDA receptors after injury (Zhang *et al.*, 1996). This study illustrated that following mechanical injury NMDA receptors of injured neurons showed a large increase in conductance at

hyperpolarized potentials when compared to non-injured neurons. This study ultimately concluded that the effect was due to a loss in sensitivity of NMDA receptors to $Mg^{2+}$ blocking. The study also showed that the ability of $Mg^{2+}$ to block NMDA currents at higher concentrations was severely diminished as well (Zhang *et al.*, 1996).

Another study revealed that mechanical injury alters AMPA receptor function (Goforth *et al.*, 2004). In this study, injured neurons showed significantly larger AMPA induced currents than non-injured neurons. These cells also exhibited larger average steady state current densities and longer decay time constants.

In contrast to AMPA and NMDA receptors, the γ-aminobutyric-acid (GABA) receptor regulates the inhibitory post-synaptic currents at the synapse. Similarly, research has shown that stretch injury induces changes in $GABA_A$ currents (Kao *et al.*, 2004). Neurons that were exposed to stretch injury have shown dramatic increase in $GABA_A$ potentiation and current density.

Despite these findings, there is still much to discover and understand about the mechanisms underlying the deficits caused by TBI. The literature reviewed by the author indicates that much research is being done on synaptic currents and the changes in kinetics and function of these currents. Since it is indicated in these studies that neurons which have undergone stretch injury show changes in all major synaptic currents, one could speculate that it would also be important to investigate how these changes affect over all network activity.

## 4.2 Materials and Methods

### 4.2.1 Neuronal Culture

All neuronal culture was performed as described in Chapter 2.

### 4.2.2 Stretch Injury to Neuronal Cultures

All cultures were injured on DIV11-12 the 6-well module described in Chapter 2. Cultures were placed in the injury chamber and the chamber was pressurized to produce 60% strain at a rate of $30s^{-1}$ (60% strain was achieved in approximately 0.02s). Following injury, cultures were incubated at 37°C in 5%$CO_2$. Control, measurements were taken from neurons located outside of the stretch zone; these neurons were considered to be non-injured. Since voltage gated sodium channels play a major role in action potential propagation, one could hypothesize that changes in the action potential of injured neurons should coincide with changes seen in the expression of voltage gated sodium channels of injured neurons. The changes in voltage gated sodium channel expression were found to occur approximately 20 minutes after injury (Iwata et al 2004, von Reyn et al 2009, Yuen et al 2009). For these reasons, all recordings were performed 30 minutes after injury. The experiments outlined in this chapter were performed in the absence of a cell free zone.

### 4.2.3 Electrophysiology of Injured Neurons

Whole cell recordings were acquired using an Axopatch 200B in fast current clamp mode. Measurements of membrane potential were filtered at 10kHz and digitized at 25kHz using a Digidata 1440A. All recordings were performed in extracellular recording solution containing: (all in mM) 140 NaCl, 4 KCl, 10 HEPES, 2 $CaCl_2$, 2 $MgCl_2$, 10

Glucose; pH adjusted to 7.4. Recordings were obtained using patch electrodes having a resistance of 4-6MΩ. Patch electrodes were filled with intracellular solution containing: (all in mM) 120 KCl, 0.2 EGTA, 30 HEPES, 5 Na-ATP, 0.4 $Na_2$-GTP, 5 $MgCl_2$, 0.1 $NaH_2PO_4$; pH adjusted to 7.2. Any additions and or substitutions to these solutions are labeled. Prior to recording, all cultures were gently rinsed in extracellular solution. All recordings were performed at 25°C.

**4.2.3.1 Passive Membrane Properties.** Once access to the cell was achieved, resting membrane potential (RMP) was monitored and recorded. For all experiments, cells were rejected if resting membrane potential was less negative than -35 mV. Input resistance ($R_m$) was measured by injecting a 30pA hyperpolarizing current.

**4.2.3.2 Action Potential Measurements.** For the following experiments, all cells were given a constant hyperpolarizing holding command to maintain resting membrane potential at -60mV. Spontaneous action potentials (AP) were recorded for 2.5 minutes at this resting potential. Action potentials (AP) were elicited by injecting cells with a brief 3ms depolarizing current (100-400pA).

## 4.3 Results

### 4.3.1 Characterization of Action Potentials and Spontaneous Activity

Cells were held at a resting potential of -60mV and stimulated via depolarizing current injection for 3ms to stimulate action potentials. Once a cell's ability to fire action potentials was verified, cells were continuously stimulated at a rate of 1Hz. During stimulation, the cells were perfused with the voltage gated sodium channel blocker TTx (1µM) to determine if action potentials were produced by inward Na currents. Neurons

exhibited inability to fire action potentials shortly after administration of TTx (Figure 4.1).

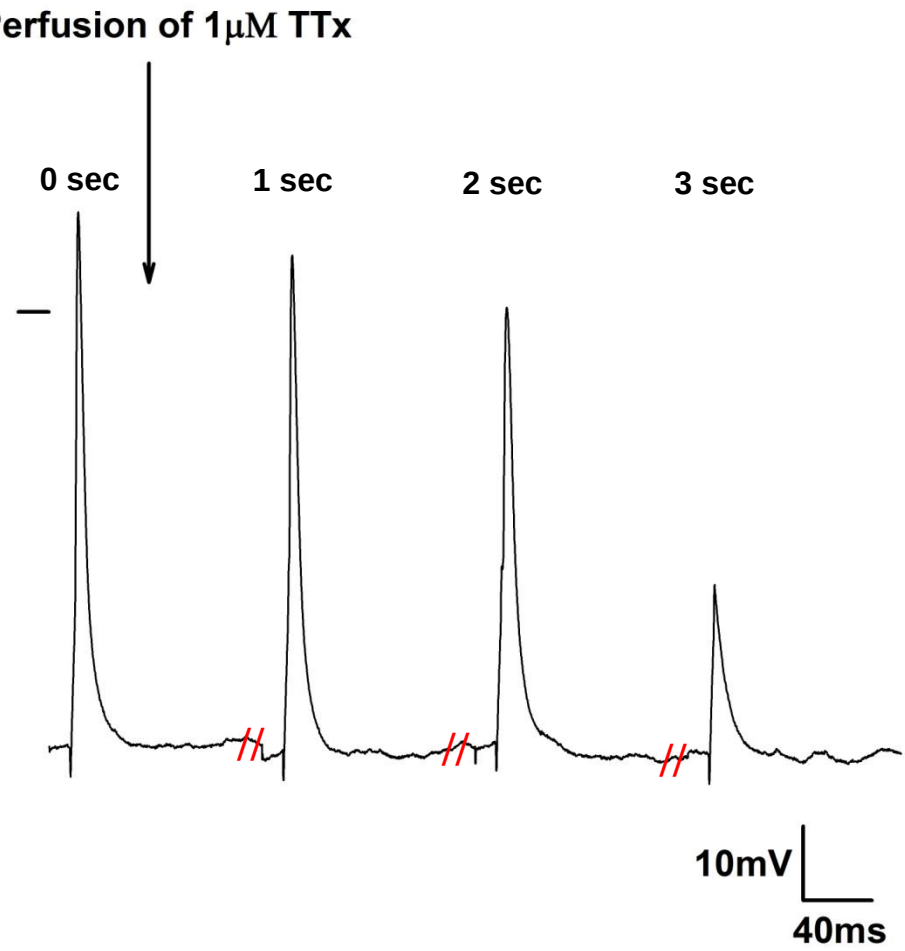


**Figure 4.1** Action potentials stimulated by brief (3ms) depolarizing stimulus (40pA) at a frequency of 1 Hz. TTx was administered during recording. Recordings show TTx diminishes action potential firing.

Spontaneous action potentials were collected by holding cells at a resting potential of -60 mV; no additional current injection was applied. Cells exhibited spontaneous action potentials and sub-threshold events (Figure 4.2, left). To investigate if spontaneous electrical activity was a result of synaptic network activity, cells were perfused with a solution containing the $GABA_A$ receptor antagonist bicuculline (100μM)

and the glutamate receptor antagonist kynurenic acid (3mM). All network activity was blocked shortly after administration of bicuculline and kynuernic acid. Also, cells exhibited a small hyperpolarization during application of drugs (Figure 4.2, right).

### 4.3.2 Comparison of Passive Membrane and Action Potential Properties

Resting membrane potential, membrane resistance, threshold for action potential, and action potential amplitude were recorded for non-injured and injured neurons, (Table 4.1). Passive membrane properties, measured as resting membrane potential (RMP) and input resistance ($R_m$), as well as action potential threshold and amplitude were not significantly different in injured neurons.

**Table 4.1** Table showing passive and action potential properties. Differences between injured and non-injured neurons did not reach significance.

| | **Non-Injured (n=10)** | **Injured (n=10)** |
|---|---|---|
| | **Passive Membrane Properties** | |
| **RMP (mV)** | -40 ± 7 | -39 ± 5 |
| **$R_M$ (GΩ)** | 0.92 ± 0.60 | 1.27 ± 0.83 |
| | **Action Potential Properties** | |
| **Threshold (mV)** | -38 ± 3 † | -35 ± 1 |
| **Amplitude (mV)** | 64 ± 14 | 69 ± 10 |

### 4.3.3 Stretch Injury Reduces Spontaneous Electrical Activity

Cultures were exposed to 60% strain (n=16) at a rate of $30s^{-1}$. Control measurements were taken outside of the stretch zone (n=13). Typical tracings of injured and non-injured cultures are shown in Figure 4.3.

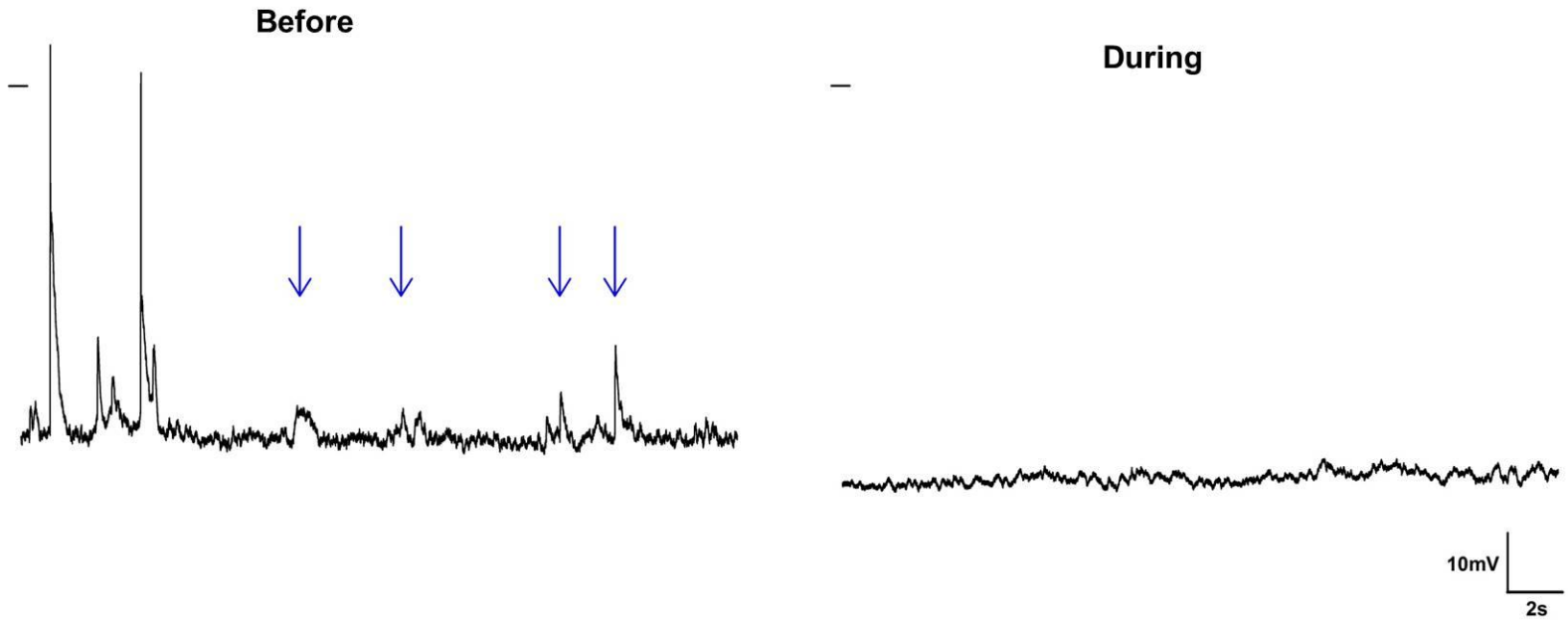


**Figure 4.2** Effect of 100µM bicuculline and 3mM kynurenic acid on spontaneous electrical activity.

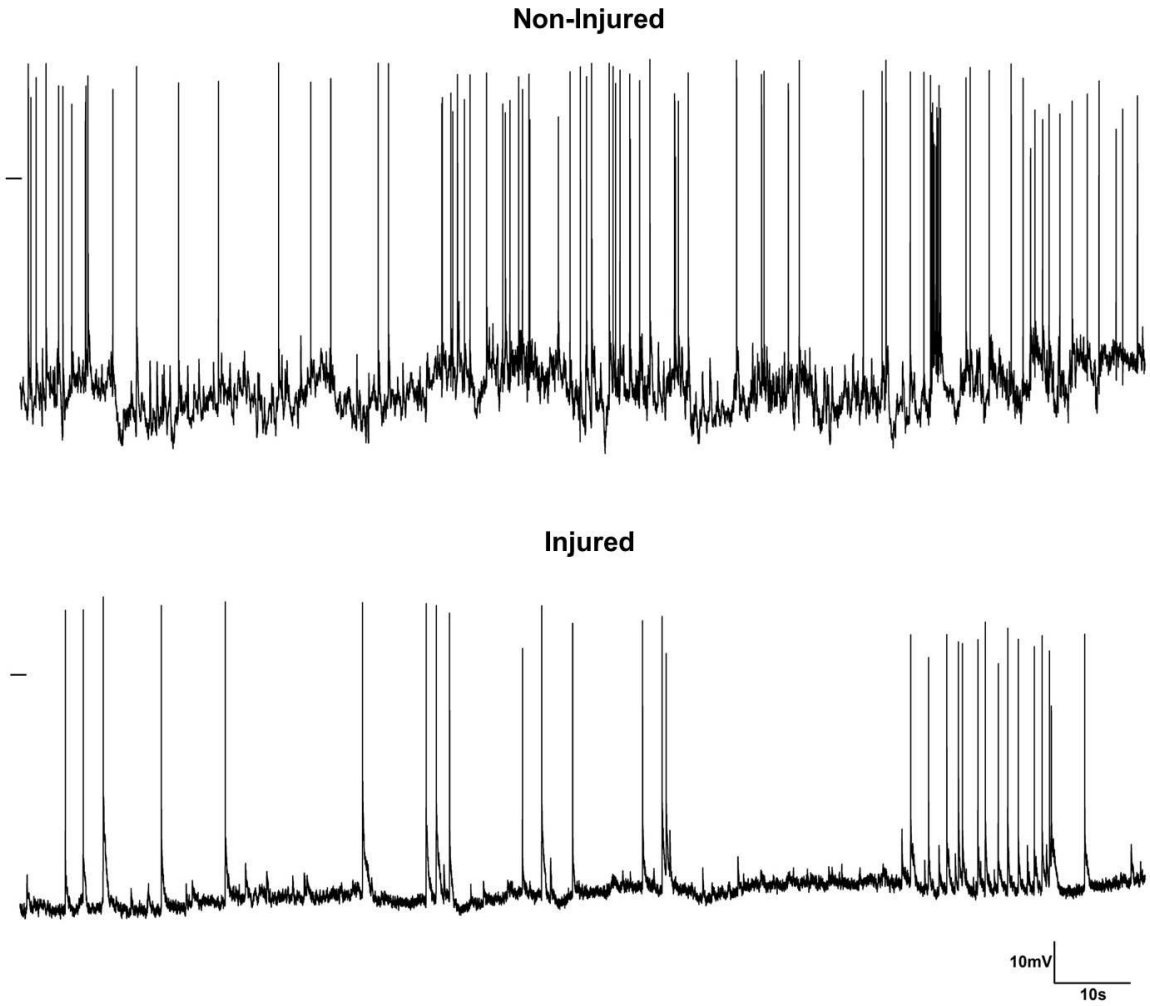


**Figure 4.3** Recordings of spontaneous electrical activity in non-injured and injured neurons.

Spontaneous events were counted and placed into two categories: action potentials and sub-threshold events, (Table 4.2). Sub-threshold events were defined as events that caused the cell to depolarize but not reach the threshold for AP generation.

**Table 4.2** Frequency of sub-threshold depolarizations and APs during a 150s recording period. Differences between non-injured and injured neurons that were found to be statistically significant via a Mann-Whitney U test ($p < 0.05$) are indicated with *.

| | Non-Injured | Injured |
|---|---|---|
| Sub-threshold | 78 ± 67 | 70 ± 31 |
| Action Potentials | 83 ± 54 | 28 ± 26* |
| Total | 161 ± 95 | 98 ± 44 |

Frequency of action potential firing was calculated as "action potentials/min" for each recording and compared, (Figure 4.4). Generally, non-injured neurons displayed higher frequencies of spontaneous action potential firing than injured neurons. Data are displayed by group (non-injured vs. injured) and by experimental day to illustrate that despite the variability between experimental days, significant differences are observed.

### 4.3.4 Action Potential Firing Pattern

Spontaneous recordings were further analyzed to investigate whether firing patterns within each group differed. This was done by analyzing the inter-AP interval for each event in a spontaneous recording session. Inter-AP interval was defined as the amount of time between the current AP in a trace and the previous AP. Inter-AP interval for all traces in each group were accumulated and plotted in histograms (Figure 4.5).

This data was also plotted as a normalized cumulative distribution function, (Figure 4.6) to identify if the two populations were significantly different.

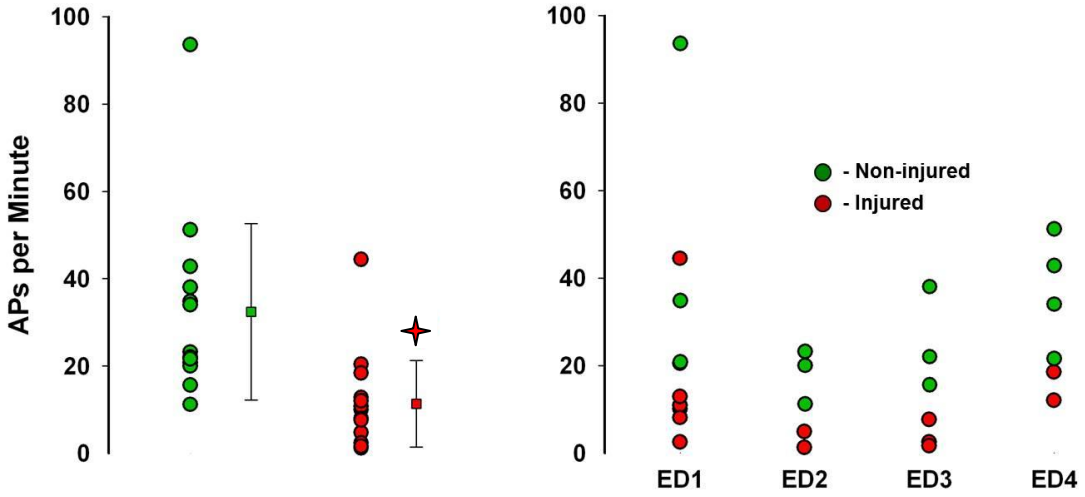


**Figure 4.4** Action potential (AP) frequency by group and experimental day (ED). Significance was determined by a Mann-Whitney U test ($p < 0.05$) and is indicated by *.

### 4.3.5 Analysis of Bursting Activity

Distribution analysis of inter-AP intervals indicated that uninjured cultures exhibited a large number of events with inter-AP intervals of 0-2s. For this analysis, a bursting event was defined as an event that had an inter-AP interval ≤ 1s. A representative burst is illustrated in Figure 4.7.

For each cell (n=13 non-injured, n=16 injured) the number of bursts were counted and distribution of bursting activity within each group was analyzed. Data were plotted in histograms illustrating the distribution of the cell-by-cell busting activities in each group, (Figure 4.8). Average number of bursts per cell was calculated and is represented in Table 4.3.

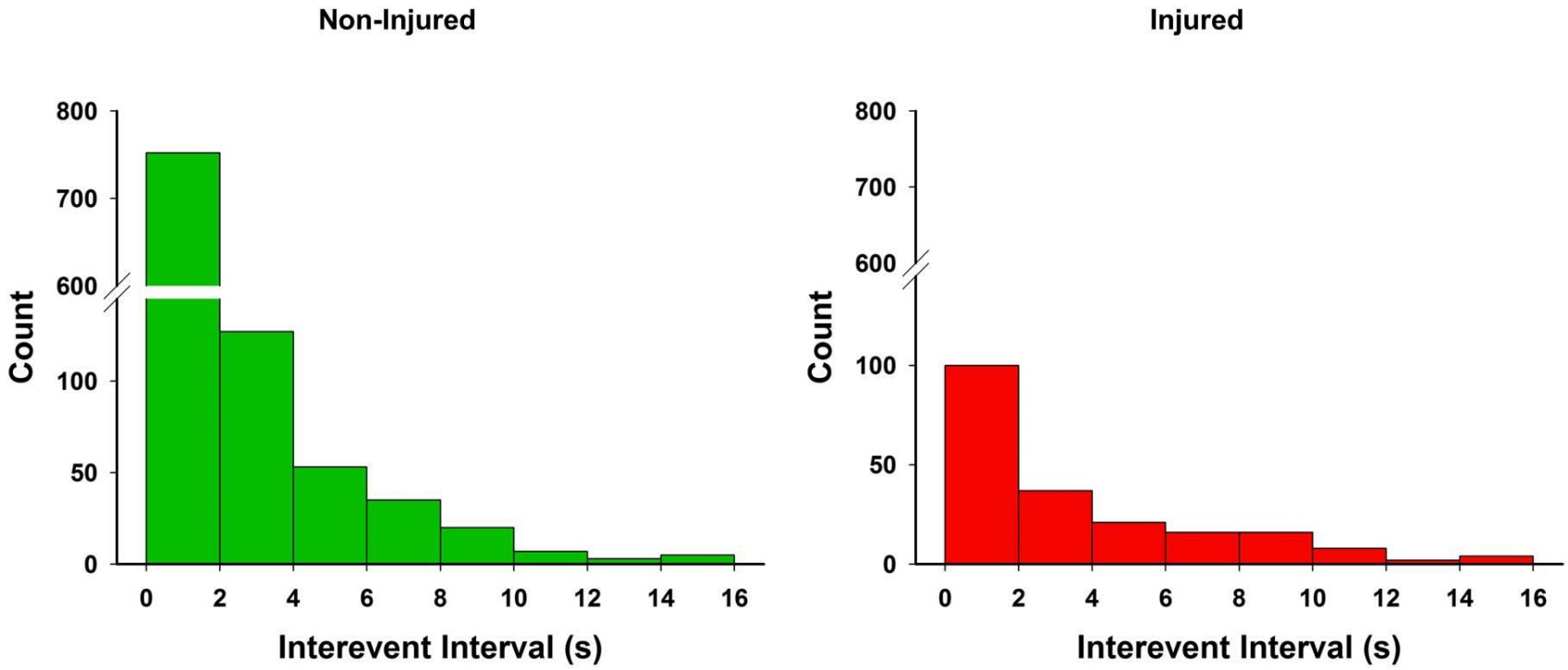


**Figure 4.5** Histograms showing the distribution of inter-AP intervals observed in non-injured (n=13) and injured neurons (n=16).

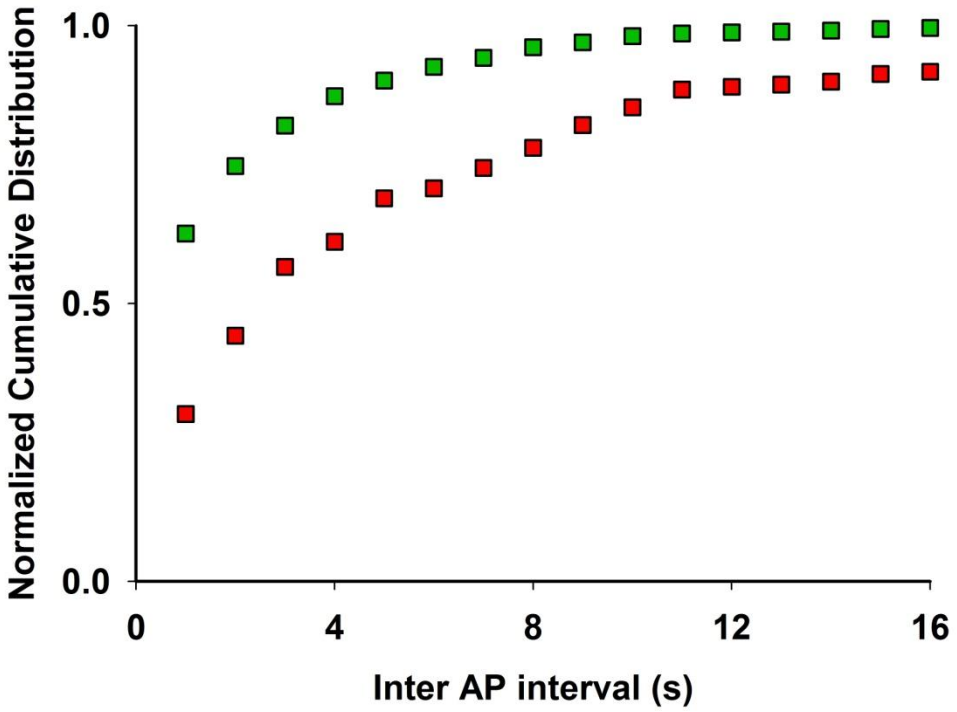


**Figure 4.6** Normalized cumulative distribution plot. Kolmogorov-Smirnov test yields that the distributions are significantly different ($p < 0.05$)

### 4.3.6 Analysis of Action Potential Waveform Properties

**4.3.6.1 Analysis of Spontaneous Action Potentials.** For each cell (n=13 non-injured, n=16 injured) a representative action potential, during spontaneous activity recording was chosen. Action potential duration at 50% amplitude ($APD_{50}$) and 90% amplitude ($APD_{90}$) was calculated for each action potential (Figure 4.9).

$APD_{50}$ for non-injured and injured neurons appeared to remain unchanged as a result of stretch injury. However, $APD_{90}$ of injured neurons was significantly increased, (Figure 4.10).

**Table 4.3** Table showing spontaneous burst activity properties. Significance determined with a Mann-Whitney U test is indicated by *.

| | Non-Injured | Injured |
|---|---|---|
| Cells tested | 13 | 16 |
| Bursting cells | 13 | 13 |
| Bursts per cell | 50 ±52 | **12** ± **19*** |

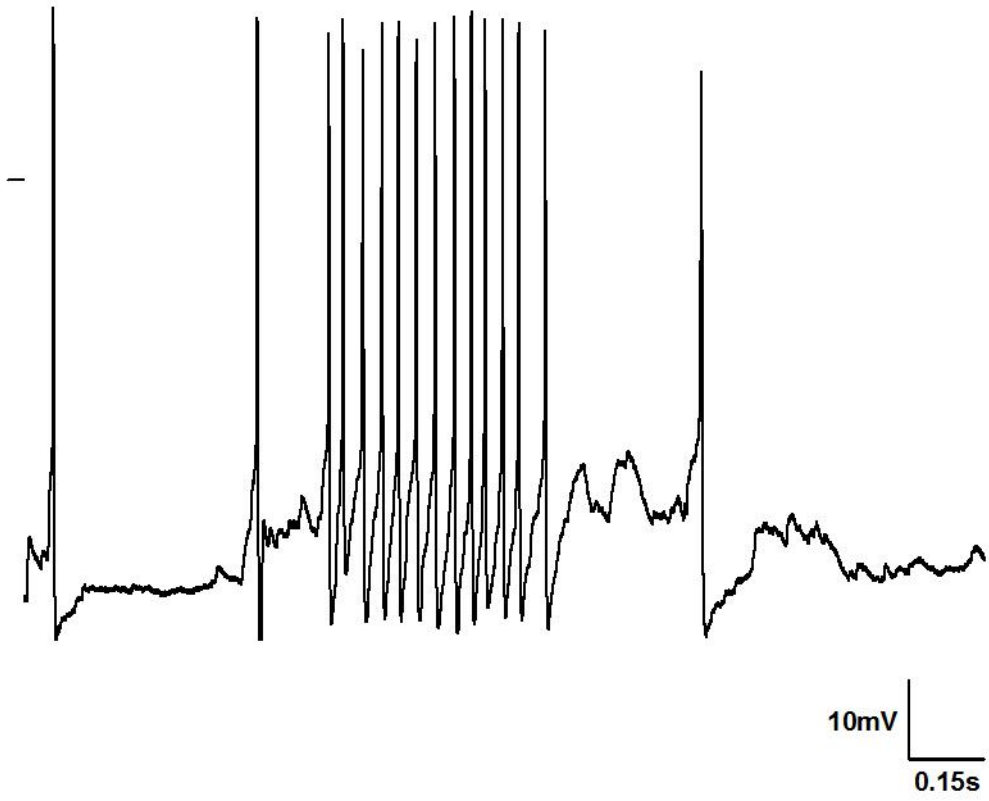


**Figure 4.7** Trace of a representative burst during recording of spontaneous electrical activity.

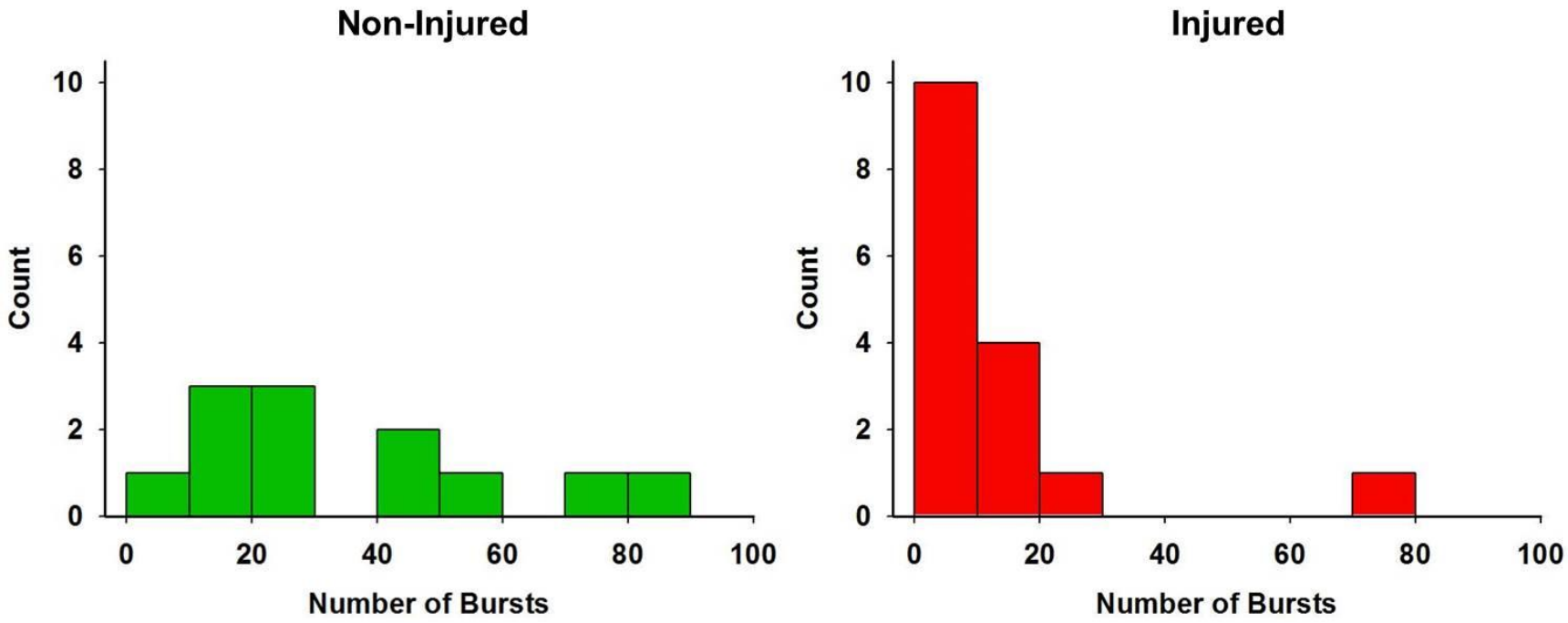


**Figure 4.8** Histograms showing the cell-by-cell counts of bursting activities observed in each 150 sec recording period.

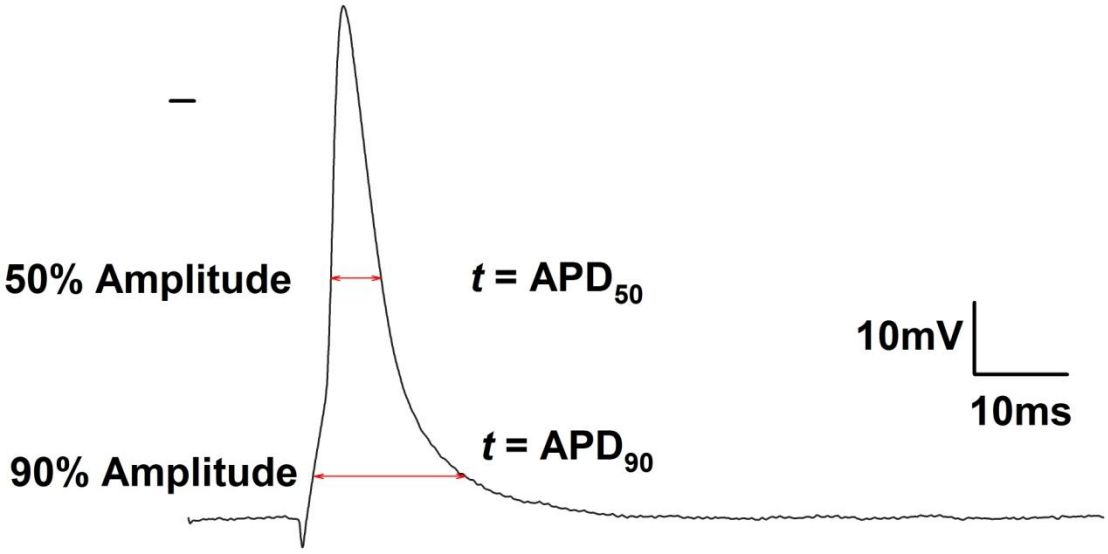


**Figure 4.9** Method for calculating action potential duration (APD). 50% and 90% amplitude were calculated with respect to the peak of the action potential.

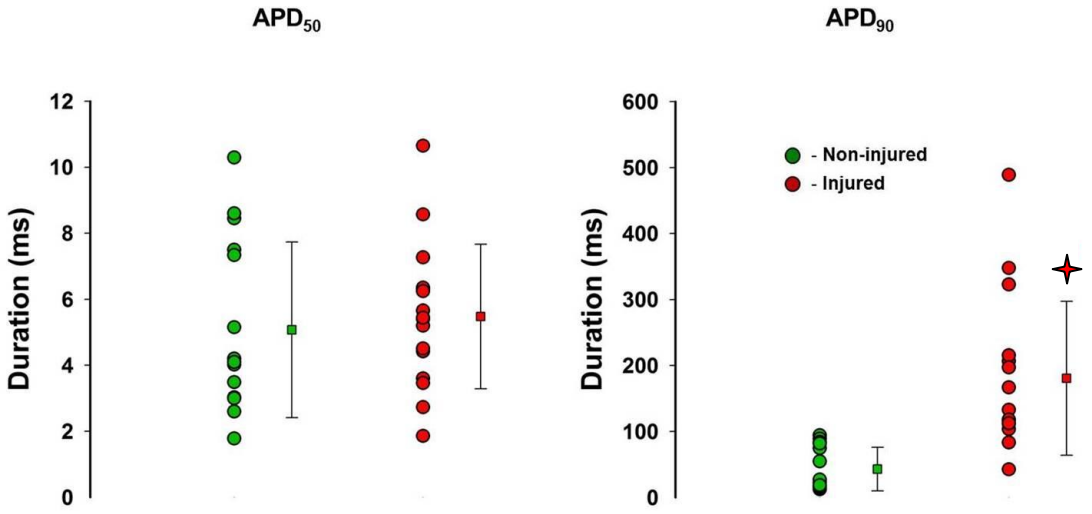


**Figure 4.10** $APD_{50}$ and $APD_{90}$ of spontaneous APs. Significance was determined by a Mann-Whitney U test. ($p < 0.05$) as indicated (*).

The increase in $APD_{90}$ of injured cultures warranted further investigation. Further inspection of spontaneous action potential recordings yielded the occurrence of three types of action potentials waveforms common to both non-injured and injured neurons (Figure 4.11). Waveform I exhibited strong after hyperpolarization (AHP). Waveform II

did not have an after hyperpolarization. Instead during action potential repolarization, a secondary depolarization occurred before the membrane potential reached baseline levels. This second depolarization decayed slowly and lasted anywhere from 150-400ms. Waveform III also did not have an after hyperpolarization, but rather returned to baseline slowly. Generally, Waveform III showed $APD_{90}$ greater than Waveform I but less than Waveform II.

Census of action potential waveforms was taken for each cell (n= 13 non-injured, n= 16 injured) and presented in Table 4.4. Cells commonly exhibited one or more action potential styles. Therefore, a census was done by noting presence or absence of each type of action potential in a cell.

**Table 4.4** Census of each AP waveform observed in non-injured and injured neurons. Some cells displayed more than one AP waveform. Significance was determined by a two-way Chi-square analysis and is indicated by *.

| | **Waveform I** | **Waveform II** | **Waveform III** |
|---|---|---|---|
| **Non-injured** | 10 | 5 | 11 |
| **Injured** | 1 | 16 | 14 |
| **$p < 0.05$** | * | * | - |

**4.3.6.2 Analysis of Stimulated Action Potentials.** For each cell (n=13 non-injured, n=16 injured) action potentials were measured via stimulation with a brief (3ms) depolarizing current (100-400pA). A representative action potential was chosen for each cell. $APD_{50}$ and $APD_{90}$ was calculated for each action potential, (Figure 4.9).

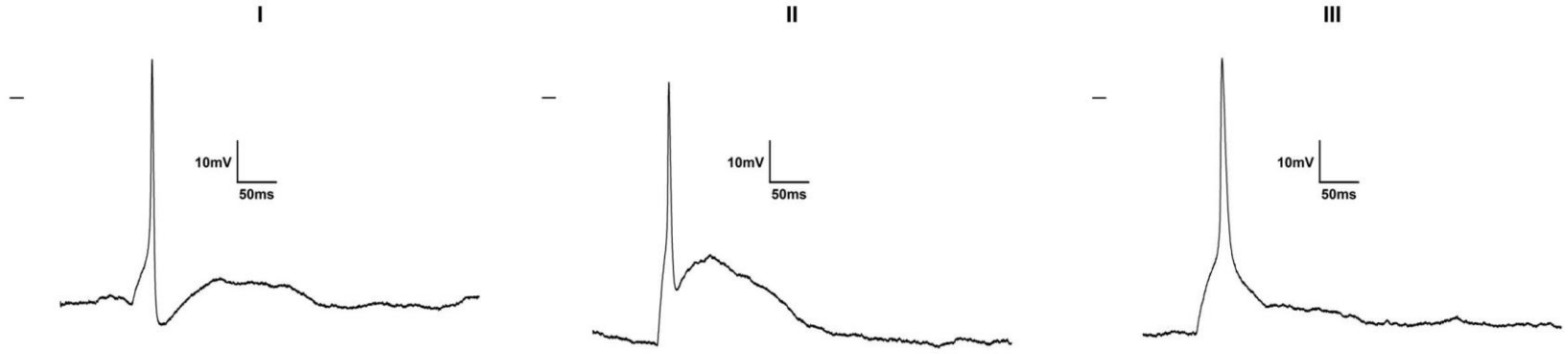


**Figure 4.11** Representative action potentials of the three types of waveforms observed in spontaneous action potential recordings.

$APD_{50}$ and $APD_{90}$ were found to be similar in both groups (Figure 4.12).

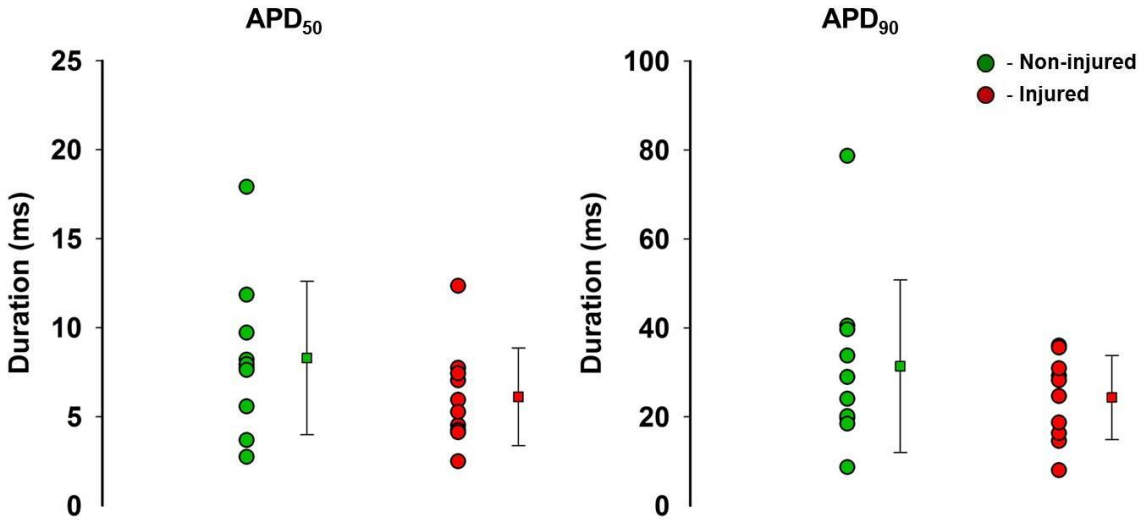


**Figure 4.12** $APD_{50}$ and $APD_{90}$ for stimulated APs in non-injured and injured neurons.

## 4.4 Discussion

This study focused on exploring electrical activity of stretch injured neuronal cultures. Primary focus for this analysis was to determine if changes in the behavior of the neuronal network and action potentials occurred subsequent to stretch injury. The most critical finding in this study was that spontaneous network activity was depressed as a result of mechanical injury. Injured cultures showed a 66% reduction in spontaneous action potential frequency after mechanical injury ($p < 0.05$). Despite the cell-to-cell variability found in the data, (Figure 4.4) it was evident that non- injured neurons generally exhibited higher action potential firing frequencies than injured neurons. Since it was verified that spontaneous action potential firing was a result of synaptic network activity (Figure 4.2), variability between experimental days might be attributed to variability in cell plating density.

Since, changes in synaptic activity showed severely depressed rates of firing, it is logical to speculate that these same changes could also yield different firing patterns. When the distribution of inter-AP interval was compared (Figure 4.5), initial observation showed a large decrease in overall number of events in neurons that had been mechanically injured. More importantly, the histograms show a clear difference in the level of activity within the 0-2s inter-AP interval range. The cumulative distribution plot showed that injured neurons not only exhibit reduced firing rates, but also exhibit an overall pattern of spontaneous action potential activity.

These findings point toward a change in bursting activity, a point confirmed by analysis of bursting activity. Injured neurons also exhibited a lowered average number of bursts per cell ($p < 0.05$), (Table 4.3). Distributions of bursting on a cell-by cell basis showed that most injured neurons exhibited less than 10 bursts per recording session, whereas non-injured neurons exhibited higher numbers of bursts per recording and, as a population, spanned a larger range of bursting frequencies, (Figure 4.8).

Aside from changes in network activity, changes were observed in the waveform of spontaneous action potentials. No changes were seen in $APD_{50}$, however, $APD_{90}$ of injured neurons was much greater than that of non-injured neurons (Figure 4.10). When the waveforms were compared, injured cultures showed almost no incidence of action potentials with an after hyperpolarization (Waveform I). Rather, the action potential most prominent for injured neurons was Waveform II. the incidence of Waveform II was found to be statistically different between the two groups, (Table 4.4). Waveform II shows the activation of a depolarizing current not seen in Waveform I or III. However, it is interesting to note that these changes were not seen in stimulated action potentials

(Figure 4.12). Non-Injured and injured neurons showed no statistical difference in $APD_{50}$ or $APD_{90}$.

Changes in the repolarization of neurons may suggest that there are changes in repolarizing currents being expressed in a cell. Currents that are widely known to be responsible for repolarization and after hyperpolarization in neurons are K currents (Storm, 1987; Wu & Barish, 1992; Korngreen & Sakmann, 2000). However, since the changes in action potential waveform do not translate to stimulated action potentials, it is likely that the change is due to alterations in regulation of K channel kinetics rather than changes in channel number or function. It is also possible that by eliciting action potentials via current stimulation, the effects of injury seen in the $APD_{90}$ of injured neurons may go unseen. Additionally, spontaneous recordings were done with no disturbances to the cell's native state. Stimulated action potentials were collected at a rate of 1 Hz. This may have created an artificial "steady-state" of activity in cells, thereby negating the natural state of the cell and masking the changes seen in spontaneous $APD_{90}$.

Furthermore, no changes were seen in resting membrane potential, input resistance, threshold, or action potential amplitude. This indicates that injured cells did not exhibit signs of compromised membrane integrity, changes in passive ionic currents, or ability to fire action potentials. The changes seen in this study point to overall changes in network activity in the form of depressed bursting and spontaneous AP firing. In addition, changes seen in $APD_{90}$ suggest a possible change in the kinetics of repolarizing $K^+$ currents.

# CHAPTER 5

# DISCUSSION AND CONCLUSIONS

In Chapter 1, the author proposed the notion of exploring the effects of strain rate more closely. In order to do this, a system that could achieve high strain rates while controlling strain and strain rate accurately and independently needed to be designed. The system showed the ability to accurately and reproducibly control both pressure pulse magnitude and rate of delivery. Testing done on cultured neurons showed morphologies and compromised cell viabilities similar to that published in the literature (Smith *et al.*,1999; Wolf *et al*., 2001; Iwata *et al*., 2004). The system is able to achieve strain rates > $100s^{-1}$.

Changes in intracellular $Ca^{2+}$ levels were used as an indicator for severity of injury. Studies done on the effects of rate showed a change in the injury response at each strain level. Maximum $F/F_0$ of the 20% injury group showed no significant differences when strain rate was modulated. However, when the time course intensity traces were compared, there were clear differences in the behavior. The $30s^{-1}$ group exhibited slow oscillating fluorescent peaks that returned to baseline intensity, whereas the $70s^{-1}$ showed rapid spiking and sustained elevation of $[Ca^{2+}]_i$. To further characterize this behavior, area under the curve was examined for each time course intensity trace. When compared, the $30s^{-1}$ and $70s^{-1}$ group statistical statistically different ($p < 0.05$).

A similar phenomena was seen with the 40% injury group. At slower rates, cultures behaved by exhibiting slow oscillations that, generally, returned to baseline. When cultures in this injury group were injured at a rapid rate, the cells experienced steep

rises in $Ca^{2+}$ and did not show signs of $Ca^{2+}$ oscillations. This behavior may reflect the threshold at which cells are capable of responding to injury. The forces produced from an injury of 40% strain at a rate of $70s^{-1}$ may elicit a $Ca^{2+}$ response that exceeds the buffering capabilities of the cell.

The same could be said about the 60% group. When injured at a strain of 60%, neither group rate produced fluorescent $Ca^{2+}$ oscillations. All cultures displayed a steep rise in $Ca^{2+}$ fluorescence, much greater than that of the 20% and 40% groups, and did not return to baseline within the measurement period. 60% strain may also represent a threshold for cell response to injury.

It is clear from the data that both rate and strain rate contribute to the injury response of stretch injured neurons. One underlying concept in this project was the idea that injuries at lower strains but higher rates could elicit cellular responses similar that of a high strain low strain rate injury. When statistical analysis was done to compare the area under the curve for the 20% strain group at a strain rate of $70s^{-1}$ and the 40% group at a strain rate of $30s^{-1}$, there was no statistical difference between the two groups ($p > 0.05$). This implies that (based on $Ca^{2+}$ response) the cultures experienced similar injuries under different loading conditions.

In terms of strain, it is clear that 40% and 60% represent the upper bound for $Ca^{2+}$ response in stretch injured neurons. The 20% strain group and 40% strain $30s^{-1}$ rate group were the only experiments that exhibited clear fluorescent $Ca^{2+}$ oscillations. It would be interesting to return to these experiments to investigate the effect of rate at lower strains. Sub-threshold strain levels that do not yield a $Ca^{2+}$ response, such as those

described in Yuen *et al.* (2009), could be tested. The strain rate could be modulated at these strain levels to elicit an injury damaging enough to produce a $Ca^{2+}$ response.

TTx experiments confirmed two main points. Pretreatment with TTx indeed reduces intracellular entry of $Ca^{2+}$ after stretch injury. However, when the rate of injury was increased, TTx was no longer capable of completely blocking the $Ca^{2+}$ response. A supplemental study could be done to see if this effect is a result of the inefficacy of TTx or an alternative mechanism of $Ca^{2+}$ elevation in rapidly stretch injured neurons. Cultures could be pretreated with TTx and injured under two conditions; in the presence of 0mM $Na^{+}$ or in the presence of 0mM $Ca^{2+}$. Under these conditions, it could be elucidated if the effect is a result of TTx no longer blocking voltage gated sodium channels or the possibility of an alternative method of $Ca^{2+}$ entry into the cytosol. It is quite possible that high strain rate injuries have exacerbated effects on alternative methods of $Ca^{2+}$ entry such as those mentioned in Wolf *et al.* (2001) (P/Q and N-type voltage gated $Ca^{2+}$ channels and $Na^{+}$-$Ca^{2+}$ exchanger).

Investigation of network activity and action potential properties yielded two major findings. First, there was a decrease in spontaneous electrical activity of injured neurons. Injured neurons not only showed a decrease in rate of action potential firing, but changes in bursting activity. It is unknown what the mechanism behind depression of spontaneous action potential firing is. However, knowing that these action potential are a product of synaptic activity, one could speculate that this phenomenon is similar to the results seen in Goforth *et al.* (2011). It would be interesting to combine the pharmacological agents used in Wolf *et al.* (2001) and Iwata *et al.* (2004) to investigate the possibility of preventing synaptic activity depression after injury. Neurons could be

injured in the presence of TTx, and ω-conotoxin MVIIC. Pharmacological agents can be washed off prior to spontaneous activity recordings to see if network activity remained intact.

Kao et al., 2004 showed that $GABA_A$ potentiation is severely increase after stretch injury indicating that there is a high potential for inhibition in injured neurons. Goforth et al 2011 showed that synaptic activity could be restored by blocking $GABA_A$ receptors with bicuculline methiodide (BMI). It would be interesting to see if spontaneous action potential firing could be restored by treating cells with BMI after stretch injury. One could speculate that positive results may suggest an over expression of $GABA_A$ channels and in parallel testing could be done to test this hypothesis.

In conclusion the work done here may be used to begin to describe the processes involved in and affected by stretch injury. It has been shown that strain rate is an important factor to consider in the injury process and in characterizing the injury model. Electrophysiological data strongly suggest the depression of spontaneous electrical activity after stretch injury. While it has not yet been looked at, it would be important to investigate these results under the strain rate paradigm.

## REFERENCES

Adams, J.H., Doyle, D., Ford, I., Gennarelli, T.A., Graham, D.I. & McLellan, D.R. (1989) Diffuse axonal injury in head injury: definition, diagnosis and grading. *Histopathology*, **15**, 49-59.

Adams, J.H., Graham, D.I. & Gennarelli, T.A. (1983) Head injury in man and experimental animals: neuropathology. *The European Journal of Neurosurgery*, **32**, 15-30.

Arbogast, K.B. & Margulies, S.S. (1998) Material characterization of the brainstem from oscillatory shear tests. *J Biomech*, **31**, 801-807.

Arbogast, K.B. & Margulies, S.S. (1999) A fiber-reinforced composite model of the viscoelastic behavior of the brainstem in shear. *J Biomech*, **32**, 865-870.

Arbogast, K.B., Thibault, L.E., Pinheiro, B.S., Winey, K.I. & Margulies, S.S. (1997) A high-frequency shear device for testing soft biological tissue. *Journal of Biomechanics*, **30**, 757-759.

Ashman, T.A., Gordon, W.A., Cantor, J.B. & Hibbard, M.R. (2006) Neurobehavioral consequences of traumatic brain injury. *The Mount Sinai journal of medicine, New York*, **73**, 999-1005.

Callister, W.D., Jr. (2007) *Materials Science and Engineering an Introduction*. John Wiley & Sons, York, PA.

Cargill, R.S., 2nd & Thibault, L.E. (1996) Acute alterations in [Ca2+]i in NG108-15 cells subjected to high strain rate deformation and chemical hypoxia: an in vitro model for neural trauma. *J Neurotrauma*, **13**, 395-407.

Chen, Y.C., Smith, D.H. & Meaney, D.F. (2009) In-vitro approaches for studying blast-induced traumatic brain injury. *J Neurotrauma*, **26**, 861-876.

Choi, D.W. (1995) Calcium: still center-stage in hypoxic-ischemic neuronal death. *Trends in neurosciences*, **18**, 58-60.

Coats, B. & Margulies, S.S. (2006) Material properties of porcine parietal cortex. *J Biomech*, **39**, 2521-2525.

Cohen, A.S., Pfister, B.J., Schwarzbach, E., Grady, M.S., Goforth, P.B. & Satin, L.S. (2007) Injury-induced alterations in CNS electrophysiology. *Prog Brain Res*, **161**, 143-169.

Ellis, E.F., McKinney, J.S., Willoughby, K.A., Liang, S. & Povlishock, J.T. (1995) A new model for rapid stretch-induced injury of cells in culture: characterization of the model using astrocytes. *J Neurotrauma*, **12**, 325-339.

Galbraith, J.A., Thibault, L.E. & Matteson, D.R. (1993) Mechanical and electrical responses of the squid giant axon to simple elongation. *J Biomech Eng*, **115**, 13-22.

Gallant, P.E. & Galbraith, J.A. (1997) Axonal structure and function after axolemmal leakage in the squid giant axon. *J Neurotrauma*, **14**, 811-822.

Geddes, D.M. & Cargill, R.S., 2nd (2001) An in vitro model of neural trauma: device characterization and calcium response to mechanical stretch. *J Biomech Eng*, **123**, 247-255.

Geddes, D.M., Cargill, R.S., 2nd & LaPlaca, M.C. (2003a) Mechanical stretch to neurons results in a strain rate and magnitude-dependent increase in plasma membrane permeability. *J Neurotrauma*, **20**, 1039-1049.

Geddes, D.M., LaPlaca, M.C. & Cargill, R.S., 2nd (2003b) Susceptibility of hippocampal neurons to mechanically induced injury. *Exp Neurol*, **184**, 420-427.

Gennarelli, T.A. (1993) Mechanisms of brain injury. *The Journal of emergency medicine*, **11**, 5-11.

Goforth, P.B., Ellis, E.F. & Satin, L.S. (1999) Enhancement of AMPA-mediated current after traumatic injury in cortical neurons. *J Neurosci*, **19**, 7367-7374.

Goforth, P.B., Ellis, E.F. & Satin, L.S. (2004) Mechanical injury modulates AMPA receptor kinetics via an NMDA receptor-dependent pathway. *Journal of Neurotrauma*, **21**, 719-732.

Goforth, P.B., Ren, J., Schwartz, B.S. & Satin, L.S. (2011) Excitatory synaptic transmission and network activity are depressed following mechanical injury in cortical neurons. *J Neurophysiol*, **105**, 2350-2363.

Graham, D.I., Adams, J.H. & Gennarelli, T.A. (1993) Pathology of Brain Damage in Head Injury. *Head Injury*. Williams and Wilkins, Baltimore, pp. 91-113.

Graham, D.I., McLellan, D., Adams, J.H., Doyle, D., Kerr, A. & Murray, L.S. (1983) The neuropathology of the vegetative state and severe disability after non-missile head injury. *The European Journal of Neurosurgery*, **32**, 65-67.

Holbourn, A.H.S. (1945) The Mechanics of Brain Injuries. *British Medical Bulletin*, **3**, 147-149.

Iwata, A., Stys, P.K., Wolf, J.A., Chen, X.H., Taylor, A.G., Meaney, D.F. & Smith, D.H. (2004) Traumatic axonal injury induces proteolytic cleavage of the voltage-gated sodium channels modulated by tetrodotoxin and protease inhibitors. *J Neurosci*, **24**, 4605-4613.

Kao, C.Q., Goforth, P.B., Ellis, E.F. & Satin, L.S. (2004) Potentiation of GABA(A) currents after mechanical injury of cortical neurons. *J Neurotrauma*, **21**, 259-270.

Korngreen, A. & Sakmann, B. (2000) Voltage-gated K+ channels in layer 5 neocortical pyramidal neurones from young rats: subtypes and gradients. *The Journal of physiology*, **525**, 621-639.

LaPlaca, M.C., Cullen, D.K., McLoughlin, J.J. & Cargill, R.S., 2nd (2005) High rate shear strain of three-dimensional neural cell cultures: a new in vitro traumatic brain injury model. *J Biomech*, **38**, 1093-1105.

LaPlaca, M.C. & Thibault, L.E. (1997) An in vitro traumatic injury model to examine the response of neurons to a hydrodynamically-induced deformation. *Annals of Biomedical Engineering*, **25**, 665-677.

LaPlaca, M.C. & Thibault, L.E. (1998) Dynamic mechanical deformation of neurons triggers an acute calcium response and cell injury involving the N-methyl-D-aspartate glutamate receptor. *J Neurosci Res*, **52**, 220-229.

Lea, P.M.t., Custer, S.J., Stoica, B.A. & Faden, A.I. (2003) Modulation of stretch-induced enhancement of neuronal NMDA receptor current by mGluR1 depends upon presence of glia. *J Neurotrauma*, **20**, 1233-1249.

Lee, A.A., Delhaas, T., Waldman, L.K., MacKenna, D.A., Villarreal, F.J. & McCulloch, A.D. (1996) An equibiaxial strain system for cultured cells. *Am J Physiol*, **271**, C1400-1408.

Lighthall, J.W., Dixon, C.E. & Anderson, T.E. (1989) Experimental models of brain injury. *J Neurotrauma*, **6**, 83-97.

Lucas, J.H. (1992) In vitro models of mechanical injury. *J Neurotrauma*, **9**, 117-121.

Lusardi, T.A., Rangan, J., Sun, D., Smith, D.H. & Meaney, D.F. (2004a) A device to study the initiation and propagation of calcium transients in cultured neurons after mechanical stretch. *Ann Biomed Eng*, **32**, 1546-1558.

Lusardi, T.A., Smith, D.H., Wolf, J.A. & Meaney, D.F. (2003) The separate roles of calcium and mechanical forces in mediating cell death in mechanically injured neurons. *Biorheology*, **40**, 401-409.

Lusardi, T.A., Wolf, J.A., Putt, M.E., Smith, D.H. & Meaney, D.F. (2004b) Effect of acute calcium influx after mechanical stretch injury in vitro on the viability of hippocampal neurons. *J Neurotrauma*, **21**, 61-72.

Magou, G.C., Guo, Y., Choudhury, M., Chen, L., Hususan, N., Masotti, S. & Pfister, B.J. (2011) Engineering a high throughput axon injury system. *J Neurotrauma*, **28**, 2203-2218.

Margulies, S.S. & Thibault, L.E. (1992) A proposed tolerance criterion for diffuse axonal injury in man. *J Biomech*, **25**, 917-923.

Margulies, S.S., Thibault, L.E. & Gennarelli, T.A. (1985) A study of scaling and head injury criteria using physical model experiments. In: Proceedings of the IRCOBI, 223-234.

Margulies, S.S., Thibault, L.E. & Gennarelli, T.A. (1990) Physical model simulations of brain injury in the primate. *J Biomech*, **23**, 823-836.

Meaney, D.F., Miller, R.T., Shreiber, D.I. & Smith, D.H. (1998) Experimental Models of Traumatic Brain Injury. *Frontiers in Head and Neck Trauma*. IOS Press, Amsterdam, Netherlands.

Meaney, D.F., Smith, D., Ross, D.T. & Gennarelli, T.A. (1993) Diffuse axonal injury in the miniature pig: biomechanical development and injury threshold. *Crashworthiness and Occupant Protection in Transportation Systems*, 169-175.

Meaney, D.F., Smith, D.H., Shreiber, D.I., Bain, A.C., Miller, R.T., Ross, D.T. & Gennarelli, T.A. (1995) Biomechanical analysis of experimental diffuse axonal injury. *J Neurotrauma*, **12**, 689-694.

Meaney, D.F. & Thibault, L.E. (1990) Physical Model Studies of Cortical Brain Deformation in Response to High Strain Rate Inertial Loading. International Conference on the Biomechanics of Impact. Lyon, France.

Miller, W.J., Leventhal, I., Scarsella, D., Haydon, P.G., Janmey, P. & Meaney, D.F. (2009) Mechanically induced reactive gliosis causes ATP-mediated alterations in astrocyte stiffness. *J Neurotrauma*, **26**, 789-797.

Morrison, B., 3rd, Cater, H.L., Benham, C.D. & Sundstrom, L.E. (2006) An in vitro model of traumatic brain injury utilising two-dimensional stretch of organotypic hippocampal slice cultures. *J Neurosci Methods*, **150**, 192-201.

Morrison, B., 3rd, Meaney, D.F. & McIntosh, T.K. (1998a) Mechanical characterization of an in vitro device designed to quantitatively injure living brain tissue. *Ann Biomed Eng*, **26**, 381-390.

Morrison, B., 3rd, Saatman, K.E., Meaney, D.F. & McIntosh, T.K. (1998b) In vitro central nervous system models of mechanically induced trauma: a review. *J Neurotrauma*, **15**, 911-928.

Palsson, B.O. & Bhatia, S.N. (2004) *Tissue Engineering*. Pearson Prentice Hall, Upper Saddle River, NJ.

Pfister, B., Oyler, G., Betenbaugh, M. & Bao, G. (2004) The effects of BclXL and Bax over-expression on stretch-injury induced neural cell death. *Mech Chem Biosyst*, **1**, 233-243.

Pfister, B.J. (2001) An in vitro model for uniaxial stretching of culutred neural cells; the roles of mechanical deformation and Bcl-2 proteins on axonal injury. The Johns Hopkins University, Baltimore.

Pfister, B.J., Weihs, T.P., Betenbaugh, M. & Bao, G. (2003) An in vitro uniaxial stretch model for axonal injury. *Ann Biomed Eng*, **31**, 589-598.

Povlishock, J.T. (1992) Traumatically induced axonal injury: pathogenesis and pathobiological implications. *Brain Pathol*, **2**, 1-12.

Prado, G.R., Ross, J.D., DeWeerth, S.P. & LaPlaca, M.C. (2005) Mechanical trauma induces immediate changes in neuronal network activity. *J Neural Eng*, **2**, 148-158.

Rzigalinski, B.A., Weber, J.T., Willoughby, K.A. & Ellis, E.F. (1998) Intracellular free calcium dynamics in stretch-injured astrocytes. *J Neurochem*, **70**, 2377-2385.

Santhakumar, V., Ratzliff, A.D., Jeng, J., Toth, Z. & Soltesz, I. (2001) Long-term hyperexcitability in the hippocampus after experimental head trauma. *Annals of neurology*, **50**, 708-717.

Smith, D.H. & Meaney, D.F. (2000) Axonal Damage in Traumatic Brain Injury. *The Neuroscientist*, **6**, 483-495.

Smith, D.H., Wolf, J.A., Lusardi, T.A., Lee, V.M. & Meaney, D.F. (1999) High tolerance and delayed elastic response of cultured axons to dynamic stretch injury. *J Neurosci*, **19**, 4263-4269.

Sotoudeh, M., Jalali, S., Usami, S., Shyy, J.Y. & Chien, S. (1998) A strain device imposing dynamic and uniform equi-biaxial strain to cultured cells. *Ann Biomed Eng*, **26**, 181-189.

Spaethling, J.M., Klein, D.M., Singh, P. & Meaney, D.F. (2008) Calcium-permeable AMPA receptors appear in cortical neurons after traumatic mechanical injury and contribute to neuronal fate. *J Neurotrauma*, **25**, 1207-1216.

Storm, J.F. (1987) Action potential repolarization and a fast after-hyperpolarization in rat hippocampal pyramidal cells. *The Journal of physiology*, **385**, 733-759.

Tavalin, S.J., Ellis, E.F. & Satin, L.S. (1995) Mechanical perturbation of cultured cortical neurons reveals a stretch-induced delayed depolarization. *J Neurophysiol*, **74**, 2767-2773.

Tavalin, S.J., Ellis, E.F. & Satin, L.S. (1997) Inhibition of the electrogenic Na pump underlies delayed depolarization of cortical neurons after mechanical injury or glutamate. *J Neurophysiol*, **77**, 632-638.

Thibault, L.E., Meaney, D.F., Anderson, B.J. & Marmarou, A. (1992) Biomechanical aspects of a fluid percussion model of brain injury. *J Neurotrauma*, **9**, 311-322.

von Reyn, C.R., Spaethling, J.M., Mesfin, M.N., Ma, M., Neumar, R.W., Smith, D.H., Siman, R. & Meaney, D.F. (2009) Calpain mediates proteolysis of the voltage-gated sodium channel alpha-subunit. *J Neurosci*, **29**, 10350-10356.

Wolf, J.A., Stys, P.K., Lusardi, T., Meaney, D. & Smith, D.H. (2001) Traumatic axonal injury induces calcium influx modulated by tetrodotoxin-sensitive sodium channels. *J Neurosci*, **21**, 1923-1930.

Wu, R.L. & Barish, M.E. (1992) Two pharmacologically and kinetically distinct transient potassium currents in cultured embryonic mouse hippocampal neurons. *J Neurosci*, **12**, 2235-2246.

Yuen, T.J., Browne, K.D., Iwata, A. & Smith, D.H. (2009) Sodium channelopathy induced by mild axonal trauma worsens outcome after a repeat injury. *J Neurosci Res*, **87**, 3620-3625.

Zhang, L., Rzigalinski, B.A., Ellis, E.F. & Satin, L.S. (1996) Reduction of voltage-dependent Mg2+ blockade of NMDA current in mechanically injured neurons. *Science*, **274**, 1921-1923.